A FUNDAMENTAL STUDY OF INJECTION, SPRAY, AND COMBUSTION CHARACTERISTICS OF HYDROTREATED VEGETABLE OIL UNDER SIMULATED DIESEL ENGINE CONDITIONS

VO TAN CHAU

A THESIS SUBMITTED IN FULFILLMENT OF THE REQUIREMENT FOR THE DEGREE
OF DOCTOR OF ENGINEERING IN MECHANICAL ENGINEERING
FACULTY OF ENGINEERING
KING MONGKUT'S INSTITUTE OF TECHNOLOGY LADKRABANG
2017

KMITL-2017-EN-D-058-218

A FUNDAMENTAL STUDY OF INJECTION, SPRAY, AND COMBUSTION CHARACTERISTICS OF HYDROTREATED VEGETABLE OIL UNDER SIMULATED DIESEL ENGINE CONDITIONS

VO TAN CHAU

A THESIS SUBMITTED IN FULFILLMENT OF THE REQUIREMENT FOR THE DEGREE
OF DOCTOR OF ENGINEERING IN MECHANICAL ENGINEERING
FACULTY OF ENGINEERING
KING MONGKUT'S INSTITUTE OF TECHNOLOGY LADKRABANG
2017

Thesis title	A Fundamental Study of Injection, Spray, and Combustion Characteristics of Hydrotreated Vegetable Oil under Simulated Diesel Engine Conditions
Student	Mr. VO TAN CHAU
Student ID	56601360
Degree	Doctor of engineering
Program	Mechanical Engineering
Year	2017
Thesis Advisor	Asst. Prof. Dr. Chinda Charoenphonphanich
Thesis Co-advisor	Prof. Dr. Kosaka Hidenori

ABSTRACT

Fossil fuels have been the essential source of energy in the global development for centuries. However, along with the continual rise in the fossil fuels consumption come the pollution and the environmental degradation. Thus, attempts have been made to mitigate the fossil fuels-related environmental impacts through the renewable and more environmentally-friendly energy alternatives. Hydrotreated Vegetable Oil (HVO) is seen as a modern paraffin based fuel promising to substitute petro-diesel. The influences of physical/chemical properties of HVO to engine performance and emissions formation have been investigated the feasibility through a sequence of experiments before applying popularity on the market. This work concentrated on the analysis of injection, spray, combustion and emission characteristics of HVO which are considered as the most important features on engine. These experiments were carried out in the injection rate-Zeuch measurement system, constant volume combustion chamber (CVCC), and rapid compression expansion machine (RCEM) respectively under direct injection (DI) diesel engine conditions. The experimental fuels were the commercial diesel fuel (B7), the neat HVO, the 10%, 20%, 30%, 50%, 80% HVO (by mass fraction) blended with diesel fuel (B7). The results indicated that bulk modulus of compressibility, injection delay, average injection rate, injection quantity were inversely correlated to HVO fraction in blend. Adjusting injection duration was required to obtain the injected fuel amount equally into combustion chamber. In addition, the findings revealed the higher discharge coefficient with HVO as well as under higher injection pressure. Regarding to spray evolution, slightly shorter in penetration length during fully developed zone was observed with higher HVO fraction in blend. The larger spray cone angle of HVO and its blends compared to diesel was caused by the difference in viscosity, density, surface tension and the higher differential pressure. The effects of HVO's fuel properties, variable oxygen concentrations and injection pressures

were clearly revealed in results of combustion and emissions. The ignition delay, the heat release rate, the flame temperature, the soot density-KL factor, the NO_x and soot-out emissions were decreased as increasing the HVO fraction in the blend. In addition, the findings revealed the similar flame profiles in which the higher flame temperature region and the darker KL density were concentrated around the spray flame upstream, regardless of the HVO mixing ratio. Besides, the decrease in the O_2 concentration resulted in the lower heat release rate, integral heat release, flame temperature, KL factor and NO_x emissions but the longer ignition delay and higher soot concentration, with the highest soot concentration observed under the 15% O_2 environment. Nevertheless, the higher pressure differential (i.e. between the injection pressure and the ambient pressure) contributed to the shorter ignition delay, higher heat release rate, early peak of the flame temperature, wider combustion area, faster soot oxidation rate and higher NO_x production.

Key words: Hydrotreated vegetable oil, DI-diesel combustion, NO_x-soot emission, Constant Volume Combustion Chamber, Zeuch-Injection Rate Method, Two Color Method.

หัวข้อวิทยานิพนธ์	**การศึกษา**คุณลักษณะ**พื้นฐานของการฉีดสเปรย์และการเผาไหม้ของเชื้อเพลิง Hydrotreated Vegetable Oil ภายใต้การจำลองการเผาไหม้แบบเครื่องยนต์ดีเซล**
นักศึกษา	Mr. VO TAN CHAU
รหัสนักศึกษา	56601360
ปริญญา	วิศวกรรมศาสตรดุษฎีบัณฑิต
สาขาวิชา	วิศวกรรมเครื่องกล
พ.ศ.	2560
อาจารย์ที่ปรึกษาวิทยานิพนธ์	ผศ.ดร.จินดา เจริญพรพาณิชย์
อาจารย์ที่ปรึกษาวิทยานิพนธ์ร่วม	Prof. Dr. Kosaka Hidenori

บทคัดย่อ

เชื้อเพลิงฟอสซิลเป็นแหล่งพลังงานที่สำคัญของการพัฒนาของประเทศทั่วโลก อย่างไรก็ตามการเพิ่มขึ้นอย่างต่อเนื่องของการใช้เชื้อเพลิงฟอสซิลนั้นเป็นผลทำให้เกิดมลพิษและความเสื่อมโทรมของสิ่งแวดล้อม ดังนั้นจึงมีความพยายามที่จะบรรเทาผลกระทบการใช้เชื้อเพลิงฟอสซิลให้สัมพันธ์กับผลกระทบต่อสิ่งแวดล้อมและต่อสิ่งแวดล้อม เชื้อเพลิง Hydrotreated Vegetable Oil (HVO) ถูกมองว่าเป็นเชื้อเพลิงที่มีพื้นฐานจากพาราฟินที่มีแนวโน้มว่าจะมาทดแทนน้ำมันดีเซลได้ อิทธิพลของสมบัติทางกายภาพและทางเคมีของ HVO ต่อสมรรถนะของเครื่องยนต์และการปลดปล่อยมลพิษได้รับการตรวจสอบความเป็นไปได้ผ่านทางการทดลองก่อนที่จะได้รับความนิยมในตลาด งานวิจัยนี้เน้นการวิเคราะห์คุณลักษณะการฉีด การสเปรย์ การเผาไหม้และการปล่อยไอเสียของเชื้อเพลิง HVO ซึ่งถือว่าเป็นคุณลักษณะที่สำคัญในเครื่องยนต์ การทดลองดำเนินการโดยใช้อัตราการฉีดเชื้อเพลิง ด้วยวิธีการวัดแบบ Zeuch, ห้องเผาไหม้ปริมาตรคงที่ (CVCC) และเครื่องอัดและขยายตัว (RCEM) ตามลำดับภายใต้สภาวะการทำงานของเครื่องยนต์ดีเซลแบบฉีดตรง (DI) สำหรับเชื้อเพลิงทดลองคือน้ำมันดีเซล (B7), เชื้อเพลิง HVO, เชื้อเพลิง HVO 10%, 20%, 30%, 50%, 80% ผสมกับน้ำมันดีเซล (B7) ผลการทดลองแสดงให้เห็นว่าค่าโมดูลัสการอัดตัวม ความล่าช้าของการฉีด อัตราการฉีดโดยเฉลี่ย และปริมาณการฉีดเชื้อเพลิงมีความสัมพันธ์เชิงผกผันกับการผสมเชื้อเพลิง การปรับระยะเวลาการฉีดให้ถูกต้องเป็นสิ่งจำเป็นเพื่อให้ได้ปริมาณเชื้อเพลิงที่ฉีดเข้าไปในห้องเผาไหม้อย่างเท่าเทียมกัน นอกจากนี้ผลการวิจัยพบว่าค่า discharge coefficient สูงขึ้นกับเชื้อเพลิง HVO และสูงขึ้นเมื่อเพิ่มความดันของการฉีดด้วย

เมื่อพิจารณาถึงการสเปรย์ของเชื้อเพลิงพบว่าความยาวของลำสเปรย์สั้นในช่วงที่หัวฉีดมีการฉีดอย่างเต็มที่ (Fully developed zone) เมื่อเพิ่มสัดส่วนของเชื้อเพลิง HVO มุมของสเปรย์มีขนาดกว้างขึ้นกับเชื้อเพลิง HVO และเชื้อเพลิงผสม HVO เมื่อเทียบกับเชื้อเพลิงดีเซล ซึ่งเกิดจากความแตกต่างของความหนืด ความหนาแน่น ความตึงผิวและความแตกต่างของความดัน ผลของคุณสมบัติของน้ำมันเชื้อเพลิง HVO

ความเข้มข้นของแก๊สออกซิเจนและความดันการฉีดแสดงให้เห็นอย่างชัดเจนต่อการเผาไหม้และการปล่อยไอเสีย ความล่าช้าการเผาไหม้ อัตราการปลดปล่อยความร้อน อุณหภูมิเปลวไฟ ค่าความหนาแน่นของเขม่า (KL factor) การปล่อยไอเสียของแก๊สไนโตรเจนออกไซด์และเขม่าลดลงเมื่อเพิ่มส่วนการผสมของเชื้อเพลิง HVO นอกจากนี้พบว่ามีเปลวไฟที่คล้ายคลึงกันในบริเวณที่มีอุณหภูมิสูงกว่าและความหนาแน่นของบริเวณสีเข้มของค่า KL มีการความหนาแน่นในช่วงบนของเปลวไฟโดยไม่คำนึงถึงอัตราส่วนการผสมของเชื้อเพลิง HVO นอกจากนั้นการลดลงของความเข้มข้นของแก๊สออกซิเจนยังส่งผลให้เกิดอัตราการปลดปล่อยความร้อนลดลง การปล่อยความร้อน อุณหภูมิเปลวไฟ KL factor และการปล่อยไอเสียของแก๊สไนโตรเจนออกไซด์ลดลง แต่พบว่าความล่าช้าของการเผาไหม้นานขึ้นและความเข้มข้นของเขม่าสูงขึ้น ความเข้มข้นของเขม่าสูงที่สุดที่ความเข้มข้นของแก๊สออกซิเจน 15% แต่อย่างไรก็ตาม ที่ความแตกต่างของความดันการฉีดที่เพิ่มขึ้น (ความดันระหว่างการฉีดและความดันในห้องเผาไหม้) ทำให้ความล่าช้าในการเผาไหม้ที่สั้นลง อัตราการปลดปล่อยความร้อนสูงขึ้น เกิดจุดสูงสุดของอุณหภูมิเปลวไฟก่อนพื้นที่การเผาไหม้ที่กว้างขึ้น อัตราการเกิดออกซิเดชันของเขม่าเร็วขึ้นและการเกิดแก๊สไอเสียไนโตรเจนออกไซด์ที่สูงขึ้น

คำสำคัญ: น้ำมันเชื้อเพลิง Hydrotreated vegetable oil, การเผาไหม้ของดีเซลแบบฉีดตรง, มลพิษไอเสียของไนโตรเจนออกไซด์-เขม่า, ห้องเผาไหม้ปริมาตรคงที่, วิธีการวัดอัตราการฉีดด้วยวิธี Zeuch, วิธี Two Color

ACKNOWLEDGEMENTS

I would like to thank King Mongkut's Institute of Technology Ladkrabang (KMITL), which gave me the opportunity for pursuing one's studies. I would like to express my sincerest gratitude to Asst. Prof. Dr. Chinda Charoenphonphanich for his supports, invaluable advices, timely inspirations during my doctoral study. I would like to reveal deep thank to my co-advisor, Prof. Kosaka Hidenori who gave me a chance to perform experiment, as well the supports, constant guidance and enthusiasm during I spent my research time in Tokyo Institute of Technology (TIT). I would like to thank Dr. Preechar Karin, Dr. Prathan Srichai, Assoc. Prof. Dr. Sato Susumu for their help and consult in experiments. I would like to thank all staffs, technicians, assistants and students of Automotive Laboratory (KMITL) and Advanced Thermo-Fluid Dynamics Laboratory (TIT) for their supporting and helping throughout my studying time.

Special thanks to Dr. Somnuek Jaroonjitsathian and PTT Public Company Ltd. for supplying experimental fuels. Sincere thanks to Dr. Nuwong Chollacoop and staffs at MTEC for supporting fuel property test.

I would like to thank for AUN/SEED-Net program-JICA that sponsored finance for my study time. I am grateful to all JICA staffs at Thailand and Japan who always take care and support me during the course of study.

I wish to express my gratitude to my parents though they could not feel their son's success. Thank parents for giving me a life and beloved brothers by my side. They are always invaluable source of support, and encouragement in my life. More than ever, I wish my parents could stand side me at this moment.

Finally, I would like to thank my engaged wife who has always stood behind me and given me the love, motivation and sharing in life.

CONTENTS

LIST OF FIGURES

LIST OF TABLES

NOMENCLATURE

K	Bulk modulus of compressibility, (MPa)
V	Volume of Zuech chamber, (m^3)
ΔV	Differential volume of Zuech chamber, (m^3)
ΔP	Differential pressure, (MPa)
ρ_f	Fuel density, (kG/m^3)
dm/dt	Mass flow rate, (mg/ms)
dP/dt	Rate of pressure changed in chamber, (MPa/ms)
Cd	Discharge coefficient
m°_{theory}	Theoretical mass of flow rate, (mg/ms)
A	Cross section of injector, (mm^2)
$n_{orifice}$	Number hole of injector
Re	Reynolds number
$V_{average}$	Flow velocity at exit of nozzle, (mm/ms)
D_{inj}	Nozzle diameter, (mm)
υ	Fuel kinematic viscosity, (mm^2/s)
S	Spray tip penetration (mm)
θ	Spray cone angle (deg)
$I_{(\lambda,T)}$	Monochromatic radiant intensity
λ	Wavelength, (nm)
T	True flame temperature, (K)
T_a	Apparent temperature, (K)
C_1	The first Planck constant
C_2	The second Planck constant
ε	Emissivity
K	Absorption coefficient
L	Optical path length
α	Empirical constant of visible spectrum (1.39)
dQ/dt	Heat release rate
γ	Specific heat ratio

CHAPTER 1
INTRODUCTION

1.1. Background of Introduction

Detection of fossil oil has played the important role to the development of the world economy which forced the great evolution in many fields such as energy, industry, transportation. Nowadays, the growth of world population, economies, industrialization of developing countries as well as the continuous industrialization of developed countries have caused the increase of oil energy consumption. According to International Energy Agency [1], global primary energy demand increases by one-third to 2040, from 13,546 million tons of oil equivalent (Mtoe) in 2013 to 17,973Mtoe in 2040 (Fig. 1.1). Oil is mostly used in mobile applications: transport accounts for over 55% of oil demand. Small-scale stationary usage such buildings, agriculture covers another 10% of oil. A third of oil is used in large-scale stationary sources in industry and power generation. Global oil demand reaches 99 million barrels per day in 2030, around 9% higher than today (Energy and Climate Change-IEA [2]). In addition, fossil fuel price depends on the size of fossil fuel reserves but the trend of fossil fuel consumption increase over time. Currently, the oil price is at around 50USD per barrel in nominal terms. However, fossil fuel price fluctuates according to economic condition and others issues. As a result, forecasting fossil fuel price are uncertain for future.

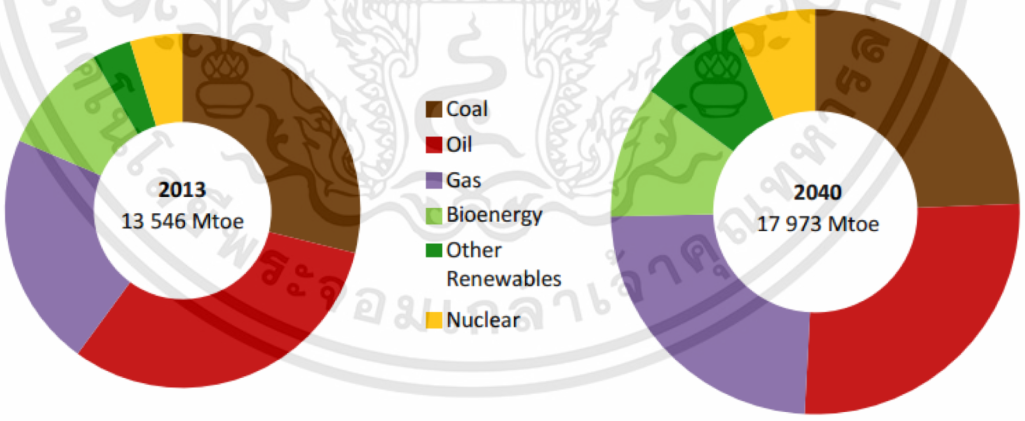

Fig. 1.1. World primary energy demand in the new policies scenario (Energy and air pollution [1]).

Despite possessing many dominant properties such as high energy density, safety, available oil reserves but fossil oil is considered to be non-renewable resources. Regarding to Shafiee and Topal [3], fossil reserves including oil, coal and gas are going to be depleted in next 35, 107, and 37 years, respectively. The role of fossil oil has been continued for dominating the global energy and accounted for 84% of total

energy use in 2030 [4]. However, pollutant emissions have been produced along the whole chain of fossil fuel life, from extraction to final use. For refining sector of crude oil, some 2 Mt of SO_2 and 1.2 Mt of NO_x emissions are released, especially, a number of Coker are produced which may have a substantial local impact. The transport sector remains a major source of air pollutants, around 56 Mt of NO_x and PM in 2015 [1]. Carbon dioxide (CO_2) is one of the greenhouse gas that contributes to global warming, causing the increase of surface temperature of the earth. CO_2 is released over 90% of energy-related emissions from fossil fuel combustion. Global CO_2 emissions increased 2.3% between 2000 and 2014, particularly driven by a rapid rise of CO_2 in power generation in countries outside the Organization for Economic Cooperation and Development (OECD). This is due to the higher level of vehicle ownership in OECD countries even though, over the past 15 years, CO_2 emissions from transport doubled in non-OECD countries as a result both of higher levels of private vehicle ownership and stronger growth in freight traffic [2].

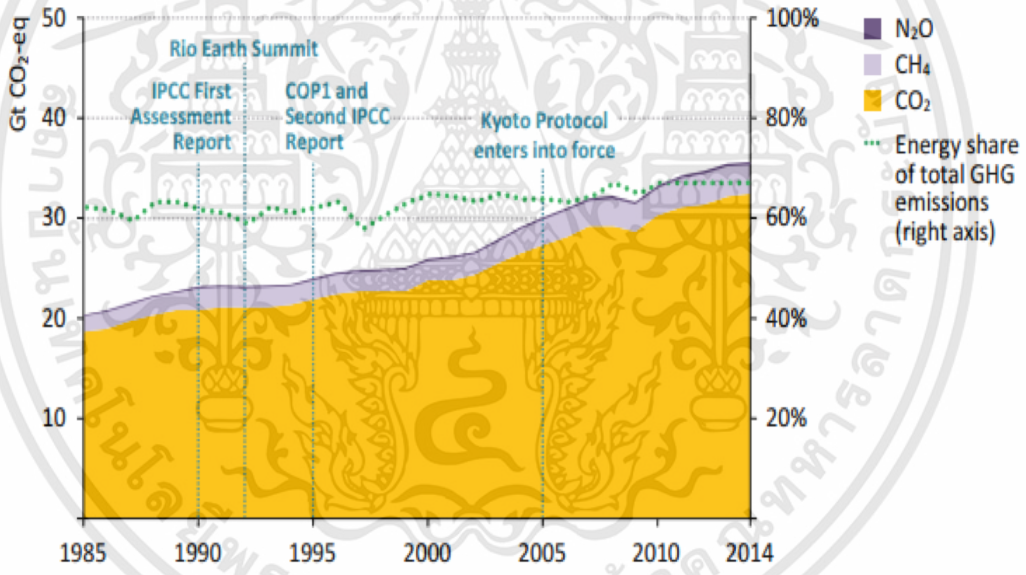

Fig. 1.2. Global anthropogenic energy-related greenhouse gas emissions by type (IEA and EC/PBL 2014) [2].

From above issues of fossil energy consumption, attempts have been made to mitigate the fossil fuels-related environmental impacts as well as solving energy crisis through the renewable and more environmentally-friendly energy alternatives. Solar, wind, geothermal, hydro, and some forms of biomass are common sources of renewable energy. The International Energy Agency reported that renewable sources account for almost 22% of global electricity generation in 2013 and project reaching near 26% increase to 2020, almost 30% in 2040. With the government policies, renewable energy is the world's fastest growing source of energy, at an average rate

of 2.6% yearly. According to REN 21 [5], renewable energy provided an estimated 19.2% of global final energy consumption in 2014. In which, the increase of renewable energy consumption is divided as 8.9% average annually coming from biomass (wood and wood waste, municipal solid waste, landfill gas and biogas, ethanol, biodiesel), over 4% as geothermal power and heat energy, 3.9% hydro-power and 1.4% is electricity from wind, solar by the end of 2014 (notably, wind power contributed 42% of electricity demand in Denmark, more than 60% in four states of Germany, 15.5% in Uruguay while solar supplied 7.8% in Italy, 6.5% in Greece, and 6.4% in Germany). Around 10% in total global primary energy consumption has been shared by the bioenergy since 2005 [5]. For using renewable energy in transportation, it showed an estimated 4% of global road transport fuel in 2015. Liquid biofuels continued to represent the vast majority of the renewable energy contribution to this sector (reaching 133 billion liters in 2015). In biofuels global production, ethanol has the highest capacity with 74%, then 22% for biodiesel and 4% for hydrotreated vegetable oil (HVO) [5]. The higher renewable energy use promotes to diminish air pollution. These efforts bring the reduction of greenhouse gas emission not only sustainable but also techno-economically competitive.

In the scope of this study, diesel fuel was used as a base-fuel and hydrotreated vegetable oil (HVO), one type of biofuel, was used as a research fuel in compression ignition engine (CI-engine). Diesel fuel is one of fossil products from refinery of petroleum crude oil. It is a mixture of hydrocarbon such alkanes, cycloalkanes and aromatic with boiling point in the range of 150^{0}C to 380^{0}C and carbon atoms per molecule in the range between C8 and C21 (Chevron [6]). The burning of diesel fuel in CI engine significantly produces emissions. As known, diesel combustion is a complicated phenomenon with the interaction between physical and chemical processes. In the direct injection (DI) diesel engine, high pressure-diesel fuel is injected into combustion chamber in the end of compression stroke. At that moment, engine has small combustion volume with high temperature and high pressure, the injected diesel spray is atomized, then it vaporizes and mixes with the hot air in chamber. Auto-ignition starts locally in the areas with completely evaporated fuel mixed with sufficient atmospheric oxygen. During this phase, injection typically continues and combustion and mixture preparation occur simultaneously. The combustion process is usually composed of ignition delay, premixed-combustion phase, diffusion combustion phase, and late combustion phase in lastly (Heywood [7]). The ignition process is strongly inhomogeneous, since liquid and gaseous phases simultaneously exist with a complex dynamic interaction. The local temperature is the decisive factor in determining the ignition lag and related processes. During ignition delay, the air-fuel mixture prepared burns quickly upon the onset of ignition. The combustion of premixed component

occurs with a slower diffusion combustion. The fuel preparation is further accelerated from the increasing release of energy. High conversion rates in auto-ignition generate high-pressure gradients and, therefore, usually high noise emissions. To avoid this, the premixed combustion is limited as much as possible. In diffusion combustion phase, the combustion is characterized by the continued injection of fuel into the existing flame. The burning rate is controlled by the rate at which mixture becomes available for burning. This mainly depends on the fuel vapor-air mixing process. In late combustion phase, heat release continues at a lower rate well into the expansion stroke due to decreasing reaction rate (The zones of reducing oxygen and gradually sinking gas temperature from expansion). A small fraction of fuel may not yet have burned and existed in soot-out emission. The efficiency of the combustion process is strongly dependent upon the charged-air, temperature, pressure, fuel, injection pressure, atomization, vaporization, interaction, etc. Equivalence ratio is used to present a measure of the relative amount of fuel and air and the first auto-ignition occurs in the regions where the fuel-air equivalence ratio is appropriate. The fuel-air mixing process has the dominant influence to soot formation in where is the rich regions and high temperature. Soot or Particulate Matter (PM) is the mix of solid/liquid organic and inorganic substances (consists of a varying number of HC and/or sulfur compounds that are deposited on soot). The exhaust particles are linked to major detrimental health impacts and size is an important factor in determining these impacts. NO_x emission strongly depends on the premixed combustion phase when combustion has the highest temperature. Soot and NOx are mainly considerations in combustion process for diesel engines. In addition, carbon monoxide (CO) is one of the incomplete combustion gas emission in CI engine which contributes to air pollution. However, CO or HC plays less of a role in diesel engine combustion. Pollutants such as NO_x, soot, CO, CO_2 and HC are directly related to the local conditions of ignition, mixture formation, and combustion in chamber. The optimization of diesel combustion conditions contributes to higher combustion efficiency and lower emission level.

As mentioned above, diesel fuel is considered as a non-renewable fuel. Therefore, the world has been confronted with energy crises due to rising fuel consumption. In addition, with the increase of emission standards being applied on many countries, the instability of oil price, requirement of lower CO_2 emission for reducing the impact to the climate change, and satisfaction of increasing energy demand, the searching for bio-based diesel fuel is being considered as a top priority in the researches relating diesel engine. Currently, these researches are forwarding to advanced techniques in order to diversify alternative fuel resources as well as upgrade new biofuel generations with many dominant properties. These generations are biomass to liquid (BTL), gas to

liquid (GTL), coal to liquid (CTL), hydrotreated vegetable oil (HVO), pyrolysis oil, synthetic fuel, hydrogen, ethanol, fuel cell, etc. They are not only sustainable but also techno-economically competitive fuel. Furthermore, they are promoted as a means to create rural development and improve trade balance. In Thailand, Ministry of Energy aims to increase the alternative energy consumption by 25% in 2021 (Twarath [8]). With policies for strengthening alternative energy development, specifically in biofuel, it is expected that biofuel can substitute by 44% oil demand (9mL/d for ethanol, 5.97 mL/d for biodiesel, and around 25mL/d for new biofuel) by 2021 as well as reduce greenhouse gas and challenges in energy crisis.

In CI-diesel engine, study on combustion phenomenon in chamber has not fully comprehended due to a series of complex physical and chemical sub-processes occur such as spray formation, vaporization, mixing, and chain branching (initial chemical reactions) without any notable conversion of energy. The ignition is therefore dependent on the starting conditions of mixture formation as following:

- The pressure and temperature of the charge;
- The temperature, viscosity, vaporization characteristics, ignitability of the fuel;
- The pressure, time, and characteristic of injection, as well as the nozzle geometry that determines the spray formation (size, distribution, and pulse of the droplets);
- Charge movement;
- The combustion chamber geometry;
- Charge composition, i.e., the oxygen component and the changes in the specific thermal capacity from the EGR, etc.

Currently, there are many difficulties in optical observation of combustion phenomenon as well as flexible adjustment in operating conditions for diesel engine in order to optimize engine conditions for matching with renewable fuels base diesel fuel. Recently, constant volume combustion chamber (CVCC) and rapid compression-expansion machine (RCEM) have become popular for diesel engine research. They can apply the wide range of engine conditions and simulate the well-defined boundary engine conditions (Naber *et al.*, [9]; Kobori *et al*., [10]). The work described in this thesis concentrates on the studies of hydrotreated vegetable oil, seen as a 2^{nd} generation biofuel, on the aspects of injection dynamics, spray behaviors, combustion characteristics, and gas emissions, particularly soot and NO_x formation under variable oxygen concentrations and injection pressures in CVCC and RCEM. The following part of this chapter presents a background of HVO before moving to main discussion.

1.2. Literature Review of Hydrogenated Vegetable Oil and Research Approach

As previous mentioned, HVO is seen as an alternative diesel fuel that has received remarkable attention for not only diesel engine application but also aviation fields. In this part, the discussion will be focused on the application of HVO to CI-engine only. The terms “hydrotreated vegetable oil”, hydrogenated vegetable oil”, “renewable diesel fuel”, “second generation biodiesel”, “paraffinic renewable diesel”, “paraffinic diesel fuel”, “non-esterified renewable diesel”, “hydroprocessed vegetable oil”, “green diesel”, “bio-hydrogenated diesel”, “hydrotreated biodiesel”, “hydrogenation derived renewable diesel” have been used interchangeably for bio-based alkanes mixtures with the chemical structure C_nH_{2n+2}, originating from vegetable oil or animal fat (Soo-Young No [11]). To avoid the misleading, “hydrotreated vegetable oil (HVO)” will be used in this thesis. For this part, a brief description of potential, prospects, researches related CI-engine of HVO will be provided.

Global production of HVO grew by some 20% to 4.9 billion liters at end 2015, with the Netherlands, the United States, Singapore and Finland as major producers (REN 21 [5]). HVO account for 4% in total biofuels global production by 2015 and a number of routes are being developed in next decades. According to Sunde *et al.* [12], HVO made from wastes or by-products (tall oil, tallow) or used cooking oil outperforms transesterified lipids, BTL with respect to both environmental life cycle impacts and costs. This is consistent with Rickard’s finding [13] who studied on the life cycle assessment of HVO from rape, oil palm and jatropha and reported that HVO has about half lower life cycle global warming potential (GWP) than conventional diesel fuel as well as the lowest environmental impact for using palm oil as feedstock. A comparison on aspects of fuel production and energy balance, fuel properties, and environmental effects (exhaust emissions and co-products) between biodiesel and renewable diesel (HVO) were carried out by Knothe [14]. Author revealed that both biodiesel and renewable diesel possess advantages in terms of carbon renewability compared to petro-diesel. The environmental benefits of renewable diesel appeared to be less compared to biodiesel in terms of PM and CO emissions. Besides, the drawback of HVO is reported such poorer lubricity, high cetane number than diesel (Hoekman *et al.*, [15]). This limits the its blending percentage by lower 50% with diesel to ensure on lifetime and electronic control of engine (Lapuerta *et al.*, [16]). In general, HVO production has the difference in comparison with other biofuels for instance of biodiesel (transesterification method), BTL (Fischer-Tropsch process). Although HVO is produced from same lipid feedstocks (vegetable oil) used for transesterified lipid production, the double bonds and oxygen in fatty acids based on triglyceride are converted to hydrocarbon by saturation of double bonds and removal of oxygen by

some methods (decarboxylation, decarbonylation, dehydration) with the presence of high temperature (300^0C÷360^0C), high pressure (30bar÷180bar), hydrogen (co-reagent) and catalyst (e.g. NiMo/γ-Al_2O_3 or CoMo/γ-Al_2O_3). Byproducts are light petroleum gas, propane and naphtha that can be used internally for energy production. The main constituent of HVO is paraffinic fuels (straight chain or branch chain hydrocarbon or both) (Caprotti *et al*., [17]). Fig. 1.3 illustrates the chemical structure of HVO which is produced by catalytic hydrogenation (Westphal *et al.*, [18]). Due to high n-paraffin profile, no oxygen, the absence of both aromatic and olefinic species, then HVO has low cold fuel properties. Therefore, n-HVO profile is upgraded by isomerizing process in order to obtain branch-chain hydrocarbon. HVO possesses several fuel advantages over biodiesel (poor oxidation stability, microorganism on fuel line parts, high density and viscosity, low calorific value (Jo-Han *et al*., [19]; Agarwal [20]) such high cetane number, narrow distillation curve, high heating value, no aromatic and ultra-low sulfur content, excellent oxidation stability (Soo-Young No [11]). These remarkable properties imply in easier ignition and more efficient combustion, lower engine emissions (Caprotti *et al*., [17]; Koyama *et al.*, [21]; Hartikka *et al*., [22]).

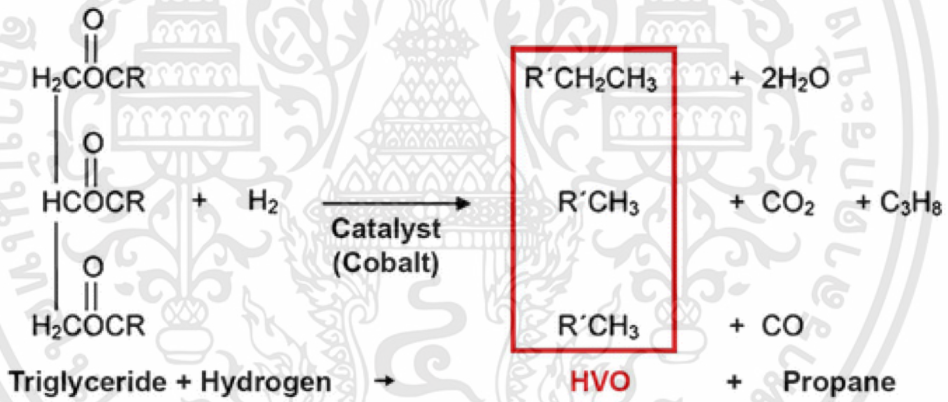

Fig. 1.3. Chemical structure of hydrotreated vegetable oil (Westphal *et al.*, [18]).

Indeed, most researchers agree that HVO has the potential for optimizing low engine emissions. This following review will mainly discuss to the application of HVO on the CI-engines. The impact HVO-blends properties on the bulk modulus was examined by Magin *et al.* [23] and showed that HVO has higher bulk modulus than diesel fuel under condition of less than 20MPa back pressure but has lower bulk modulus than biodiesel. An explanation for this could lie in the hydrocarbon structure (the presence of aromatic ring, naphtenes, branched paraffins, n-paraffin, olefins, degree of unsaturation etc.) which causes different viscosity and density. These results are especially important in the injection systems that rely on the hydraulic force transferal to open a fuel injector. An increase of bulk modulus advances the actual injection timing on mechanical injection system, then contribute to higher NO_x formation. However, the influence of the bulk modulus is not tested in the common

rail fuel injection system in the study. Sugiyama *et al*. [24] investigated the spray and combustion characteristics of HVO under the engine dynamometer and vehicle tests and documented that, in comparison with the diesel fuel, the HVO exhibited the similar spray penetration, spray angle, Sauter mean diameter (SMD) and the identical NO_x emissions but lower hydrocarbons (HC) and particulate matter (PM). The HC and PM reductions were attributable to the high cetane number and non-aromatics of the HVO. This is consistent with Pflaum's research [25], who reported that the substitution of the petro-diesel fuel with the HVO fuel could reduce the PM by almost 50% and HC and CO by 50% each; but that NO_x remained unchanged in the chassis dynamometer test and was slightly lower in the engine dynamometer test. Kim *et al*. [26] investigated the engine performance and emissions associated with the use of biodiesel and iso-HVO (HVO); and reported that the iso-HVO exhibited a better engine performance and lower total hydrocarbons (THC) and CO emissions, despite the similar levels of NO_x and PM. The findings were attributable to a more complete combustion of the HVO due to its narrow carbon-chain distribution (C15-C18). Aatola *et al*. [27] examined the effects of variable fuel injection timings in a turbocharged air-cooled common-rail heavy-duty diesel engine on the NO_x-PM tradeoff using the neat HVO fuel and the 30%vol. HVO blended with diesel. The results revealed that the HVO reduced the engine emissions without engine modifications or its control; but that, during the early injection timing, NO_x increased in the case of the 30%-HVO blend. Interestingly, their findings are consistent with the experiments on the heavy-duty engines and city buses by Kuronen *et al*. [28] and Murtonen *et al.* [29], the diesel-powered passenger cars by Kopperoinen *et al.* [30], the New European Driving Cycle (NEDC) vehicles by Somnuek *et al*. [31], and the heavy duty-typical buses by Erkkila *et al.* [32]. In addition, Hulkkonen *et al*. [33] investigated the effects of the HVO fuel on the global spray characteristics under the non-evaporative condition; and documented that the lower final boiling point, viscosity and density of the HVO contributed to the shorter liquid fuel penetration, higher spray tip velocity, and wider spray angle, resulting in the lower spray-cylinder wall interaction and better air-fuel mixing. Furthermore, Somnuek *et al.* [34] experimented with variable blends of gas-to-liquids (GTL) and HVO on a direct injection (DI) engine and reported that the higher GTL and HVO fractions shortened the ignition delay in both the pilot and main combustion. In addition, the emissions, particularly the PM, and the fuel consumption were lower, but the NO_x emissions exhibited an upward trend, regardless of the injection strategies. In regard to the soot oxidation and the surface structure, Matti *et al*. [35] reported that both the HVO and diesel fuels possessed the similar soot oxidation and surface structure, despite their chemical composition differences (i.e. cetane and aromatics). Moreover, other research of Matti [36] reported a further 25% reduction in NO_x and PM from the use of HVO

could be achieved by the adjustment of certain engine parameters. Meanwhile, Mizushima *et al.* [37] investigated and compared the effects of the HVO and fatty acid methyl esters (FAME) fuels on the emissions characteristics from a diesel engine; and documented that the HVO outperformed the FAME while the former's NO_x emissions were comparable to the ultra-low sulfur diesel. On the other hand, Singh *et al*. [38] experimented with the hydro-processed renewable diesel (HRD) fuel in the engine dynamometer using the European stationary cycle (ESC); and reported the significant reductions in PM, HC, and CO but that NO_x was substantially higher, vis-à-vis the diesel fuel. Nonetheless, the HRD emitted 29% less NO_x than the biodiesel fuel, which is contrary to Westphal's result [39], who reported the considerably lower NO_x from the HVO, according to the EU III threshold limit.

In fact, the emissions reduction results are still inconclusive, particularly with regard to the effects of variable HVO blends on the NO_x emissions. In addition, it is recognized the existence of inconsistent results for spray characteristics of HVO compared to diesel fuel. From the brief review of the application of HVO on CI-engine and under author's knowledge, no studies included a sequence of investigations of injection dynamics, fuel spray behaviors, combustion characteristics and exhaust gas emissions combinations of hydrotreated vegetable oil. Some studies only compare different fuels on a narrow-specific engine condition and from these studies, the conclusions about the effects of HVO on engine were obtained. To achieve fully understanding on the HVO feasibility, the overall objective of this study is determined as following section.

1.3. Research Objectives

Located in tropical area, Thailand has strongly potential source for producing vegetable oils, especially Palm oil, Jatropha curcas, Microalgae. Because of the limitation in blending ability and effective use of biodiesel in CI-engine and with policy for promoting biofuel development, the use of Hydrogenated vegetable oil (HVO) will contribute higher biofuels fraction for substituting petro-diesel, increase economics efficiency as well as more friendly-environment. The aim of this study is to provide the evaluation of fuel properties of hydrotreated vegetable oil to fuel injection, spray formation, combustion and emissions efficiency, increase blended ratio of bio-component in commercial diesel fuel.

From the aforementioned literature review of HVO researches, the content of this research is to focus on fundamental fuel injection, spray behaviors, combustion and emission characteristics, especially the NO_x and soot formation, given the variable oxygen concentrations and injection pressures, for hydrogenated vegetable oil and its blends under simulated diesel engine conditions. The work described in this research is separated in terms of:

A) The investigation on injection characteristics of hydrogenated vegetable oil and its blends by using high pressure fuel injection system.

B) Visualization of hydrogenated vegetable oil and its blends on spray characteristics in constant volume combustion chamber (CVCC) under non-vaporize condition.

C) Study combustion and emission characteristics of hydrogenated vegetable oil and its blends, given the variable oxygen concentrations and injection pressures, by using two-color method in a rapid compression expansion machine (RCEM).

The experiments were conducted at Automotive Laboratory, King Mongkut's Institute of Technology Ladkrabang, Thailand and Advanced Thermo-Fluid Dynamics Laboratory, Tokyo Institute of Technology, Japan. The tested fuel included commercial diesel fuel (B7-blended 7% palm methyl ester), neat HVO and HVO-diesel blends were provided by PTT Research & Technology Institute, Thailand. Fuel properties were checked at National Science and Technology Development Agency (NSTDA) and PTT. Ltd.

1.4. The Structure of Thesis

This thesis consists of 5 chapters. The current chapter is seen as an introduction. It presents the general background of this research, the literature review of HVO researches, the approach of research and scope of work.

Chapter 2 provides a description of methodology for injection characteristics. The experimental apparatus and testing conditions are showed in this chapter. In addition, the analysis of testing fuels is provided as well as used to explain for the results of following experiments. The results and discussions of injection characteristics are described for HVO and blends in this part.

Chapter 3 studies spray behaviors of HVO and its blends in CVCC under non-vaporize conditions. This chapter presents the research method, experimental conditions, results and discussions of spray characteristics. The spray development is visualized and discussed with various ambient pressures and injection pressures.

Chapter 4 shows the combustion and emission characteristics of HVO and blends in RCEM under various EGR conditions and injection pressures. In this chapter, the research method, experimental setup & conditions, and testing procedure are introduced. The result of ignition delay, heat release rate, soot formation, NOx emission are discussed.

Chapter 5 concludes this thesis by summarizing the obtained results and the prospect of possible future directions.

CHAPTER 2
INJECTION CHARACTERISTICS OF HYDROTREATED VEGETABLE OIL ON A DIESEL ENGINE COMMON RAIL SYSTEM

2.1. Introduction

Diesel engine emissions have been contributing to environmental pollution, especially NO_x and particulate matter (PM). In diesel engines, the combustion is primarily controlled by the fuel injection process. The start of injection therefore has a significant effect in the engine, which relates large amount of injected fuel at the beginning of injection to produces a strong burst of combustion with a high local temperature and high NO_x formation. As known, diesel engines utilize an internal mixture formation that produces an inhomogeneous distribution of air and fuel within the cylinder in terms of both location and time. There is only a very short time available for mixture formation in diesel engines. The parameters such injection pressure, start of injection, length of injection, nozzle geometry, etc. have played the central role to increasing large amount of mixture formation energy. As a result, how to adjust operating engine parameters or re-design chamber or improve fuel properties combination to achieve with homogeneous diesel combustion that allows the reduction of emissions and fuel consumption is the vital missions. To do that, it is necessary, on the one hand, to achieve the fastest ignition of the fuel vapor and, on the other hand, to burn as completely as possible all the injected fuel while avoiding

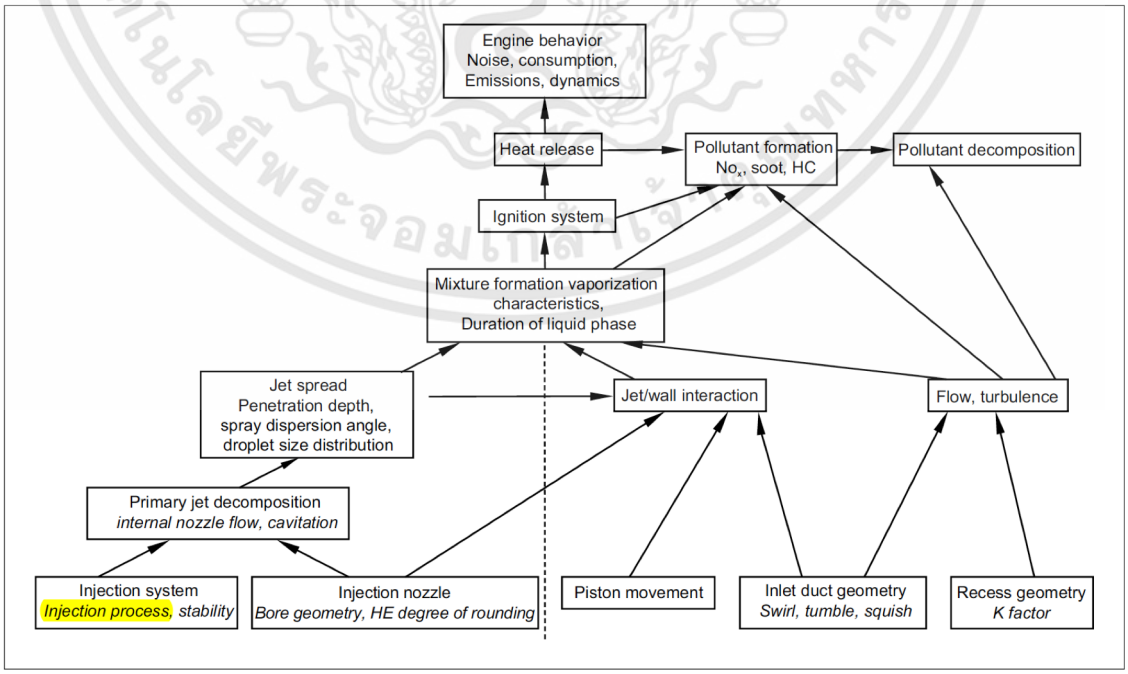

Fig. 2.1. Processes involved in mixture formation and combustion in diesel engines [40].

high peak combustion temperatures. When these two basic conditions are fulfilled, the pollution generated by diesel combustion is very low with the avoidance of extreme pressure peaks. Thereby, fuel injection process must be considered as the first important influence on the sequence of atomization, spray evolution, air-fuel mixing, and hence the engine performance along with its pollutant emissions and noise as seen in Fig. 2.1. This figure illustrates the primary factors linking to combustion efficiency and exhaust gas emissions.

The control of fuel mass flow rate is not only heat release rate in combustion to achieve the desired smooth running but also the trade-off between soot and NO_x through precisely control of injection rate shape to provide high accurate as possible fuel mass per work cycle. On this aspect, Payri *et al.* [41] built a model that can quickly simulate mass flow rate for many operation points and calculate the injected mass using few inputs such rail pressure, back pressure, energizing time, etc. Error from the model showed within 5% compared with realistic experiment. With the flexibility of the common rail system in modern diesel engine, study on the effect of the parameters of common rail system on the injection rate under Bosch long tube method was conducted by Yu *et al*. [42]. This research concluded that the primary parameters including injection pressure, electronic control signal (drive voltage, injection pulse) had significant effect on injection rate. This is consistent with other researches (Mulemane *et al*., [43]; Henein *et al.*, [44]). Except Bosch long tube's method, several studies on injection rate used Zeuch's method, for instance, Lucio's research [45] with advanced injection strategies using common-rail system, provided a proper definition of actual injection start by the first positive values of the injected volume; Ishikawa *et al.* [46] studied multiple injection in CDI (Common rail-direct injection) diesel engine. This paper pointed out the advantage of Zeuch's method which was employed on the developed injection rate meter on the aspects of high accurate detection of small injected fuel quantity and sharper detection of injection termination during injection process. This conclusion is agreed with Arcoumanis's finding [47]. In the effort in further improving particulate matter (PM) and NO_x emissions by exact controlling injection rate according to engine conditions (speed, load, swirl ratio, pulse timing and duration), Hwang *et al.* [48] investigated the effect of fuel injection rate on the pollutant emissions in DI diesel engine and concluded that there are the optimum injection rates according to engine speed and load; other research by Nishimura *et al*. [49] reported that the optimal amount of fuel injected in initial injection rate and controlling injection pressure have great reduction of NO_x emission and combustion noise. Interestingly, these findings are consistent with the experiments on the heavy/medium duty DI-diesel engine with varying the injection rate patterns to compare combustion, emissions and fuel consumption by Tanabe *et al.* [50] and

Benajes *et al*. [51]. The notable results presented a significant influence on NO_x, soot emissions concerning directly from the change in the premixed and diffusion combustion.

Besides the accurate control of the injected fuel amount to get low exhaust emissions, smooth operation, and minimum fuel consumption, other researchers have demonstrated the use of alternative fuel which promises to reduce engine emissions. Recently, a combination of use in oxygenated fuel and optimum injection rate has been well described by Tinprabath *et al.* [52]. This research examined injection flow characteristics with mixing ratios of 10%, 20%, 30%, 40%, 50% biodiesel blended with diesel, and pure biodiesel originating rapeseed. The result presented that the different fuel properties such higher in viscosity and density of biodiesel caused a decrease of discharge coefficient at low injection pressure. A further study on the effect in the wide variation range of viscosity and density to injection rate was done by Dernotte *et al*. [53] and showed that high viscosity induced a decrease up to 10% in discharge coefficient at low injection pressure difference but interestingly, at high pressure difference, fuel density remained the only fuel property driving the mass flow rate. It is noted that the larger in viscosity of biodiesel causes higher flow friction loss and greater Sauter Mean Diameter (SMD) which make mass flow rate reduction (Bang *et al*., [54]; Seykens *et al.*, [55]; Som *et al*., [56]; Desantes *et al*., [57], Dong Han *et al*., [58]). In addition, with the high in cloud point and pour point, biodiesel flow characteristics in cold condition are also described by Tinprabath *et al*. [59] and showed that the discharge coefficient for all test fuels are lower than at room temperature and only a change in viscosity or density can impact on the flow rate. It is well-known that cavitation phenomenon strongly affected on injection process, under occurrence of cavitation, discharge coefficient suddenly drops which accompanies the collapse of the mass flow rate, an increase in the spray angle and velocity outlet. These tendencies appear in all experiments and have been observed by other researchers (Desantes *et al.*, [60]; Payri *et al*, [61]; Benajes *et al*., [62]; Payri *et al*., [63]; Badock *et al*., [64]).

From above point of views, it is necessary to know the physical properties of injection characteristics of biofuels base diesel fuel inside the injector in order to improve the characteristics of biofuel, injector geometry, injection strategy, engine chamber and thus achieve higher engine efficiency. However, under literature review of HVO researches as shown in the previous part (1.2) and author's knowledge, studies on injection dynamics flow for HVO is very limited. This study was carried out to reach a new understanding of injection rate behaviors of HVO, the relationship between discharge coefficient and the percentage of HVO in the blends, and the relationship between discharge coefficient and injection pressure, back pressure, injection length command.

2.2. Research Methodology-Injection rate Zeuch Method

In this study mainly focused on the injection characteristics which consists of injection rate, injection delay, discharge coefficient, injection quantity, and others relevant parameters. By Zuech's method which has high accurate detection of small injected fuel quantity and sharper detection of injection termination during injection process (Arcoumanis *et al*., [47]), the HVO's injection characteristics were performed. The tested fuel was injected into constant volume chamber filled full with the same tested fuel at a certain pressure (back pressure). At the time of injection occurred, the pressure in chamber increased in proportion corresponding with the injected fuel quantity. By using the fuel bulk modulus of compressibility (K) derived from pressure rise (ΔP) according to Eq. (1), the equation of injection rate (dm/dt) is formed based on the conservation of mass as shown in Eq. (2).

$$K = V\frac{\Delta P}{\Delta V} \quad (1)$$

$$\dot{m}_{measured} = \frac{dm}{dt} = \rho_f \frac{V}{K}\frac{dP}{dt} \quad (2)$$

Injection rate profile obtained by Eq. (2) is displayed in Fig. 2.2. From this figure, it can be divided into 3 phases: injection delay, transitional zones (needle opening and

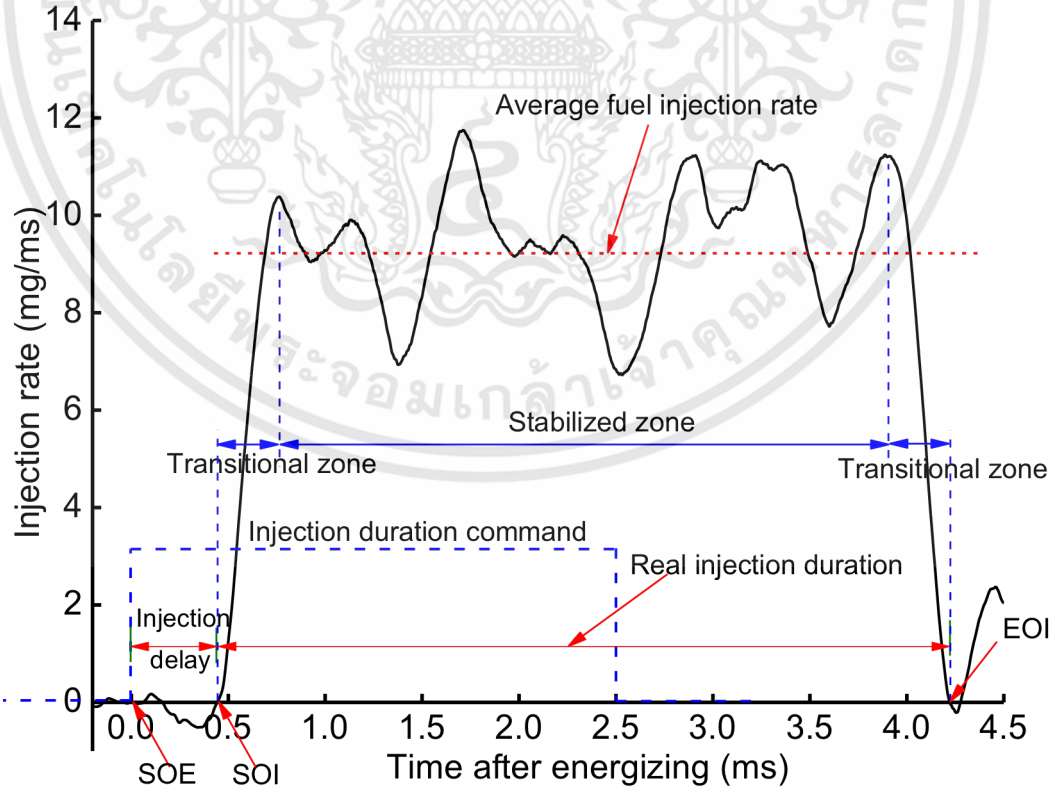

Fig. 2.2. Definition of typical fuel injection rate (diesel fuel, Pi = 100MPa, P_b = 4MPa, 2.5ms energizing time).

needle closing), and stabilized zone (fully opening needle). The injection delay refers to the period of time from starting point of energizing (SOE) to starting point of injection (SOI) in which the curve initially changes from negative value to zero and positive value (Lucio *et al*., [45]; Dong Han *et al.,* [58]; Munsin *et al.,* [65]). The effective injection duration was counted from SOI until end of injection (EOI). The quasi-steady state period of 1.5ms to 3.5ms after starting of energizing was applied for the averaged value of mass flow rate and discharge coefficient.

Based on Dernotte's work [53], discharge coefficient is defined as a ratio between the measured mass flow rate ($\dot{m}_{measured}$) and theoretical mass flow rate ($\dot{m}_{theoretical}$) derived from the combination of the continuity equation and Bernoulli equation as shown in Eq. (3) and Eq. (4):

$$C_d = \frac{\dot{m}_{measured}}{\dot{m}_{theory}} \quad (3)$$

$$\dot{m}_{theory} = n_{orifice} . A . \sqrt{2\Delta P . \rho_f} \quad (4)$$

The average velocity ($V_{average}$) was used to calculate Reynolds number (Re) as shown in Eq. (5) and Eq. (6) (Tinprabath *et al*., [52]):

$$V_{average} = \frac{\dot{m}_{measured}}{n_{Orifice} . A . \rho_f} \quad (5)$$

$$Re = \frac{V_{average} . D_{inj}}{\nu} \quad (6)$$

2.3. Injection rate set-up and test procedure

2.3.1. The analysis of experimental fuels

Seven types of fuel chosen in this research are commercial diesel fuel at Thailand (B7-blended 7% Palm Methyl-ester) as a reference fuel, neat Hydrotreated Vegetable Oil (HVO) and blends of HVO in ratios of 10%, 20%, 30%, 50%, and 80% by mass with

Table 2.1. Fuel properties

Fuel analysis	Standard	Diesel fuel (B7)	H10	H20	H30	H50	H80	Neat HVO
Viscosity @40^{0}C (cSt)	ASTM D445	3.235	3.126	3.088	2.960	2.901	2.740	2.637
Density (Kg/m^3)	ASTM D4052	823.5	818.8	814	807.5	799.9	786.5	778
Surface tension (mN/m)	ASTM D1590	26.38	26.09	25.89	25.76	25.56	24.91	24.84
Formula	Master 3625	$C_{14.28}H_{26.43}$		$C_{14.23}H_{27.17}$		$C_{14.09}H_{29.36}$	$C_{14.09}H_{29.36}$	$C_{14.03}H_{30.1}$

diesel fuel. Fuel properties are listed in Table 2.1. Because the fluid characteristics involved during the injection process are somewhat different than the parameters which affect the combustion. Therefore, some of the fuel properties which will be used for analyzing in this part are presented.

The lower viscosity of HVO than B7 of about 18.48% is caused by shorter chain length and paraffinic fuel. In addition, commercial diesel fuel with 7% palm methyl-ester contributes higher viscosity due to the presence of unsaturated compounds (Soo-Young No, [11]; Borhanipour *et al.,* [66]). The lower viscosity results in less friction flow, thus less deposit formation and more accurate operation in injector. It also results in better atomization, smaller droplet size and wider angle of fuel spray in engine combustion (Borhanipour *et al.,* [66]; Pandey *et al*., [67]). Similarly, density of HVO is 5.52% less than B7 due to the fact that it is basically a mixture of n-paraffinic and iso-paraffinic, with lower chain length and smaller molecular weight (Soo-Young No, [11]; Lapuerta *et al*., [16]). This causes, not only the influence in delivery of fuel mass to the combustion chamber due to looser particles in the packs of substance, but also retarded injection timing which contributes to lower temperature combustion (Pandey *et al*., [67]). In regard to surface tension, HVO has 5.84% less than diesel. To anticipate the evolution of the fuel properties, it is necessary to characterize their impact and their potential on every phase affecting the combustion process.

2.3.2. Experimental set-up and test conditions

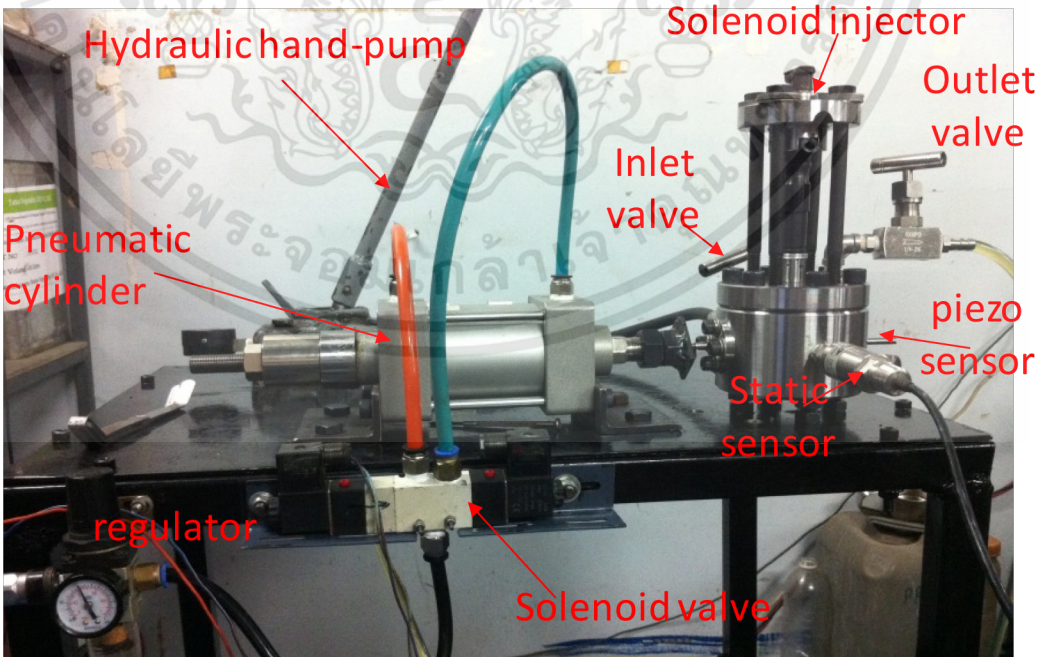

Fig. 2.3. Assembly of injection measurement system

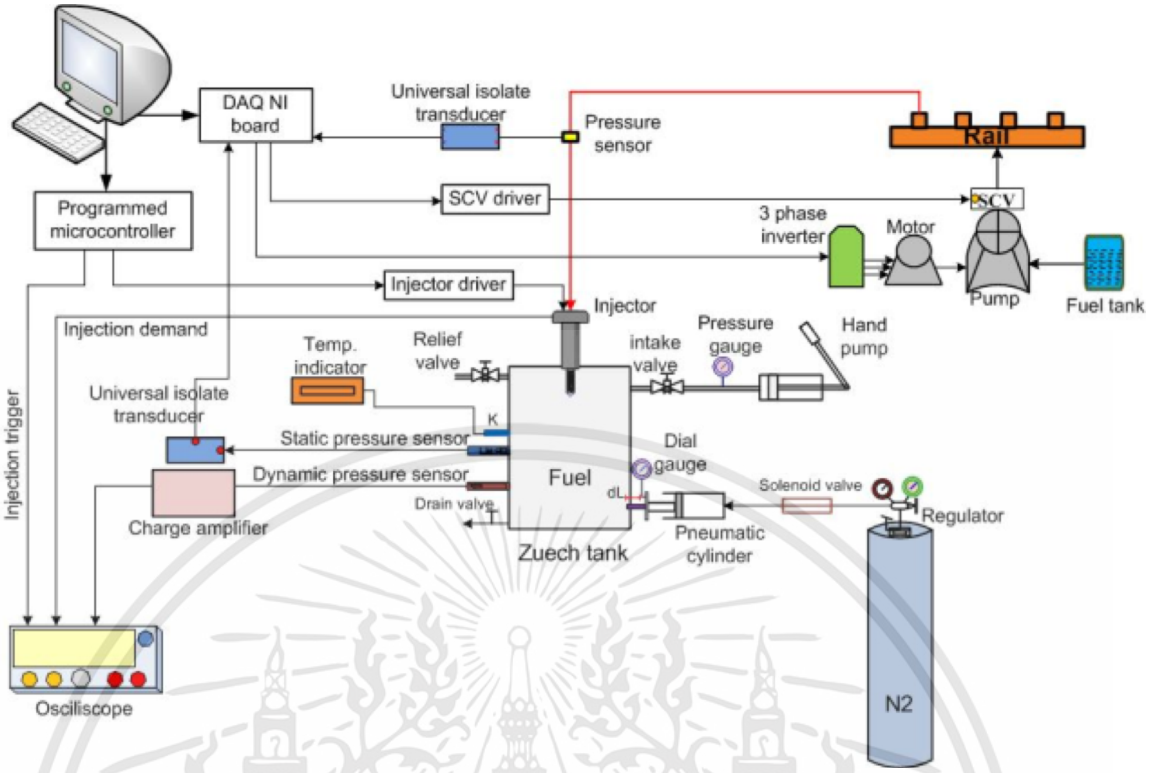

Fig. 2.4. Overall schematic arrangement of experimental apparatus

Fig. 2.3 shows the practical setup for measuring injection characteristics and Fig. 2.4 illustrates the overall schematic of experimental apparatus. A single-hole solenoid diesel injector with diameter of 0.2mm was installed on the top of the Zeuch chamber which has 40cm^3 in capacity. To determine injection rate, the tested fuel was fully filled into the chamber by hydraulic hand pump until it reached the desired back pressure, i.e. 4MPa, measured by a static pressure sensor. Then, the tested fuel was injected by the common rail injection system (the 2nd generation) which driven by a three phases electric motor through an inverter, resulting in a steep pressure rise in chamber measured by a piezo-electric pressure transducer sensor. Then, this pressure signal was transmitted to charge amplifier and recorded by oscilloscope with real time synchronously. The injection demand and trigger time were controlled by a programmable microcontroller that is actuated by the Electric Drive Unit (EDU) to inject fuel into the Zeuch chamber.

To measure fuel bulk modulus, high pressure of nitrogen (N_2) gas was connected with pneumatic cylinder. Then, it was used to push plunger located with a dial gauge to measure the displacement of plunger. The movement of the plunger into the chamber caused the reduction of volume chamber lead to increase pressure. By using Eq. (1), the bulk modulus of fuel was determined and used as a calibrating factor for injection rate calculation. It was noted that the same back pressure in injection rate measurement was employed in determining bulk modulus.

Experiments were carried out at constant temperature 301K ± 2K. Table 2.2 shows the experimental test conditions. The result of 15 injection times continuously at each test condition was recorded and averaged following the aforementioned injection rate analysis method. Fuel blends were carried out only at 4MPa of back pressure, 2.5ms of energizing time and various injection pressures. The comparison between HVO and diesel was conducted at various energizing times, injection pressures, and back pressures.

Table 2.2. Experimental conditions

Fuels	B7, H10, H20, H30, H50, H80, HVO
Back pressure P_b (MPa)	2, 4, 6
Rail pressure P_{inj} (MPa)	40, 60, 80, 100, 120
Energizing time (ms)	0.5, 1.0, 1.5, 2.0, 2.5
Orifice diameter (mm)	0.2

2.4. Results and discussion

2.4.1. Fuel bulk modulus of compressibility

Bulk modulus of compressibility implies the resistance of liquid to uniform compressibility. Fig. 2.5 shows the relationship between bulk modulus of HVO fraction in blend and various back pressures. From this figure, the bulk modulus proportionally

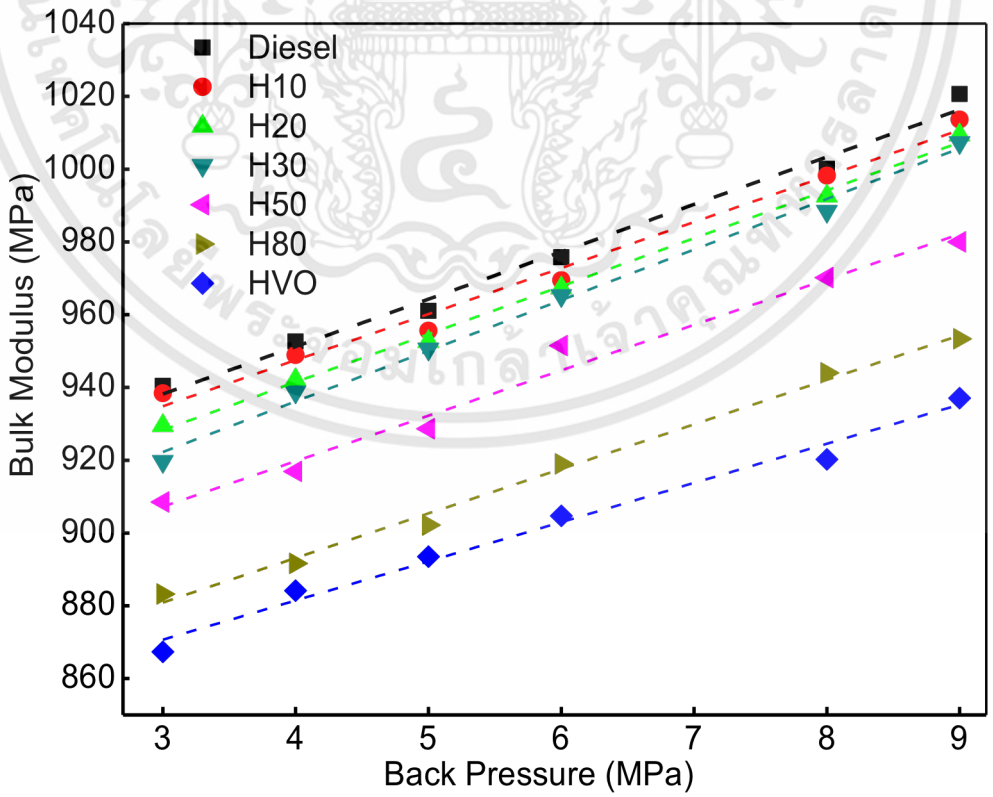

Fig. 2.5. Effect of HVO fraction (by mass) on fuel bulk modulus of compressibility.

increases with the decrease of HVO fraction in blend. This is due to the impact of molecular structure of diesel fuel such as unsaturated component (mixed with 7% FAME), aromatic composition, cycloalkane, branched alkane, etc. caused more difficulty in compressing fuel in the same volume chamber than straight chain length structure as explained by Lapuerta *et al*. [16], André *et al*. [68].

In addition, at applied higher back pressure, the compressibility of liquid is lower owing to the tightly packed molecules as well as the compression of the molecules themselves causes opposite among intermolecular repulsion. This leads to the linear increase of bulk modulus as increasing back pressure. HVO has smaller bulk modulus than diesel fuel around 7.57% for all back pressures. The smaller in fuel bulk modulus will retard to engine injection timing that thus to shift in the combustion timing and NO_x emission formation (André *et al*., [68]; Heywood, [7]).

2.4.2. Hydraulic injection delay

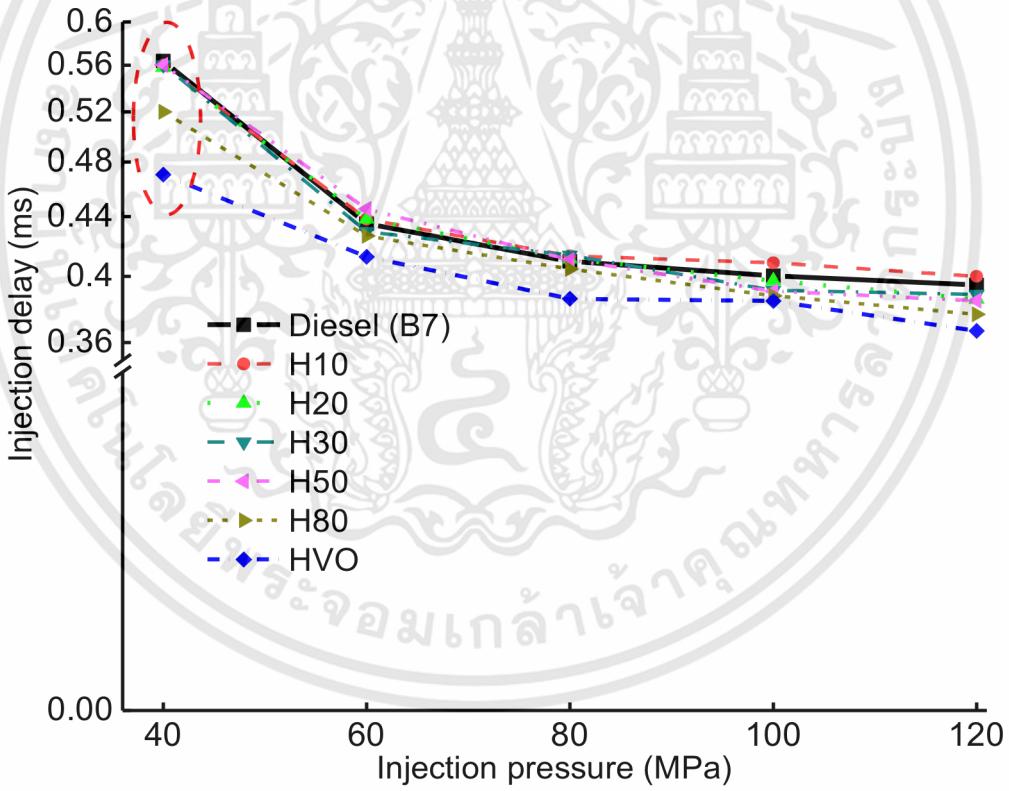

Fig. 2.6. Hydraulic injection delay of all test fuels under t=2.5ms and P_b=4.0MPa.

Fig. 2.6 shows the hydraulic injection delay of all tested fuels at 4.0MPa of back pressure, 2.5ms of energizing time with injection pressures in range of 40MPa to 120MPa. All the injection delay data lie in range of 0.36ms to 0.56ms. It is clearly observed that HVO and blends have earlier injection timing than B7 under same start

of energizing time and injection pressure due to smaller viscosity results in lower resistance force for needle lift and faster fuel flow out of control chamber immediately after solenoid valve opening. From this figure, diesel and blends of HVO with the mixed ratio up to 50% display the insignificant difference of the hydraulic injection delay. As reported, higher bulk modulus leads to earlier injection timing with in-line pump-line nozzle fuel injection system but in the common rail system, the injection pressure is constantly maintained at the desired injection pressure, the fuel flows through the orifice at a timing controlled electro-mechanically. Therefore, the influence of the bulk modulus is expected negligibility in the opening needle timing. Hence, viscosity mainly controls the start of injection timing. These observations are consistent with other findings (Dong Han *et al*., [58]; Andre *et al*., [68]). Furthermore, the hydraulic injection delay shows a downward trend as increasing of injection pressure. This can be explained by pressure differential between the controlled volume of injector and at exit orifice which leads to faster needle lift (Dong Han *et al*., [58]; Henein *et al.,* [44]).

2.4.3. The effective injection duration

Effective injection duration counted from SOI until EOI is displayed in Fig. 2.7. According to this figure, effective injection duration is prolonged as compared to the current command duration of 2.5ms. This depends on the rate of opening and closing

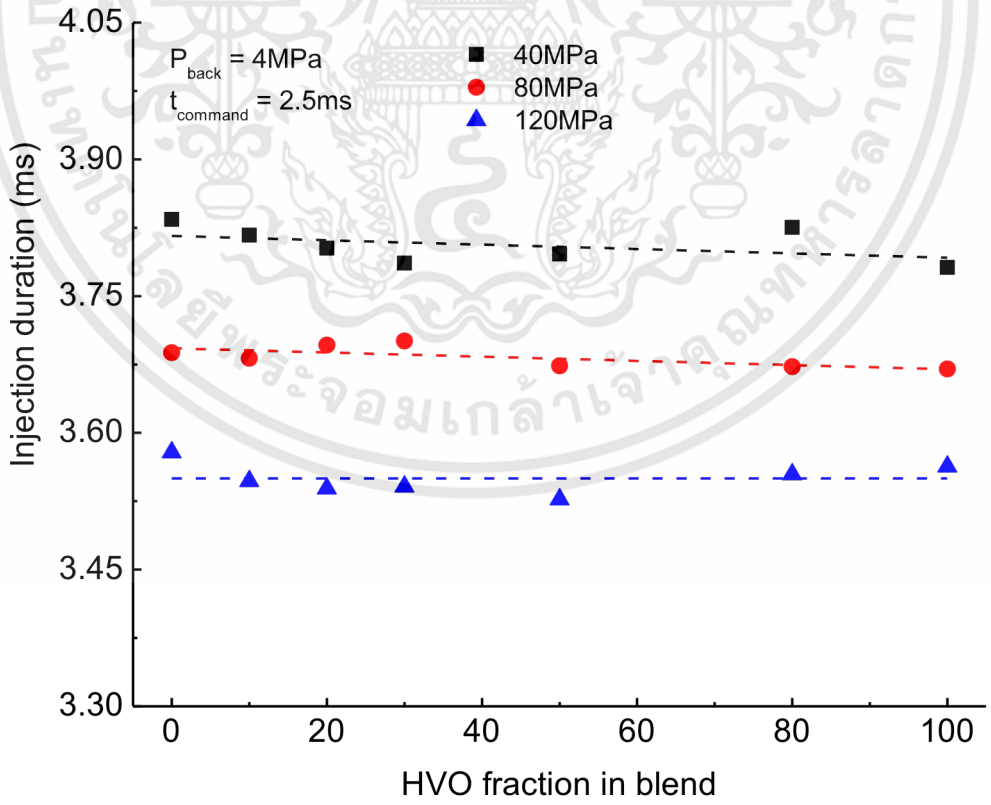

Fig. 2.7. Effective injection duration of all test fuels at 2.5ms of energizing time, P_b = 4.0MPa.

needle, needle lift during fuel delivery, nozzle type and fuel properties (Henein *et al.,* [44]). This figure also shows a reducing trend of the effective injection duration (earlier closing) as increasing injection pressure due to reducing the effect of viscosity so as to descend the resistance of needle closure process. Therefore, increased fuel injection pressure difference enhances to lift and close needle more rapidly. Also, the effective injection duration is hardly affected by HVO fraction in blends. This may be caused by the compensative effect of the low bulk modulus of HVO fraction which tends to prolong injection while it's small viscosity causes less friction.

2.4.4. The mass flow rate

Mean mass flow rate during quasi-steady state period calculated from 1.5ms to 3.5ms with various injection pressures was displayed in Fig. 2.8. Slightly higher mean injection rate of diesel is attributed by larger inertial fore from higher density (Dernotte *et al.,* [53]; Desantes *et al.,* [57]). HVO with lower injection rate may cause the shorter in spray penetration and air-fuel interaction in surrounding environment of chamber. It is also seen that HVO and blends had insignificantly difference in mean mass flow rate. In addition, injection rate increases when increasing injection pressure owing to higher flow capacity (Henein *et al.,* [44]; Dong Han *et al*., [58]).

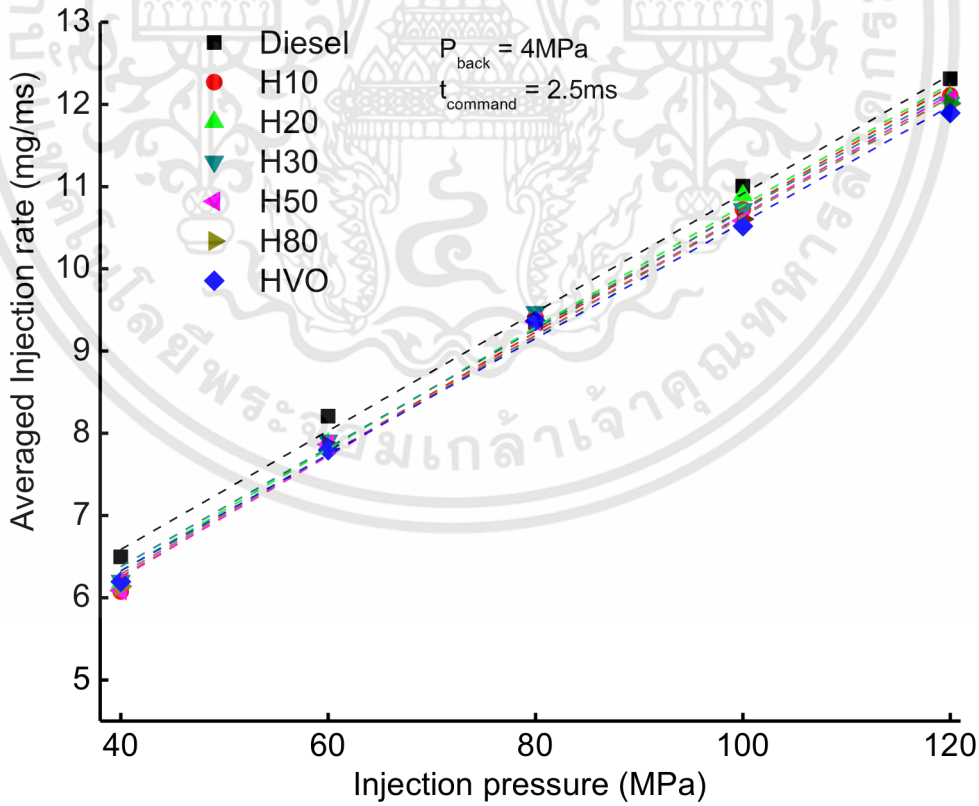

Fig. 2.8. Mean injection rate of all fuels at stable injection period of 1.5ms-3.5ms.

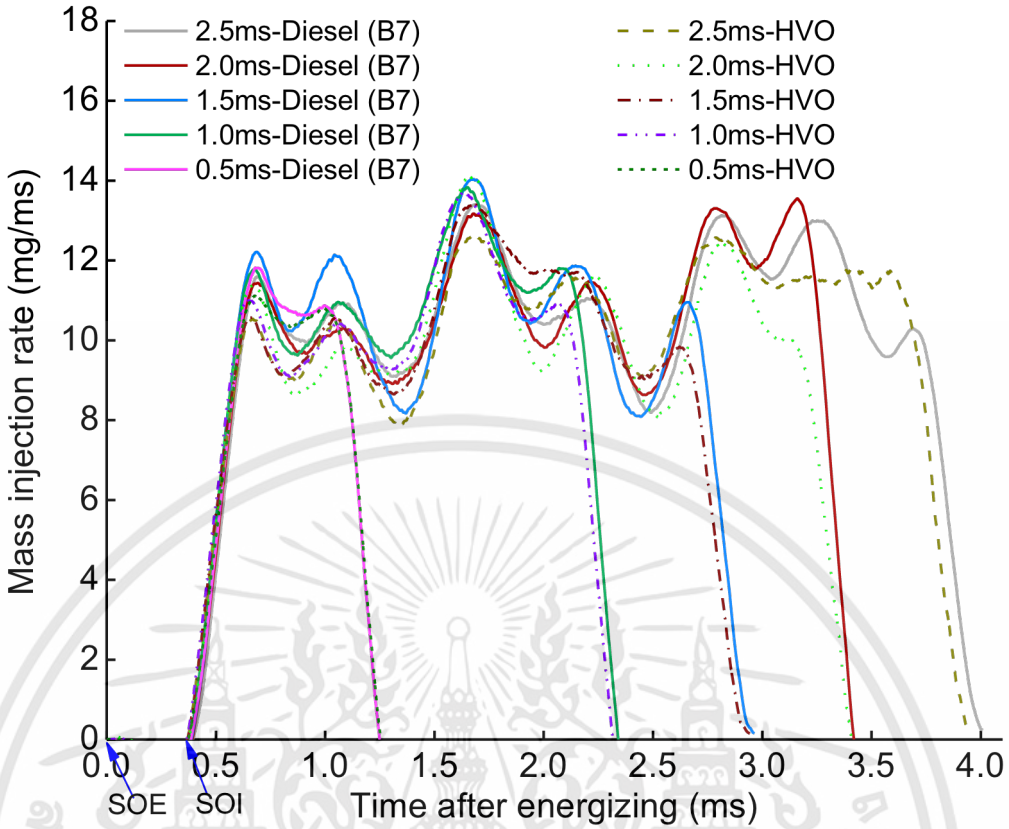

Fig. 2.9. Mass injection rates of diesel and HVO at Pinj=120MPa, Pb=4MPa and various injection durations (0.5ms, 1.0ms, 1.5ms, 2.0ms, 2.5ms).

The mass flow rate for various energizing times of diesel and HVO under 120MPa of injection pressure can be seen in Fig. 2.9 as representative. The results of mass injection rate under 0.5ms of energizing time for both fuels show the extreme short in steady phase of injection process due to incompletely needle opening. For each fuel, the change in energizing time from 0.5ms to 2.5ms produces the insignificant difference in the hydraulic injection delay as well as the averaged value of mass flow rate after fully opening needle. Besides, longer energizing time of 0.5ms, 1.0ms, 1.5ms, 2.0ms, and 2.5ms produces longer effective injection duration corresponding 0.864ms, 1.959ms, 2.574ms, 3.027ms, 3.612ms for diesel and 0.880ms, 1.949ms, 2.574ms, 3.031ms, 3.571ms for HVO. Furthermore, HVO's falling slopes show slight earlier closure than B7 at each condition. It is possibly due to its lower viscosity which causes fast-down the needle process. This finding confirm the primary influence of viscosity on two period of needle opening and needle closing. Fig. 2.10 presents the impact of back pressure on the averaged injection rate between HVO and diesel. According to this figure, there is no significantly difference in injection rate when varying back pressures in range from 2MPa to 6MPa.

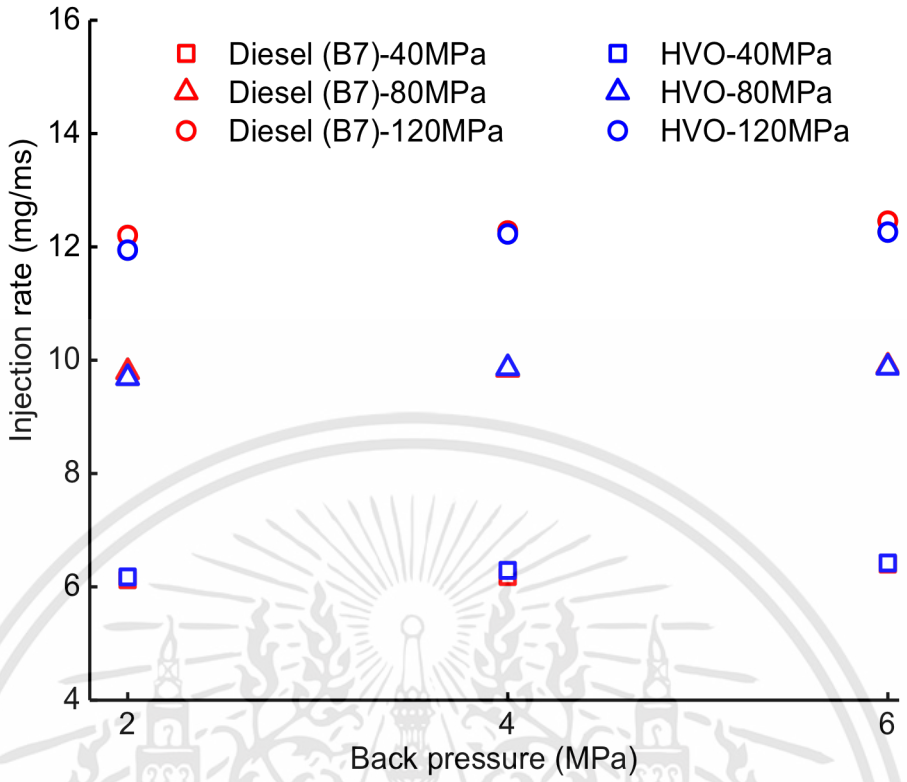

Fig. 2.10. Mean injection rate of diesel and HVO at 2.5ms, different P_{inj}, and P_b.

2.4.5. The fuel injection quantity

Fuel injection quantity at different injection pressures for all fuels under 4.0MPa of back pressure, 2.5ms of energizing time is calculated from integration of injection rate curves by Simpson's rule and depicted in Fig. 2.11. Diesel has higher injection quantity than HVO and blends due to higher density (Dernotte *et al.*, [53]; Desantes *et al.,* [57]). More specifically, diesel fuel approximately increases 5.85% the injected fuel amount at all injection pressures compared to neat HVO, averagely.

Fig. 2.12 shows the injection quantity of all injection pressures from 40MPa to 120MPa with various energizing times between HVO and diesel as representative. Generally, diesel has higher the injection quantity than HVO for all energizing times and injection pressure as same propensity with Fig. 2.11. Also, from this graph, with increased injection pressure, injection quantity increases due to enhancing the flow capacity. It is noted that the distance of injection quantity line between 0.5ms and 1.0ms energizing time is larger than the others. It can be explained by partial opening needle at 0.5ms. On this viewpoint, the needle lift in multiple injection strategy of HVO will be affected by dwell-time and then injection timing, injection quantity.

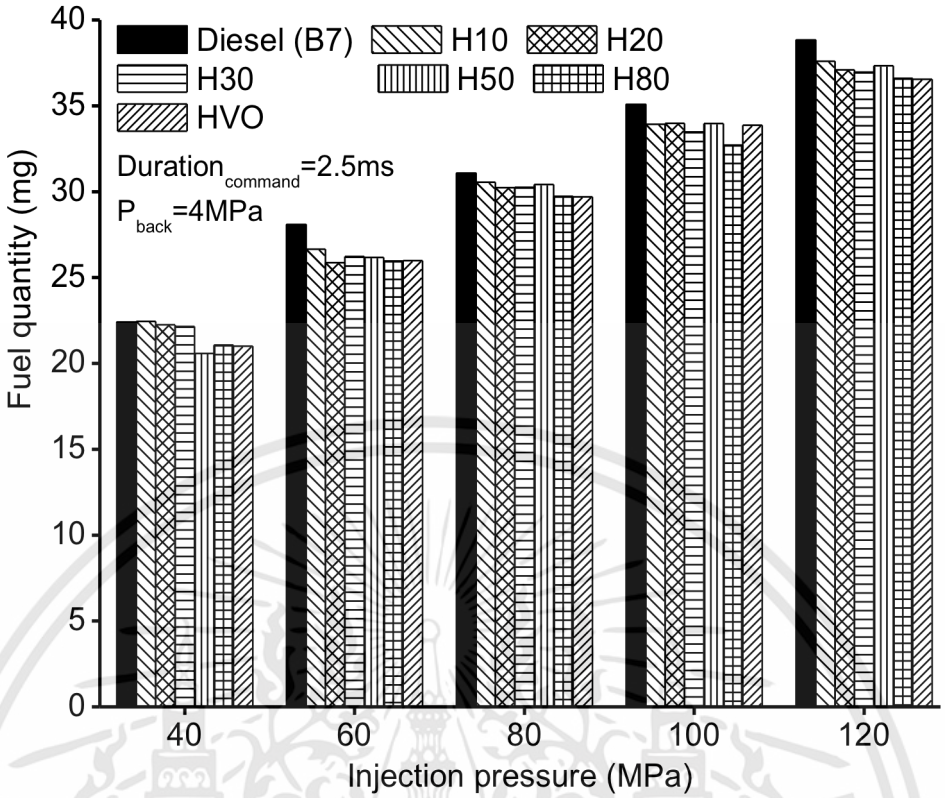

Fig. 2.11. Fuel injection quantity of all fuels at stable injection period of 1.5ms-3.5ms.

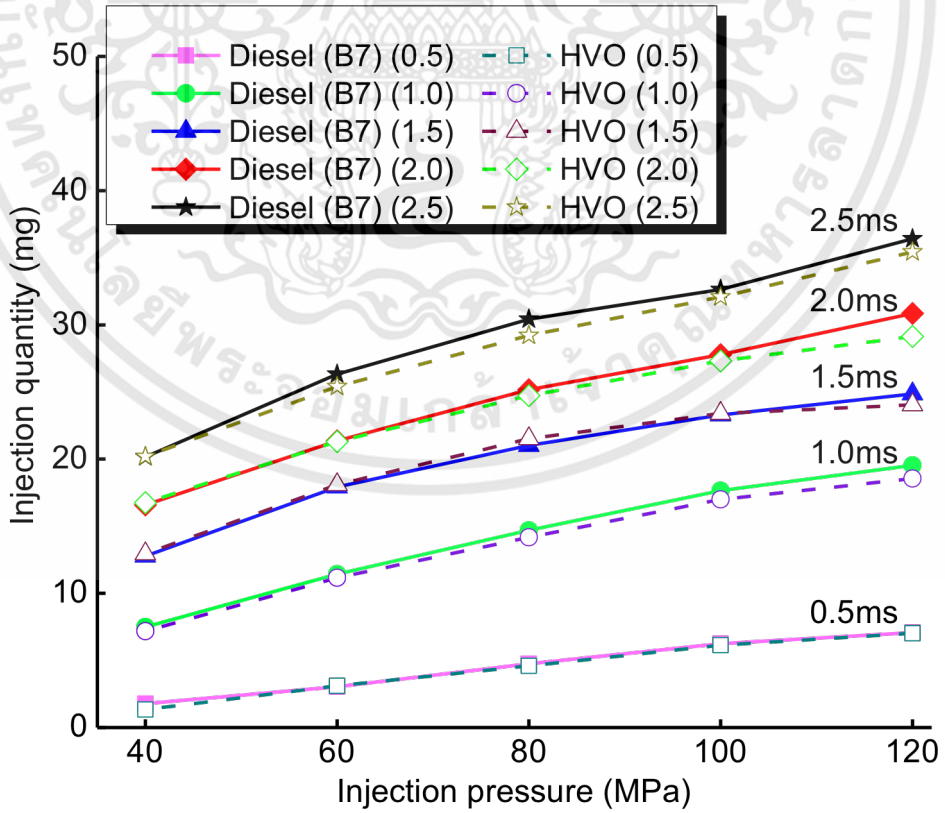

Fig. 2.12. Injection quantity of HVO and diesel at P_b=4MPa, various injection durations and injection pressures.

2.4.6. The discharge coefficient

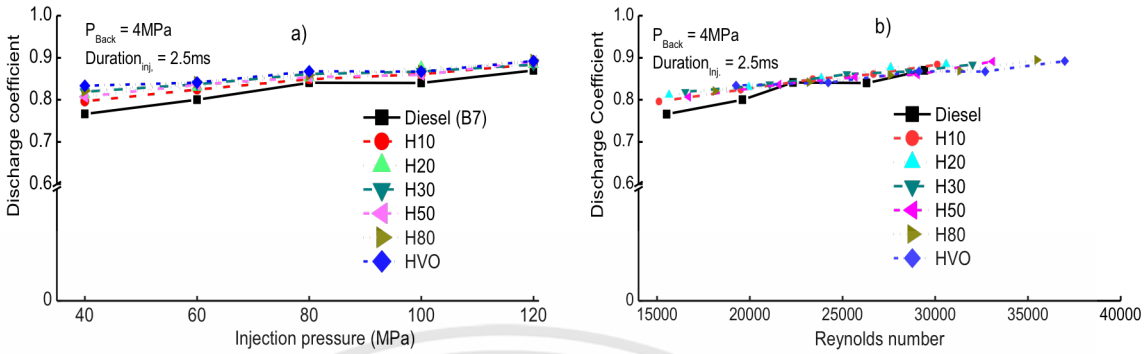

Fig. 2.13. Discharge coefficient versus injection pressure (a) and discharge coefficient versus Re for all test fuels at 4MPa back pressure and 2.5ms energizing time.

Discharge coefficient analyzed according to Eq. (3) is plotted versus with different injection pressures in Fig. 2.13(a). From this figure, HVO and its blends have higher discharge coefficient than diesel as the effect of smaller viscosity and density makes lower friction loss. An approximate higher about 8.7%, 5.1%, 3.2%, 3.2%, 2.5% of discharge coefficient corresponding with 40MPa, 60 MPa, 80 MPa, 100 MPa, 120 MPa of injection pressure is recognized with HVO, compared to diesel fuel. In addition, an increasing trend of discharge coefficient is observed with higher injection pressure in the studied injection pressure range. This is because the higher injection pressure reduces the influence of viscosity which leads to lower pressure loss. This result has similar propensity with other researches (Tinprabath *et al.,* [52]; Dernotte *et al.,* [53]; Benajes *et al.,* [62]; and Boudy *et al.,* [69]).

Cavitation phenomenon in injector represented by Reynolds number (Re) and cavitation number strongly impacts to discharge coefficient. According to Desantes's work [60], critical cavitation appearing in orifice injector will result in the decrease of discharge coefficient due to vapor formation in the outlet section of nozzle hole. From Fig. 2.13(b), it is observed that there is no critical cavitation in the studied range of injection pressure. In this condition, discharge coefficient only depends on Re. From left side to right side of Re number axis in Fig. 2.13(b), the increase of Re causes the increase of flow out effective velocity, higher turbulent level results in higher discharge coefficient. Furthermore, the increase of HVO fraction in blends produces higher Re number due to smaller viscosity. This will be attributed that HVO and its blends will be better in mixture formation.

Fig. 2.14(a) shows the discharge coefficient for various energizing times at different injection pressures. Under low injection pressure and energizing time from 0.5ms to 1.0ms, it is clearly seen the incompletely needle opening causes low discharge coefficient and after that as increased energizing time causes slightly higher discharge

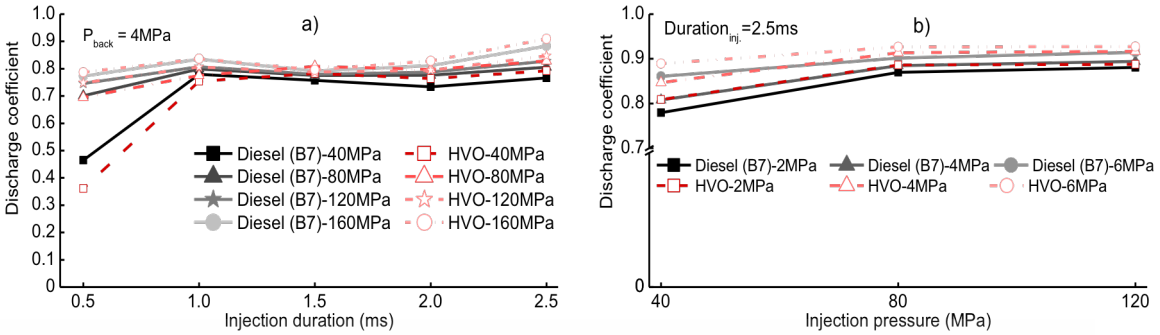

Fig. 2.14. The impact of different injection durations to discharge coefficient at 4MPa back pressure (a) and the impact of various back pressures to discharge coefficient at 2.5ms

coefficient due to less pressure loss and fully needle opening. Fig. 2.14(b) displays the impact of back pressure to discharge coefficient. Increasing trend of discharge coefficient is observed with higher back pressure at a constant injection pressure. It is attributed by the smaller pressure differential which causes smaller pressure loss.

2.5. Conclusion

This study was carried out to reach a new understanding of injection rate behaviors of HVO, the relationship between discharge coefficient and the percentage of HVO in the blends, the relationship between discharge coefficient and injection pressure, back pressure, energizing time. Some conclusions are summarized as follows:

(1) HVO, its blends and B7 have similar to injection characteristics. Because molecular structure of B7 contains such unsaturated component, aromatic composition, cycloalkane, branched alkane which causes larger bulk modulus than HVO and blends. The bulk modulus proportionally increases with the decrease of HVO fraction in the mixture as well as linearly increases with higher back pressure. Neat HVO has smaller bulk modulus than B7 around 7.57% for all back pressures.

(2) Earlier injection timing is observed with HVO and its blends due to mainly smaller viscosity. Mixing ratio of HVO over 80% in blend shows clear difference of hydraulic injection delay as compared to B7. Also, higher pressure differential reduces hydraulic injection delay. Moreover, the direct effect of various energizing times on NOx emission is predicted insignificantly due to seemly unchanged hydraulic injection delay.

(3) Longer effective injection duration compared to energizing times is obtained with all fuels. A reducing trend of the effective injection duration (earlier closing) is found as increasing injection pressure. The effective injection duration is hardly affected by HVO fraction in blends.

(4) Slightly higher mean mass flow rate was observed with diesel. This difference is mainly due to higher density of diesel. Higher mass flow rate is also recorded as

increasing injection pressure for all fuels. This is caused by the increase of flow capacity. In addition, there is negligible change for both fuels in the averaged value of injection rate under same injection pressure with various back pressures and energizing times.

(5) Viscosity is primary influential parameter on two period of needle opening and needle closing while density mainly impacts to mass flow rate in period of fully development.

(6) Diesel has higher injection quantity around 5.85% than HVO and blends owing to larger density. The difference in injection fuel quantity under same injection pressure for both fuels will cause the different energy input that influences to engine performance. However, higher in heating value of HVO may improve this drawback. Besides, the use of too short energizing time in multiple injection strategy should be considered on side of dwell-time to obtain the expected injection quantity.

(7) HVO and blends have higher discharge coefficient because of lower friction loss from smaller viscosity. An increasing trend of discharge coefficient is exhibited as increasing injection pressure. Higher pressure differential produces smaller difference in discharge coefficient between HVO and B7.

(8) Critical cavitation condition is not found in the studied range of injection pressure, and discharge coefficient of nozzle increases linearly with Re. Under low injection pressure and short energizing time contributes to low discharge coefficient.

CHAPTER 3
SPRAY VISUALIZATION OF HYDROTREATED VEGETABLE OIL IN CVCC UNDER NON-VAPORIZING CONDITION

3.1. Introduction

The diversity of alternative fuels and the corresponding variation in their physical and chemical properties, coupled with simultaneous changes in advanced techniques for CI engine (high injection pressure, exhaust gas recirculation, etc.), needed to improve efficiency and reduce emissions. Therefore, the influences of physical/chemical properties of new bio-based diesel fuel are investigated its feasibility through a sequence of experiments before applying popularity on the market.

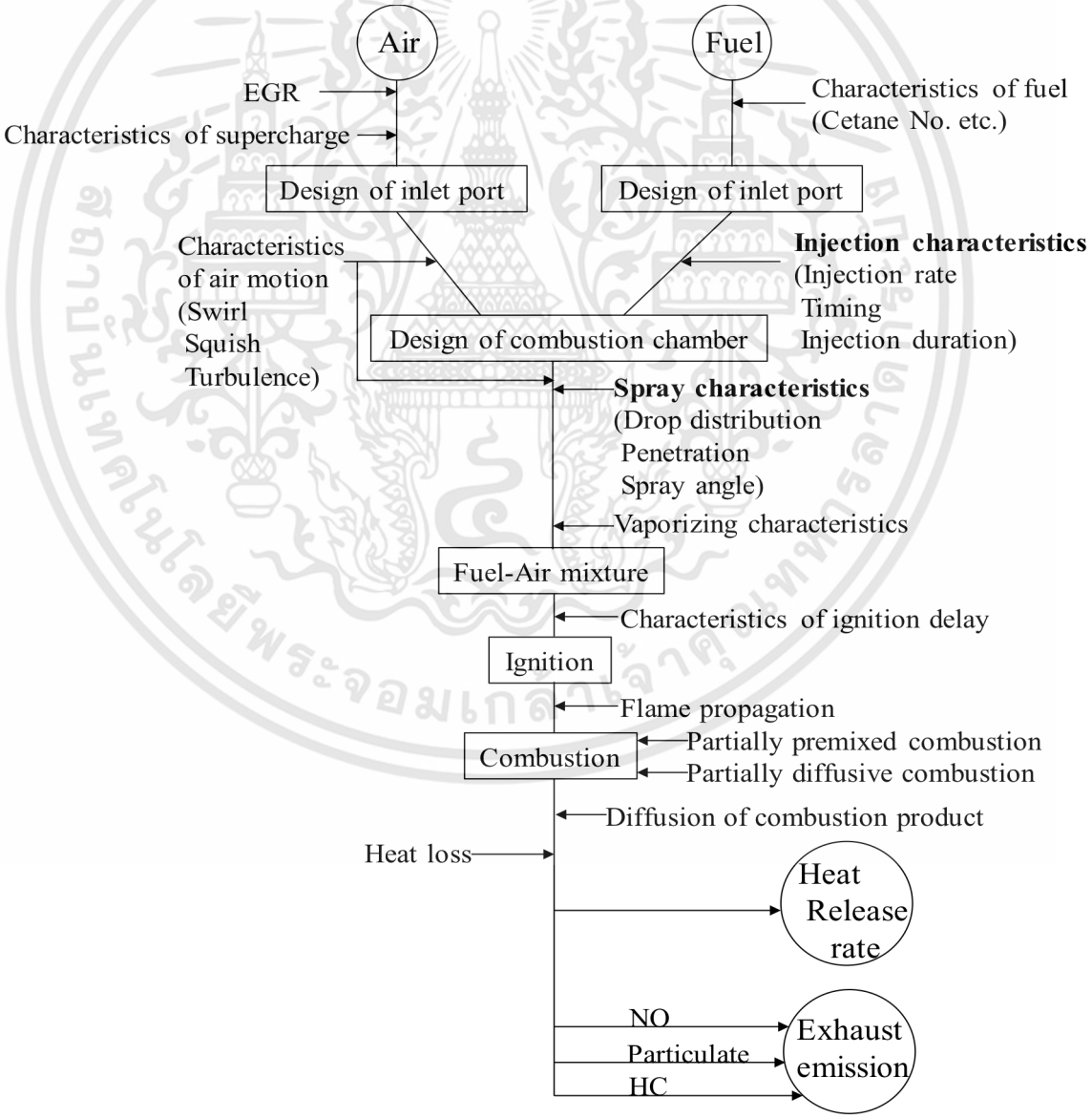

Fig. 3.1. Block diagram of diesel combustion [70].

Researches relating injection mas flow rate have firstly provided further understanding the impact of fuel properties (viscosity, density, bulk modulus), injector geometry, injection system on the flow characteristics inside nozzle, then contributes to air-fuel mixing process in combustion chamber. Besides, the spray structure in engine chamber also have strong effect on combustion characteristics as seen in logical diagram in Fig. 3.1 (Hiroyasu *et al*., [70]). Accordingly, the effect of injection pressure, ambient pressure, fuel properties, etc. on the spray penetration, spray cone angle, spray velocity, spray volume known as macroscopic fuel spray characteristics in the combustion chamber are influential keys on mixture formation (air entrainment, air-fuel mixing, temporal evolution of the mixture). Basically, the diesel combustion is strongly controlled by a fuel spray injected into air at high pressure and temperature. However, the occurrence of this process is extremely transience in engine chamber. Hence, accurate description of the behavior of atomizing and vaporizing fuel spray are important for any types of bio-based diesel fuel to comprehend and describe the processes of air-fuel mixing and subsequent combustion.

Nowadays, the constant volume combustion chamber has truly become effective instrument for optical access relating diesel engine research because experiments can be conducted at controlled environmental engine conditions with small amounts of test fuels. The data obtained in this facility is useful for numerical model of heterogeneous combustion to predict the spray behavior, combustion phenomenon and combustion efficiency due to the well-defined boundary conditions and the wide range of employed conditions. Dernote *et al.* [71] examined the influence of fuel density, viscosity, and surface tension on spray development and droplet size distribution in non-vaporizing conditions. The results revealed that the increase of fuel density and viscosity by 100kg/m^3 and 6.5mm^2/s, respectively, induced longer spray tip penetration (up to 7%) with a narrower spray angle (drop of up to 3deg) in quasi-stationary conditions, and larger sauter mean diameter–SMD (up to 23% or 3um). Furthermore, an increase in surface tension from 18 to 30nM/m did not cause any significant changes in droplet size or spray development. Hillamo *et al.* [72] investigated the diesel spray penetration and velocity with different nozzle tips, various gas densities and injection pressures under non-evaporative condition and reported that the smaller size of nozzle hole, higher gas density generated slower penetration. Shorter injection delay, longer tip penetration corresponded with higher injection pressure. Wang *et al*. [73] concluded that a hollow cone with wide spray angle, initial spray plug at the tip and vortexes in the opposite direction at the rear part of spray featured for spray behavior under low-back pressure ambient condition while a solid cone and the formed vortexes in middle part of the spray corresponded with high back pressure ambient condition. Furthermore, spray tip penetration, cone angle, gas

velocity, area of air entrainment and SMD of alcohol fuels decreased as increasing ambient back pressure in this study. The effect of very high injection pressure (up to 250MPa) on the macroscopic spray characteristics was clarified by Delacourt *et al*. [74] and reported that spray velocity decreased very quickly over time regardless of injection pressure as well as injection pressure had little influence on the diesel spray cone angle. However, it is noted that higher injection pressure caused larger spray volume. In addition, with high gas density in ambient condition, spray cone angle tended to be wider and less penetration. These indicated an increase in spray atomization quality. The result of spray angle conflicts with Wang's finding [73] but most of these obtained results consist with other researches Tinprabath *et al.* [52], Hillamo *et al*. [72], Suh et al. [75], Payri *et al.* [76]. Chen *et al*. [77] had same conclusion with Dernote [71] about the relatively lower viscosity and surface tension to smaller droplet size. Moreover, it was observed that the smallest droplet size distributed within a region near the injector nozzle tip and grew larger along the axial and radial direction. Regarding to the factors impacting on SMD, a larger of SMD was caused by increasing ambient pressure or decreasing injection pressure (Kihm *et al*., [78]); using solenoid driven injection system instead of using piezo-driven injection system (Suh *et al*., [79]); rising radial distance and axial distance from nozzle tip (Labs *et al*., [80]); high viscosity and surface tension (Gao *et al*., [81]). Recently, some typical bio-base fuels developed were investigated the global spray characteristics for instance, HVO fuel by Hulkkonent *et al*. [33], biodiesel by Ghurri *et al.* [82], DME by Lee *et al*. [83] and generally revealed that the different fuel properties from alternative fuels, especially for viscosity and density, strongly impacted on spray evolution and air-fuel interaction, and subsequently affected on engine combustion and emission formation.

Although numerous approaches have been taken to predict and understand environmental diesel combustion, diesel combustion processes are very complex and detailed mechanisms are not well understood. Especially, under literature review of HVO researches as shown in the previous part (1.2) and author's knowledge, existing researches on the spray behavior for hydrotreated vegetable oil (HVO), given the variable injection pressures and ambient pressures, which subsequently affected on combustion and its associated pollutant emissions, are very limited. Therefore, this research part primarily focused on the effects of various injection pressures and ambient pressures (gas densities) on the spray characteristics of five HVO-diesel blends under the simulated diesel engine condition-nonvaporizing condition in a constant volume combustion chamber (CVCC).

3.2. Research methodology and analysis of the spray images

Based on the change of gas density in constant volume combustion chamber (CVCC), shadowgraph technique is used to visualize liquid spray penetration and flame development through the light of fuel spray which is reflected on two concave mirrors and recorded by high-speed video camera (Settles, [84]). Fig. 3.2 shows the schematic arrangement of shadowgraph system. The uniform light beam from light source (Lamp type 904, Xe 300W) reflected on the concave mirror 1 (D=200mm, f=3970mm) and passed through CVCC to the concave mirror 2 (D=200mm, f=3970mm). Then, the reflected ray from concave mirror 2 entered the high-speed camera. The image of fuel spray has high sensitivity with environmental density variation in CVCC and allows to observe the spray development. The great advantage of this technique is its extreme simplicity.

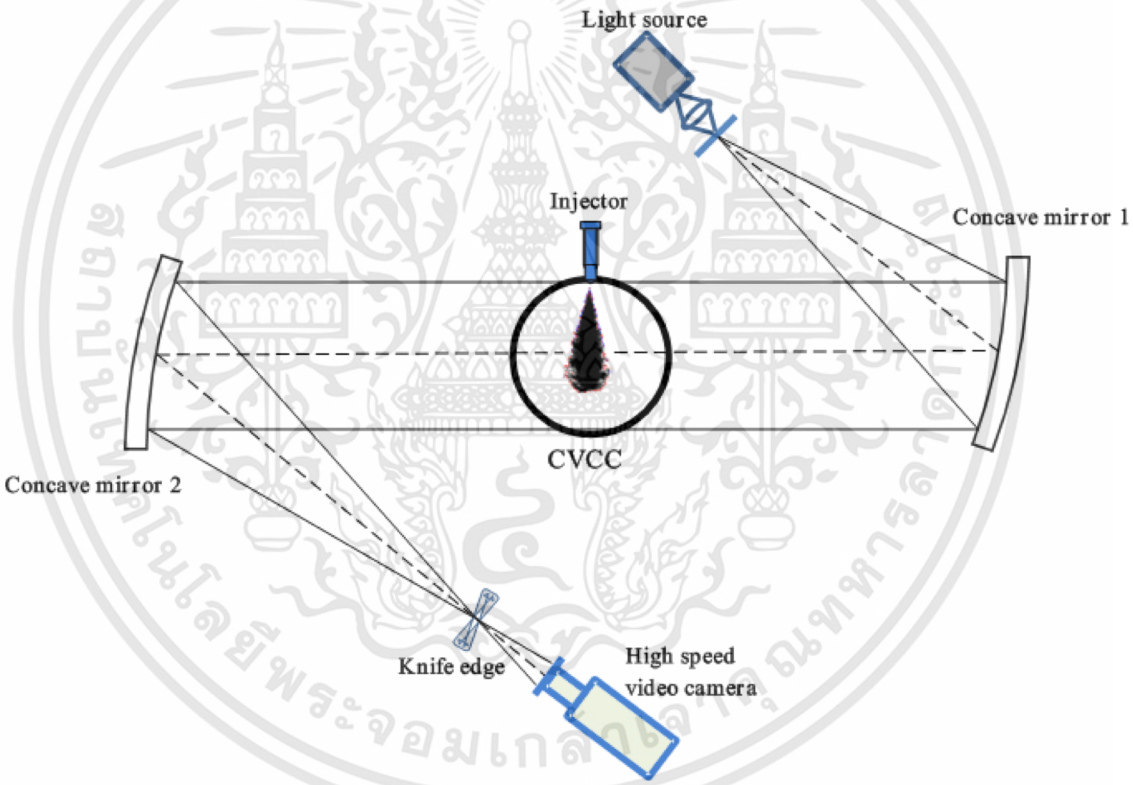

Fig. 3.2. Schematic arrangement of shadowgraph system.

Fuel spray shape obtained by this technique is displayed in Fig. 3.3. From this figure, spray tip penetration (S) is determined as the distance between the nozzle tip and leading edge; spray cone angle θ is defined by the intersection between spray and injector at a specified distance (1/2*S) (Denotte *et al.,* [53]). Meanwhile, spray tip velocity is the velocity of leading edge and is determined by two consecutive images at the defined time intervals.

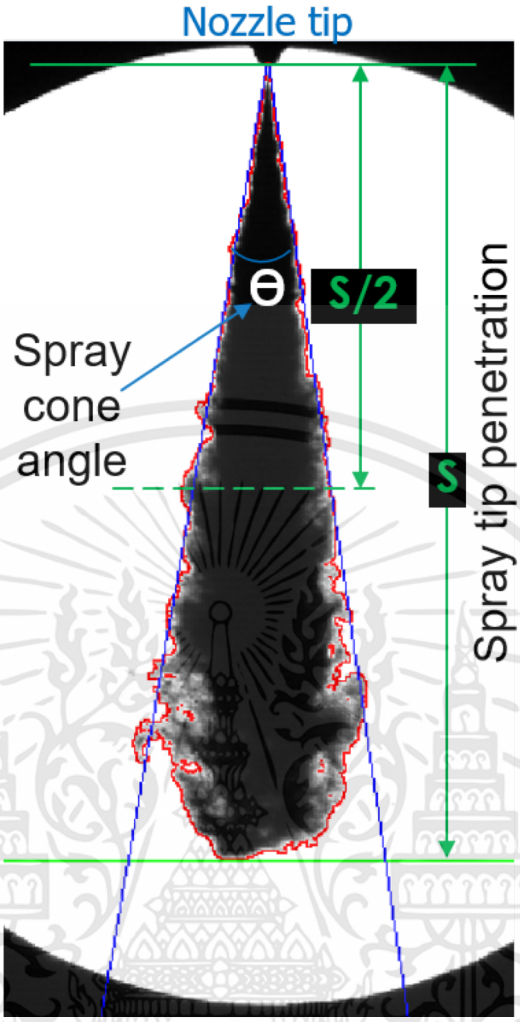

Fig. 3.3. Definition of spray parameters (HVO, P_{inj}=100MPa, P_a=4.0MPa, 2.5ms.

Based on spray tip penetration and the cone angle, spray volume is calculated using the following Eq. (7) (Chen et al., [77])

$$V = (\pi/3)S^3[\tan^2(\theta/2)]\frac{1+2\tan(\theta/2)}{[1+\tan(\theta/2)]^3} \quad (7)$$

The averaged cone angle was derived from 10 sets of spray images for each condition to verify repeatability. The calculated spray results can be determined by using a digital image processing program [53] which was built from aforementioned definitions. In general, there are three main steps. First, the background is subtracted from spray region and then it is converted to a negative value, in which the selected threshold for spray area was the pixels where the light intensity had dropped to 70% percent of the maximum intensity of image. Second, the image is binarized and detected the border. Third, from the border spray detection, spray parameters are measured.

3.3. Schlieren set-up and test procedure

3.3.1. Analysis of experimental fuels

In the present study, the experimental fuels are same with previous injection rate test. However, more fuel properties are analyzed to verify the its influence on the macroscopic spray characteristics. Surface tension is one of those properties that represents the force resistance of droplet deformation and subsequent atomization. According to Dernotte *et al.* [53], fuel viscosity, density, and surface tension have been demonstrated to influence the spray characteristics in non-vaporizing condition. Table 2.1 shows that surface tension of HVO has 5.84% less than diesel. This result may lead to higher injection velocity, decreased mean droplet size diameter (Suh *et al.,* [79]), shorter penetration as well as the better atomization process (Grimaldi *et al*., [85]).

3.3.2. Experimental set-up and test conditions

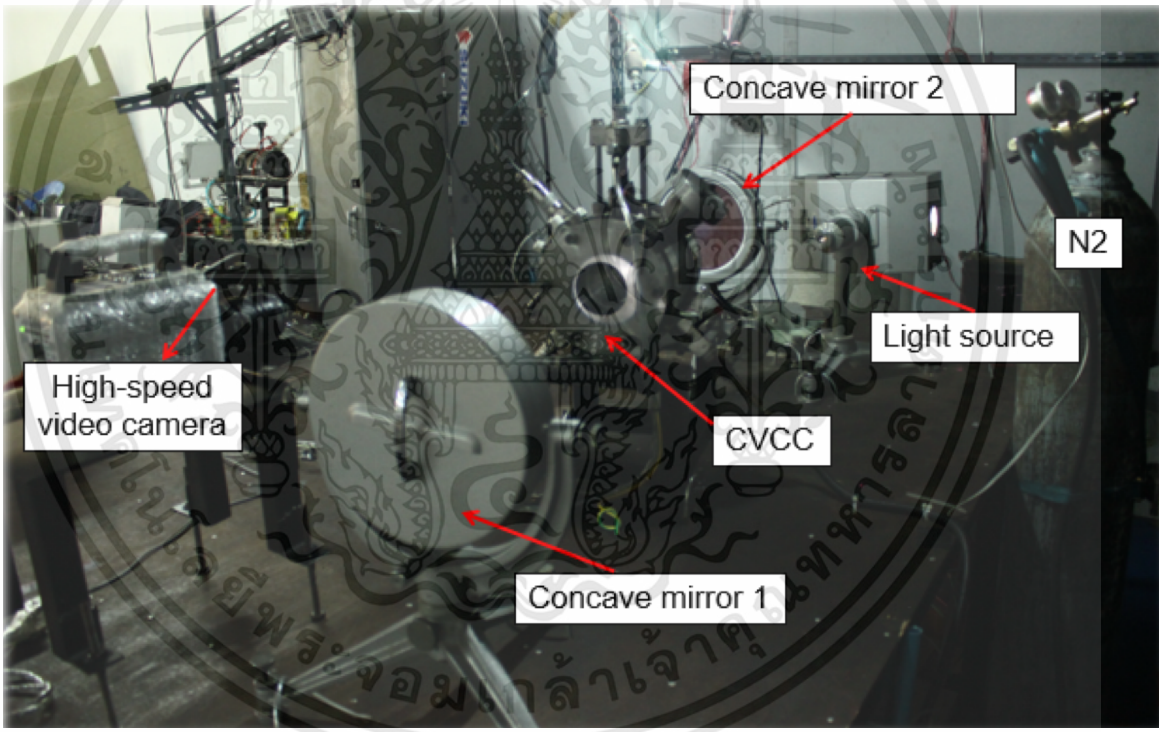

Fig. 3.4. Photograph of the Schlieren setup.

Fig. 3.4 shows the practical setup for measuring spray and Fig. 3.5 illustrates the overall schematic of experimental apparatus. The experiments were carried out using a constant volume combustion chamber (CVCC) with 80mm in diameter, 30mm in depth. The CVCC was fitted with quartz windows in both sides for observing optical spray assessment. A static pressure sensor was used to monitor ambient gas pressure in chamber. A single-hole solenoid injector, 0.2mm in nozzle diameter, was installed on the top of CVCC in order to inject fuel in range of 40MPa to 180MPa of injection pressure. Injector was connected to the common-rail system (high pressure pump type

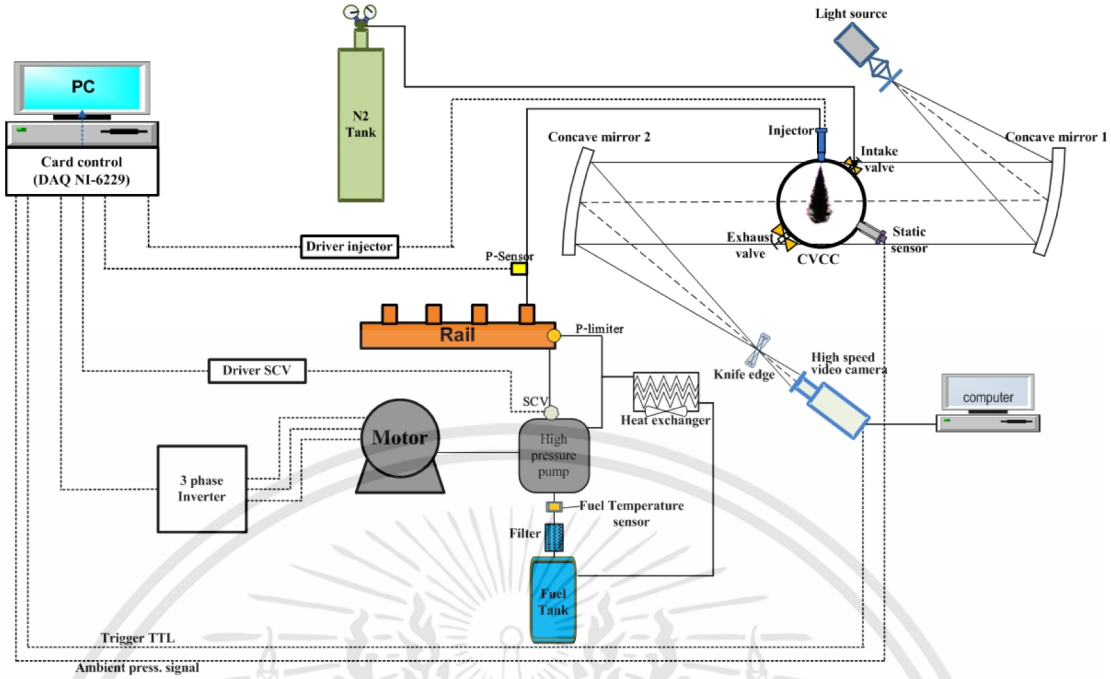

Fig. 3.5. Schematic representation of spray measurement.

Denso). In addition, a cooling-water system was applied to the injector to maintain the nozzle and fuel temperature at 301K±2K. A transducer sensor (Gems 3100 series type 3100B2200S2TB000RS) was installed on the high fuel pressure pipe to observe fuel injection pressure. To simulate a diesel engine condition (ambient gas density) at the end of compression stroke in case of non-vaporizing condition, the N_2 gas at the given pressure was provided into CVCC. Then, high injection fuel pressure was injected into CVCC. At the time of fuel injection, the high-speed camera (Photron FASTCAM mini UX100), coupled with a Nikkon lens 50mm f/1.4, also recorded spray evolution in CVCC at frame rate of 10,000fps, shutter of 1/64,000 second, resolution of 640x480 pixels^2. Signal of injector and camera trigger were synchronized and activated by LabVIEW program and micro controller. After each fuel injection, the quartz windows were cleaned and vacuumed to prevent fuel condensation in chamber.

Table 3.1 shows the experimental spray conditions, in which the test fuel samples were the B7 (as the reference fuel), the neat HVO, the 10% (H10), the 20% (H20), the

Table 3.1. Experimental spray conditions

Fuels	B7, H10, H20, H30, H50, H80, HVO
Ambient pressure P_b (MPa)	1.0, 1.5, 2.5, 4.0
Gas density (kg/m^3)	11.18, 16.78, 27.97, 44.75
Rail pressure P_{inj} (MPa)	40, 80, 100, 120, 160
Energizing time (ms)	2.5
Orifice diameter (mm)	0.2
Repeat	10 times/condition

30% (H30), the 50% (H50), the 80% (H80) HVO by mass fraction blended with B7. The HVO-B7 blends were only tested at 4.0MPa of ambient pressure for clarifying the effect of the mixing ratios, meanwhile B7 and HVO were experimented with different ambient pressures from 1.0 - 4.0MPa to investigate the impact of gas density (from 11.18-44.75kg/m^3) representing the gas density at TDC of conventional diesel engine on spray characteristics. The injection pressure was changed from 40MPa to 160MPa, injection duration was constantly kept at 2.5ms. The ambient gas temperature for non-vaporizing condition in this experiment was 301K ± 2K. some fuel vaporization may occur at this temperature. However, the rate of vaporization is slow relative to the rate of penetration. This indicates that the amount of fuel vaporization was small. The measurements were taken 10 times under each experimental conditions to verify the repeatability. Prior to beginning each test fuel, the fuel filters were replaced and fuel pipe was cleaned.

3.4. Results and discussion

3.4.1. Temporal shadowgraph spray development

In diesel engine, spray penetration and mixing process have strongly influenced to the combustion. Prior to the study of combustion of HVO blends, study of jet penetration is important. It can provide further explanations for the effects of fuel properties on mixture formation. Shadowgraph images shown Fig. 3.6 are the spray development for each fuel at 80MPa injection pressure and 4.0MPa ambient pressure, 301K room temperature. By observing directly, the first spray image appears after 0.5ms (time after the start of injection signal) and later images demonstrate the developing spray progress. A delay exists between the injection signal and the fuel jet exit from the nozzle orifice. This is mainly due to solenoid operation, needle inertia, and fluid inertia (Hulkkonen *et al*., [33]). Running until 3.5ms after the start of injection signal, the spray evolution achieves wall impingement. Also, the tip of spray displays the increase of turbulence level. This implies that more ambient gas entrains into fuel spray and rises the spray volume. The spray configuration has the steady cone shape up to around middle of spray. In addition, it is clearly seen that HVO spray exhibits shorter penetration than diesel while blends exposes the similar spray development. Through this, the HVO's combustion characteristics and exhaust emissions could be improved in that the air utilization in cylinder increased and fuel impingement decreased.

The sequence shadowgraph images spray development for case of various ambient gas densities in chamber of the B7 and HVO under 100MPa injection pressure is shown in Fig. 3.7 as representative. Similarly, all tests exist a delay of the injected fuel into

chamber and this interval time is within from 0.5ms to 0.8ms. By visual observation, higher gas density (higher ambient pressure) corresponds low spray tip penetration, wide spray angle, and strong turbulence level. This implies that fuel has a well mixed with air and the subsequent more homogenous combustion. Besides, the spray is recognized that it has the fast spray velocity and reaches wall chamber quickly around 1.4ms after the start of injection trigger under low ambient gas density (1.0MPa) while it reaches wall chamber at 2.4ms and 2.9ms after the start of injection trigger corresponding with 2.5MPa and 4.0MPa ambient pressure, respectively. On contrast, under higher injection pressure, spray velocity is faster as well as penetration length, cone angle, and spray volume become larger as seen in Fig. 3.8. Moreover, the perturbation regions of spray occur earlier at higher injection pressures by comparing the images under different pressures at 1.5ms after start of injection trigger. This effect is due to the higher spray speeds under high injection pressures making the sprays penetration and interaction with air faster and stronger (Chen *et al.*, [77]). Therefore, a combination of higher injection pressure and gas density has promoted to be well mixed with air and ready to the improved combustion.

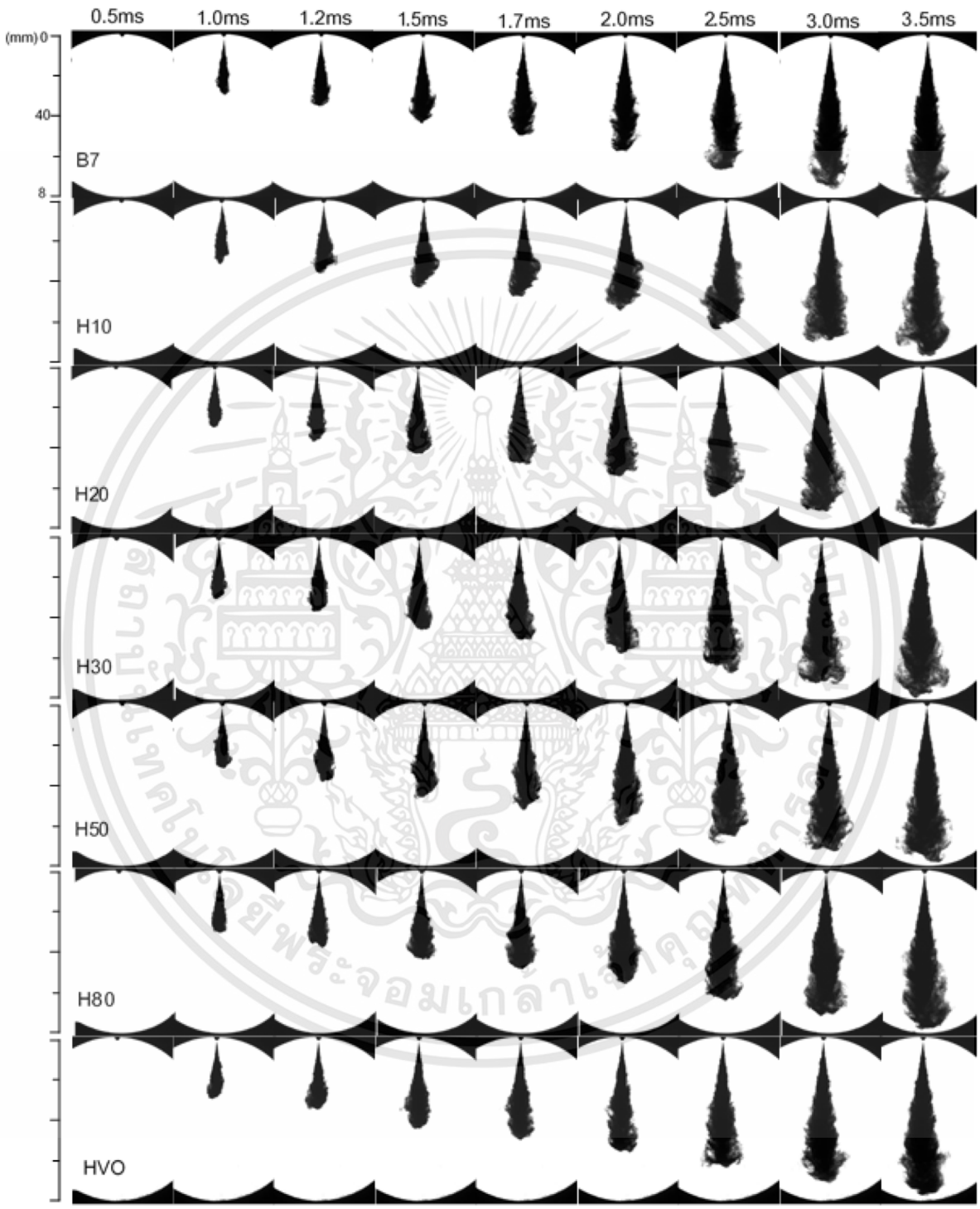

Fig. 3.6. Temporal spray development for fuel blends at P_{inj}=80MPa, P_a=4.0MPa.

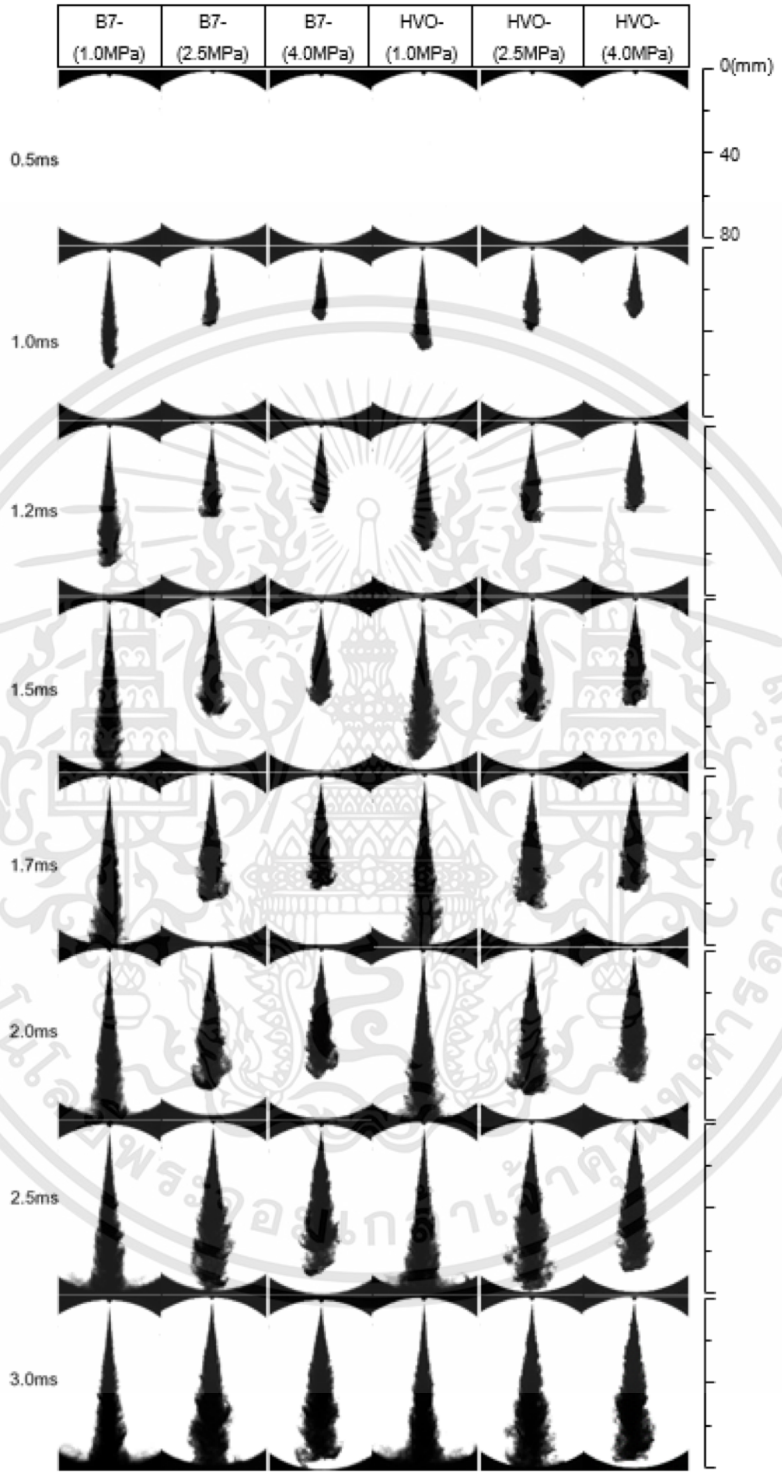

Fig. 3.7. Temporal spray development for various ambient pressures at P_{inj}=100MPa, 2.5ms.

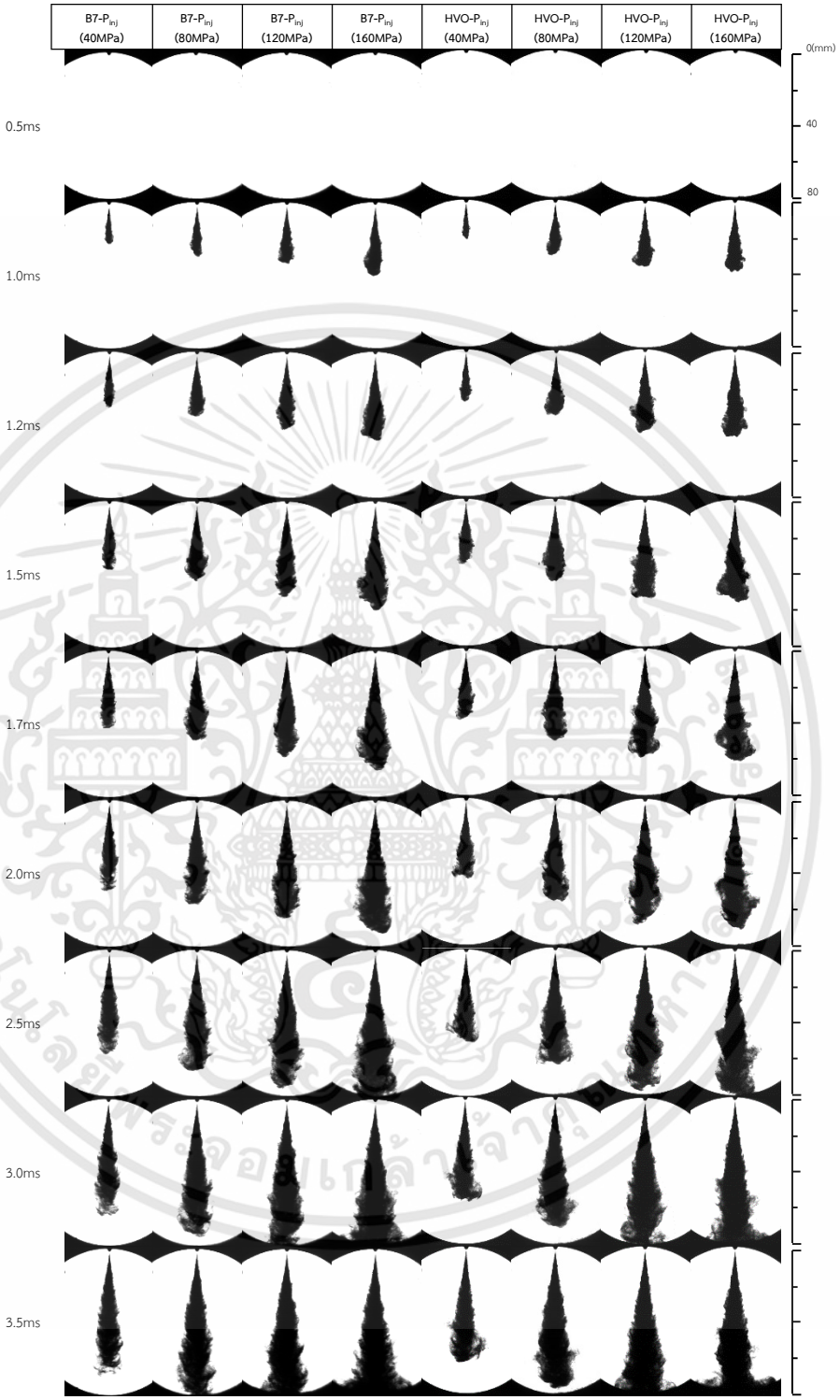

Fig. 3.8. Temporal spray development for various injection pressures at P_a=4.0MPa, 2.5ms.

3.4.2. Temporal spray tip penetration

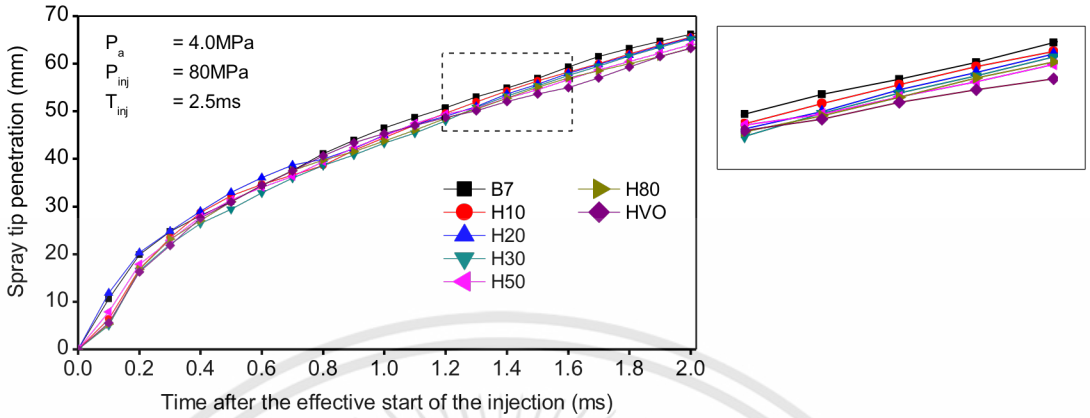

Fig. 3.9. Spray penetration for all fuels at P_{inj}= 80MPa, P_a=4.0MPa.

Spray tip penetration is an important factor that influences on air utilization and fuel-air mixing rate in the combustion chamber. Because the actual start of injection was difference for each fuel and injection parameter, the penetration curves were fixed to start at relative origin depending on hydraulic delay between electronic start of injection and actual start of fuel injection to see the differences in fundamental spray characteristics with different fuel types, injection pressures, and ambient gas densities. Fig. 3.9 shows the spray tip penetration of all the fuels at same injection pressure (80MPa) and ambient pressure (4.0MPa). The general spray penetration trend of the test fuels is the longer length along with time until wall impingement. Meanwhile, penetration length seen is slightly the shortest with HVO and the longest with B7. The difference for both fuels is about 5.1% on average at typical quasi steady period of 1.0ms-1.5ms. This can be explained by smaller viscosity, density and narrower distillation value of HVO than B7 that causes better evaporation during injection, the particles of HVO spray lost momentum easily (Ghurri *et al.*, [82]; Lee *et al.*, [83]). It is also noted that HVO blends has similar penetration.

The effect of gas density (ambient gas pressure) range from 11.16kg/m^3 to 44.75kg/m^3 on spray penetration is exhibited in Fig. 3.11. From this figure, full development time of fuel spray is longer as increasing the ambient gas pressure. The reason is that the ambient pressure is higher, the ambient gas density is also higher. This means that the development of spray is interrupted by the ambient gas particle (increasing the aerodynamic drag); thus when the ambient pressure is higher, the penetration length is shorter. This result is consistent with other findings (Tinprabath *et al.*, [52]; Payri *et al.*, [76]; Lee *et al.*, [83]; Song *et al.*, [86]). By comparing between HVO and diesel, the penetration length of HVO is shorter than diesel spray. This reason is similar to Fig. 3.9.

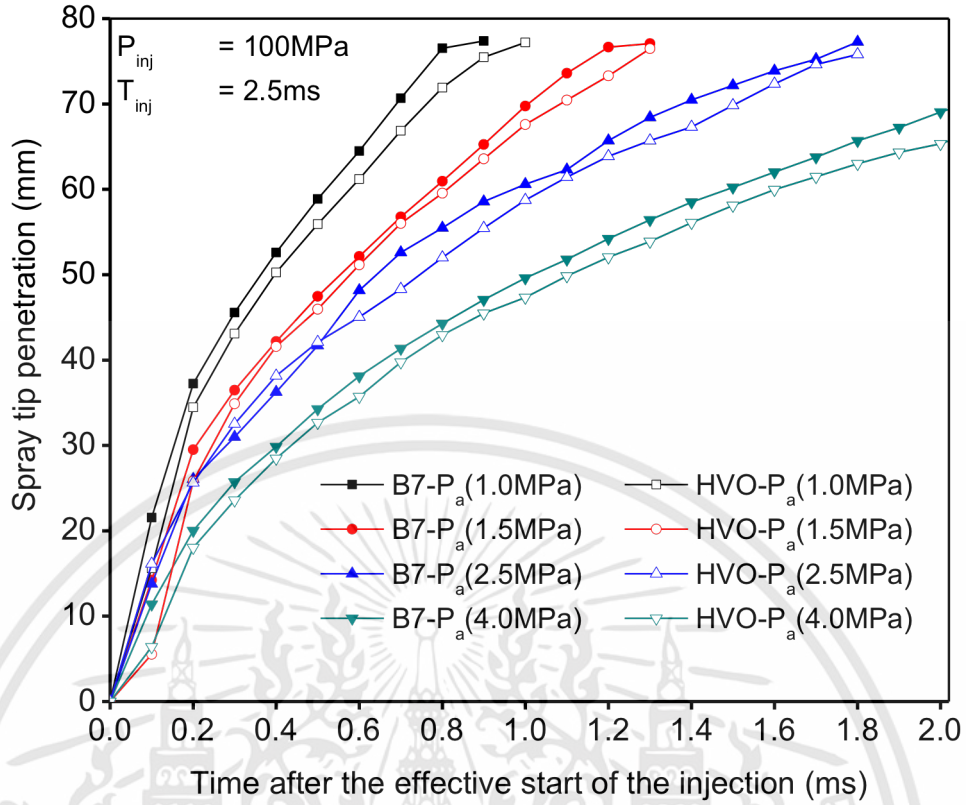

Fig. 3.11. Spray penetration length of HVO and B7 at P_{inj}= 100MPa, and various P_a (1.0, 1.5, 2.5, 4.0MPa).

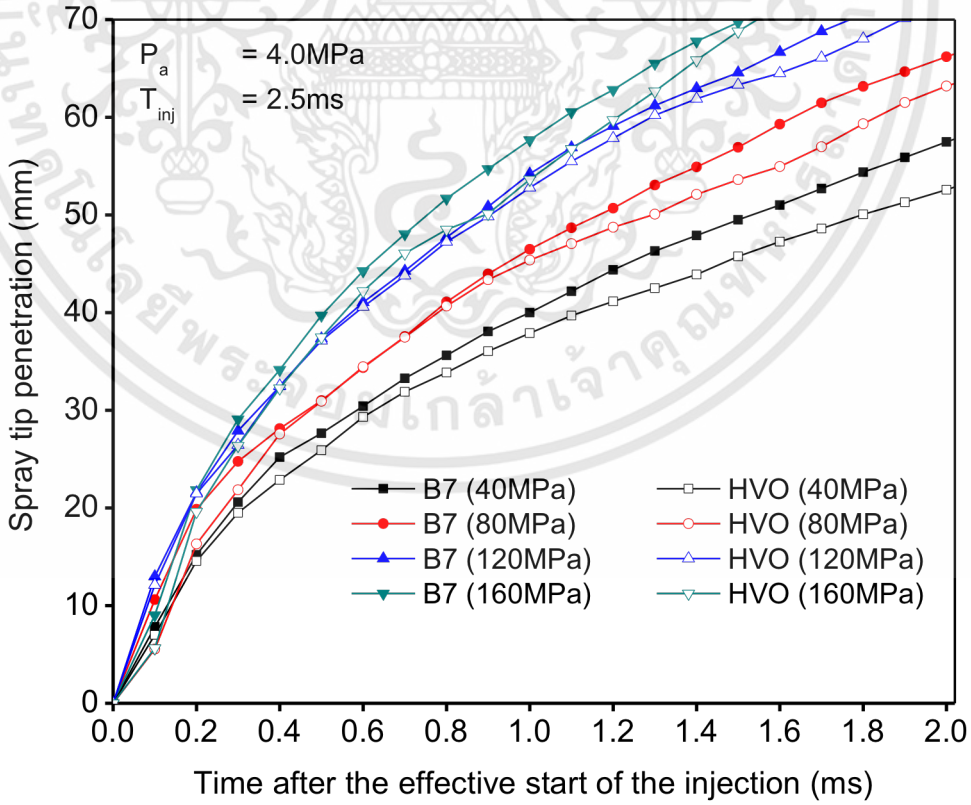

Fig. 3.10. Spray penetration length of HVO and B7 at P_a= 4.0MPa, and various P_{inj} (40, 80, 120, 160MPa).

Fig. 3.10 shows the effect of injection pressure on spray tip penetration under

constant ambient pressure and injection duration. The most noticeable trend shown by penetration data in this figure is the increase in penetration with an increase in injection pressure. For instance, with HVO, at 1.3ms after the effective start of the injection, the spray tip penetration is 42mm at 40MPa compared with 60mm under 120MPa of injection pressure. One possible explanation is higher spray momentum achieved by higher injection pressure. These trend has been observed by many other researches (Delacourt *et al.*, [74]; Chen *et al.*, [77]; Suh *et al.*, [79]; Ghurri *et al.*, [82]). In addition, it seems the spray penetration is quicker at early stage of injection (0ms-0.7ms) and slower in later stage. This means that initial spray velocity is higher at the early stage. The reason is that the spray has larger droplet size at near nozzle tip which causes higher momentum while smaller droplet size at further nozzle distance is as a result of spray atomization (Ghurri *et al.*, [82]). One the other hand, it can be clearly seen the difference of penetration for HVO and diesel at the further time because the higher viscosity and density of diesel enable the spray to have the higher momentum and could reach slightly longer penetration length.

3.4.3. Temporal spray cone angle

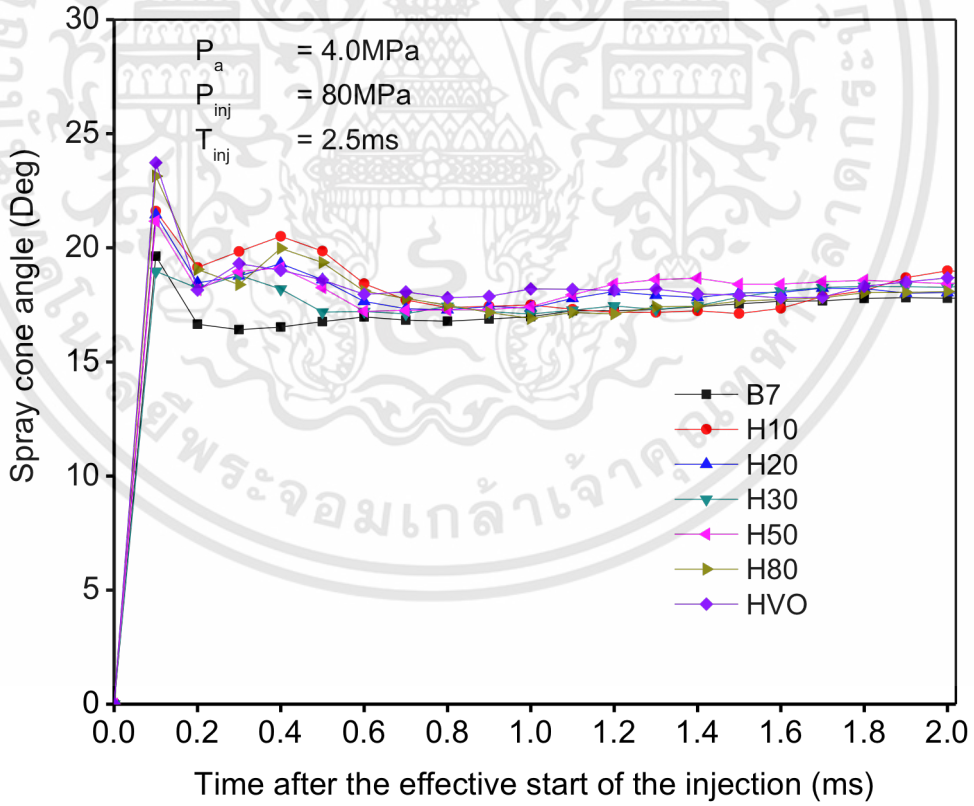

Fig. 3.12. Spray cone angle of different fuels at P_{inj}=80MPa, P_a=4.0MPa

The experimental results of spray angle at different fuel blends under constant injection pressure and ambient pressure are shown in Fig. 3.12. A comparison of spray angle for fuels was carried out at quasi-steady region of the spray of 1.0ms-1.5ms after

the effective start of the injection. It can be seen that spray angle development is divided into two parts, the first part rapidly increases to maximum angle and this transient progress (0ms-0.4ms) is set as acceleration phase. The later part is the deceleration of angle to steady angle phase. This tendency is similar to previous researches (Tinprabath *et al.*, [52]; Song *et al.*, [86]). For the comparison among the test fuels, HVO shows the slightly wider spray angle than that of B7 (from 0.2-1.1 degrees wider). Meanwhile, blends have similar angle. The slight difference between HVO and B7 may be mainly caused by smaller viscosity and density of HVO results in smaller droplet size and stronger turbulence level at exit of the orifice (Dernotte *et al.*, [53]). As the wider spray angle, HVO has smaller fuel concentration at nozzle tip area under the same mass flow. Lower concentration may reduce the soot emissions due to better air-fuel mixing. This result was similar with earlier studies by Hulkkonen [33].

Fig. 3.13 shows the effect of ambient gas pressure (ambient gas density) on the cone angle at constant injection pressure of 100MPa. Generally, the spray cone angle increases with the increase of the ambient gas pressure. This result is suitable with study of Delacourt [74], Suh [79]. It can be explained that the increase of ambient gas pressure leads to the increase of resistance on the spray and slows down the spray movement which results in stronger ambient gas entrainment. In the quasi-steady

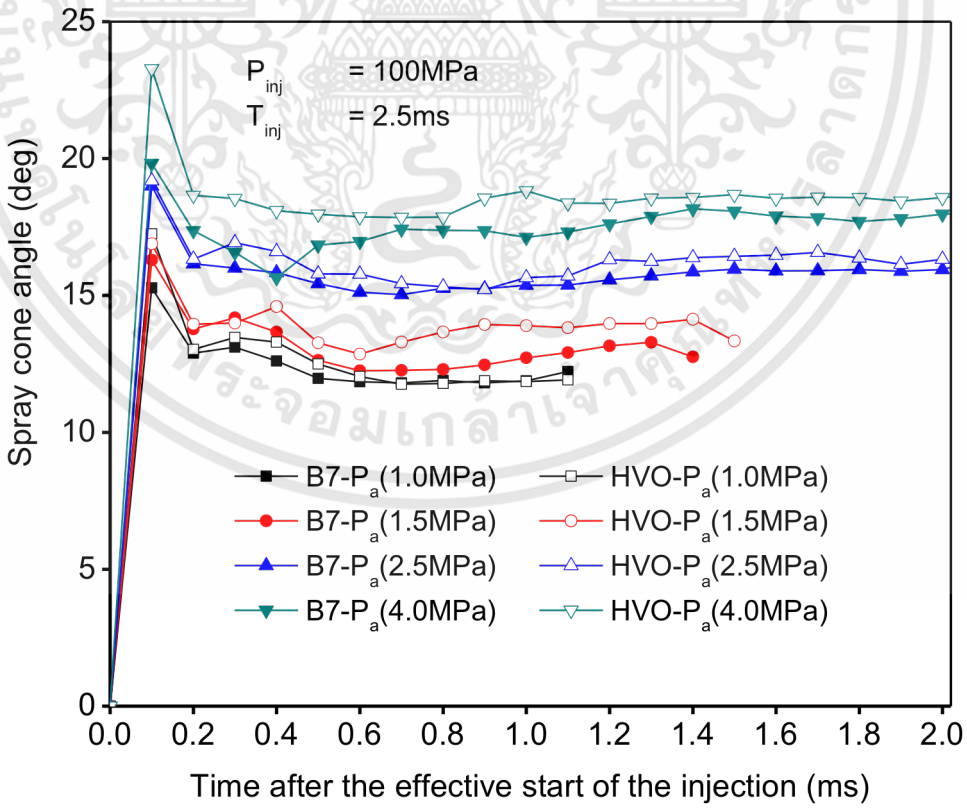

Fig. 3.13. Spray cone angle of HVO and B7 at P_{inj}= 100MPa, and various P_a (1.0, 1.5, 2.5, 4.0MPa).

period, an increase of ambient pressure from 1.0MPa until 4.0MPa caused the rise of spray angle about from 11.9deg to 17.2deg, approximately.

Fig. 3.14 indicates the result of spray angle carried out with various injection pressures (40MPa and 120MPa) under constant ambient pressure (4.0MPa) as representative. This figure shows an increase in spray angle with an increase in injection pressure. Specifically, an increase in injection pressure from 40MPa to 120MPa in quasi-steady angle region period of 1.0-1.5ms after the effective start of the injection averagely induces a slight increase of 0.6 to 2.4deg in spray angle. Increasing the injection pressure raises the turbulence level into the orifice and then the dispersion on spray at the exit of the injector. This result is consistent with other findings (Tinprabath *et al*., [52]; Wang *et al*., [73]; Lee *et al*., [83]).

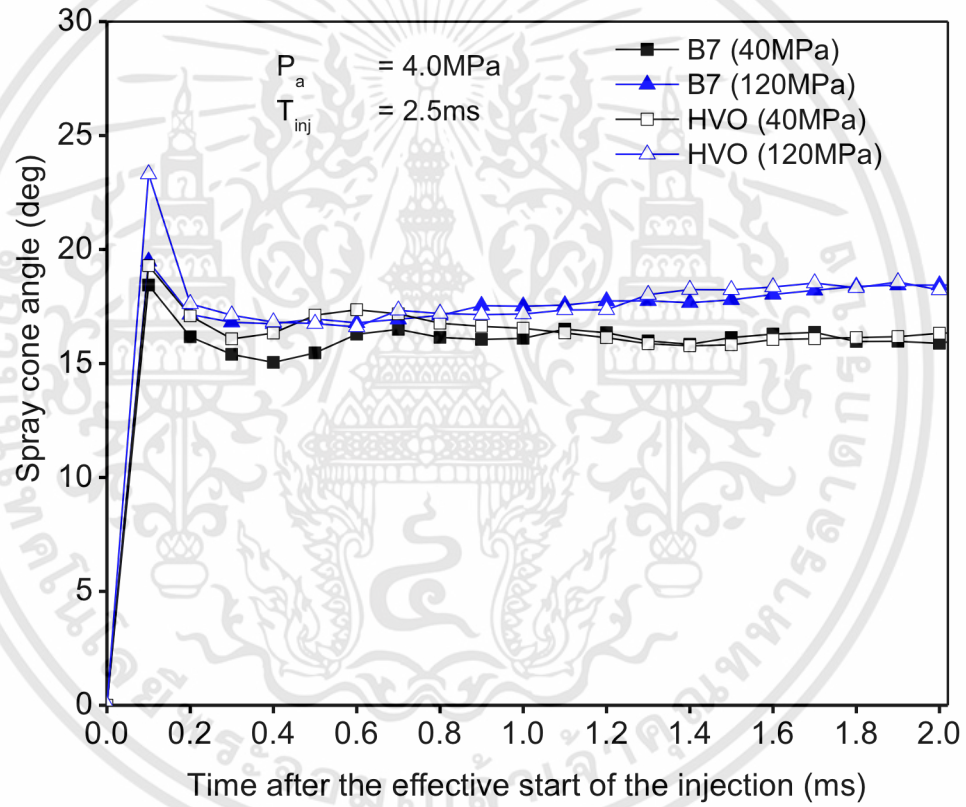

Fig. 3.14. Spray cone angle of HVO and B7 at P_a= 4.0MPa, and various P_{inj} (40, 80, 120, 160MPa).

3.4.4. Temporal spray tip velocity

With the difference of the spray penetration in the two sequential images from same spray and the known time step between the images, the spray tip velocity was determined. The results of spray tip velocity for all test fuels under constant injection pressure (80MPa) and ambient gas pressure (4.0MPa) are indicated in Fig. 3.15. The acceleration, maximum velocity, and deceleration of spray tip were found in profile.

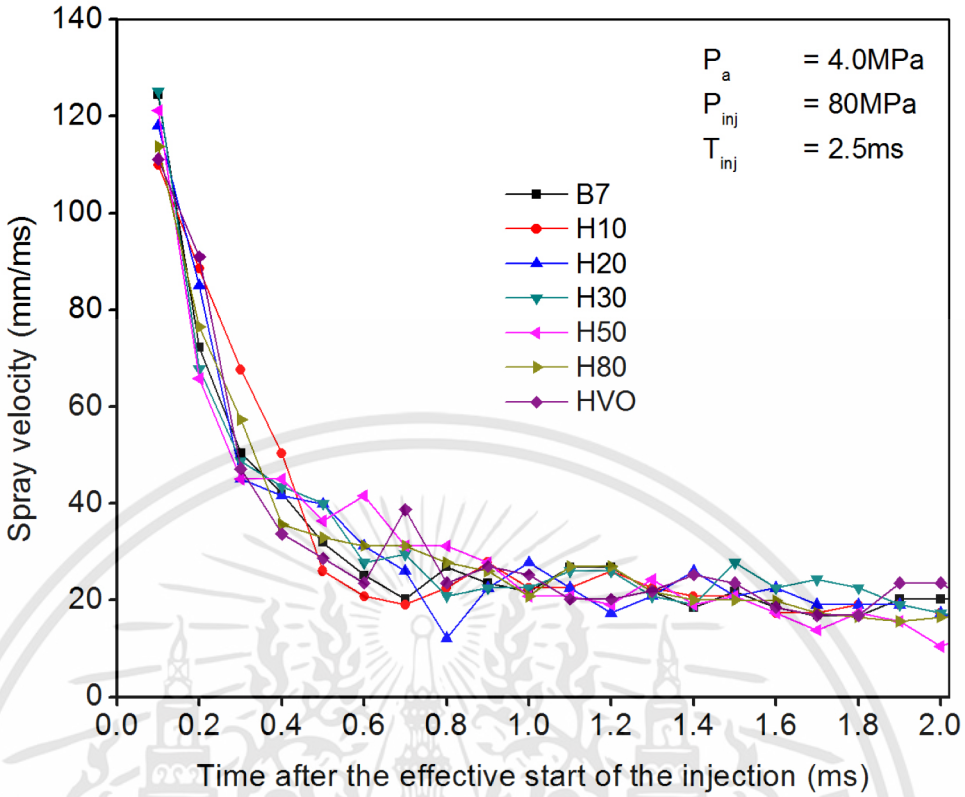

Fig. 3.15. Spray tip velocity comparison among test fuels at P_{inj}=80MPa, and P_a=4.0MPa.

Spray tip accelerates at begin of the spray injection. After acceleration, spray tip reaches maximum velocity before deceleration. Velocity maximum is located 5-10mm from nozzle orifice with all tested fuels. Clear difference in maximum velocity was found between HVO and B7. The spray tip velocity of HVO seems to be slightly lower than the velocity of B7. The maximum velocity was approximately 12-18m/s lower with HVO than B7. This may be attributed to the fact that the relatively higher density and bulk modulus of B7 increases the velocity of fluid exiting the nozzle compared with HVO (Chen *et al.*, [77]). In the deceleration phase, velocity difference between the tested fuels is not as clear.

The effect of different gas densities (ambient gas pressure) on spray tip velocity is presented in Fig. 3.16. In the figure, the higher ambient gas pressure contributed to smaller spray tip velocity, a phenomenon attributable due to increasing aerodynamic drag on droplet. In addition, the fuel spray velocity quickly reaches the chamber wall (velocity drops to zero) under low ambient gas pressure. This implies that the applying high ambient gas pressure can prevent fuel impingement which subsequently reduces emissions.

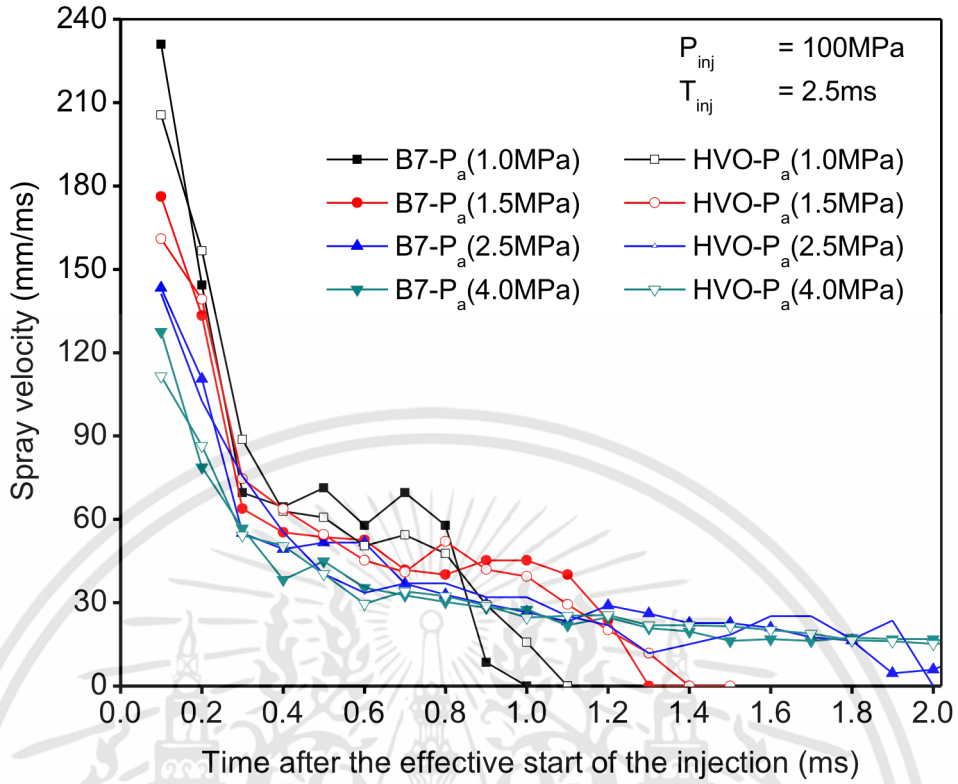

Fig. 3.16. Spray tip velocity comparison between HVO and B7 at P_{inj}=100MPa, and different ambient pressures.

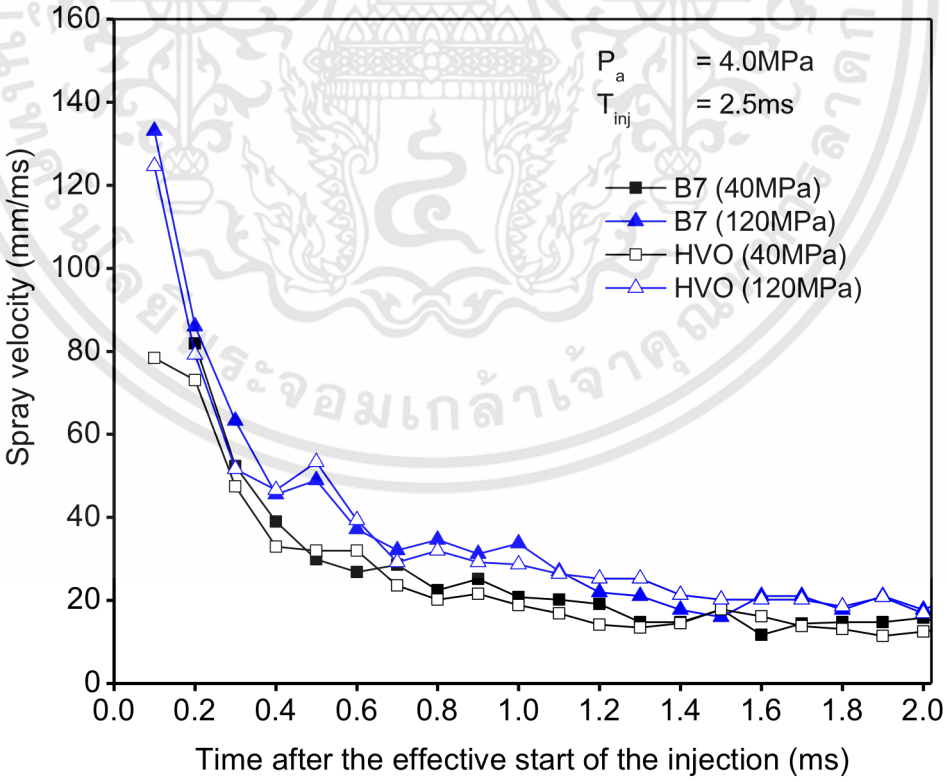

Fig. 3.17. Spray tip velocity comparison between HVO and B7 at P_a=4.0MPa, and different injection pressures.

Fig. 3.17 shows the effect of injection pressures (40MPa and 120MPa) on spray tip

velocity for HVO and B7 as representative. As observed, spray tip velocity is higher when injection pressure is higher. This is reasonable due to increasing flow rate and spray momentum as rising injection pressure. The maximum velocity was approximately higher in 60m/s for B7 and 46m/s for HVO when pressure differential increased from 40MPa until 120MPa. This result is similar to Hulkkonen's study [33]).

3.4.5. Temporal spray volume

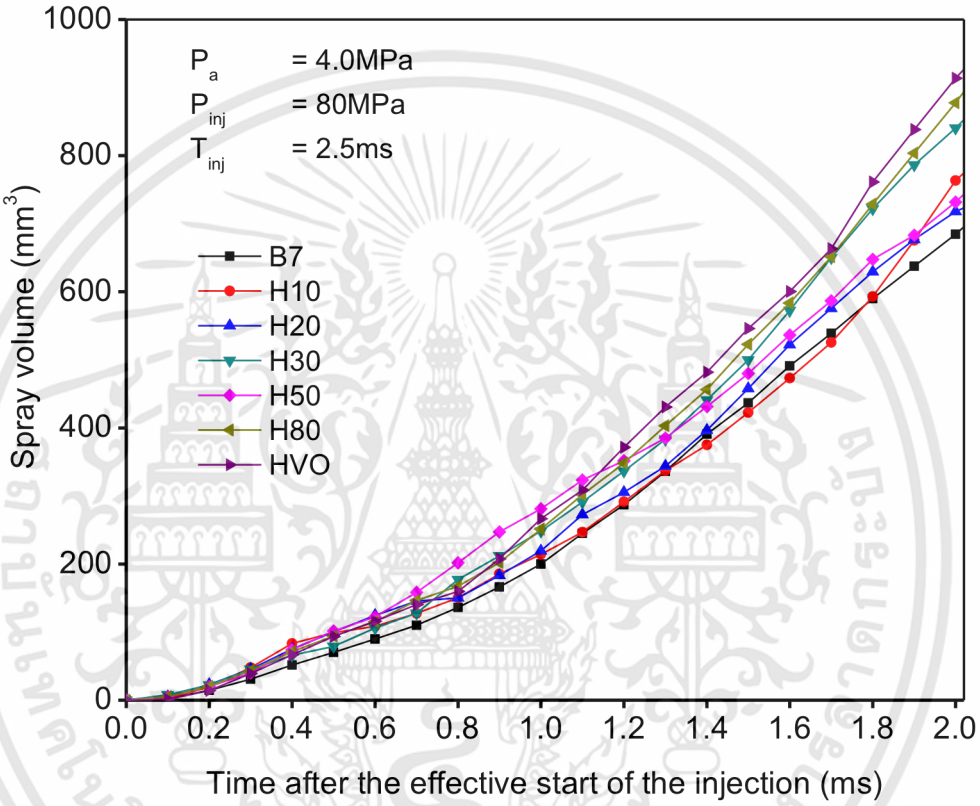

Fig. 3.18. Spray volume for different test fuels under constant P_{inj}=80MPa, P_a=4.0MPa.

Fig. 3.18 shows the calculated spray volumes of different test fuels used in this study with time after the effective start of the injection. Larger spray volume can be found with HVO fuel and the smallest with B7. For example, at 1.3ms after the effective start of the injection, spray volume is 336, 337, 343, 383, 385, 403, and 430mm^3 corresponding to B7, H10, H20, H30, H50, H80, and HVO, respectively. The distribution in spray volume for different fuels follows the same trend as spray cone angle which wider spray cone angle generates larger spray volume. From this result, it can be explained that the larger spray volume is caused by stronger turbulence intensity results in higher gas entrainment rate (Wang *et al.*, [87]). Smaller in viscosity, density, surface tension is mainly responsible for this phenomenon.

Fig. 3.19 compares the spray volumes of HVO and B7 as representative, given the same injection pressure of 100MPa, under 1.0, 1.5, 2.5, and 4.0MPa ambient pressure.

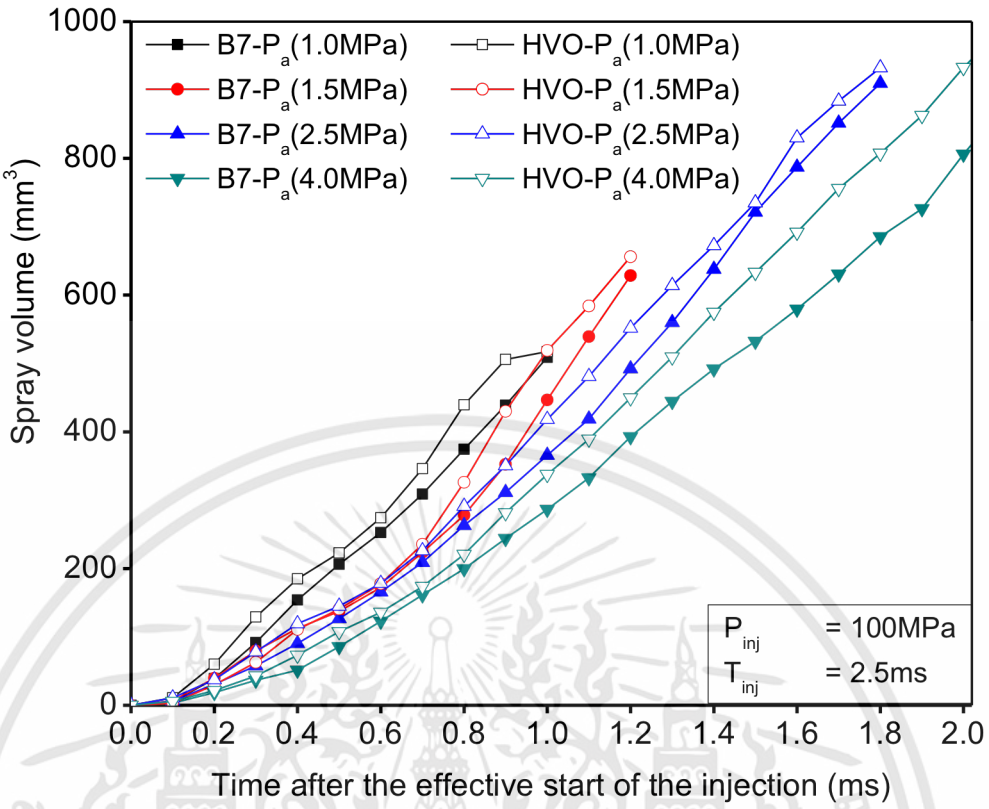

Fig. 3.19. Spray volume for HVO and B7 under constant P_{inj}=100MPa, and different ambient pressures (1.0, 1.5, 2.5, 4.0MPa).

According to this figure, an increase in ambient pressure results in a decrease in the spray volume in the short period of time, as has been observed in shadowgraph images of Fig. 3.7. This phenomenon is related to the fast spray development under low ambient gas pressure. However, full development time of fuel spray is longer as increasing the ambient gas pressure. This results in larger spray volume in later spray developing progress. Other speaking, there is an increase in the gas entrainment with an increase in the ambient gas density (ambient pressure) due to two causes: first as a direct result of the increase in ambient gas density, and second, as a result of the increase the dispersion angle with an increase in gas density (Naber *et al.*, [9]). The second cause is in accordance with the developing trend of spray penetration under different ambient pressures as shown in previous section.

Fig. 3.20 shows effect of injection pressure differential on spray volume development. Larger spray volume can be found at higher injection pressure. For instance, spray volume of HVO increases from 156mm^3 to 631mm^3 at 1.3ms after the effective start of the injection as the injection pressure is increased from 40MPa to 160MPa. This is considered as the effect of higher injection pressure delivering fuel faster as well as higher spray velocity, wider spray angle which enhance air-fuel mixing (higher air entrainment) (Hulkkonen *et al.*, [33]; Dung *et al.*, [88]; Dodge *et al.*, [89]; Wang *et al.*, [90]). Besides, the applying high injection pressure help to optimize the

trade-off of spray volume and droplet size which subsequently promotes the complete combustion (Chen *et al*., [77]).

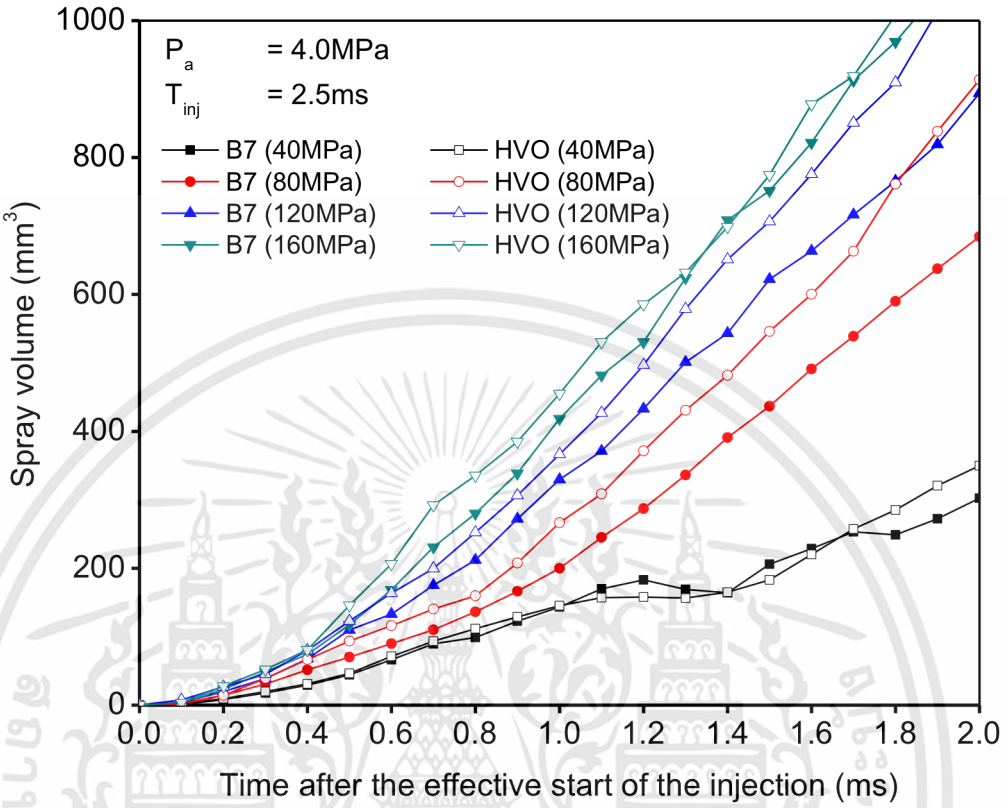

Fig. 3.20. Spray volume for HVO and B7 under constant P_a=4.0MPa, and different injection pressures (40, 80, 120, and 160MPa).

3.5. Conclusion

In this work, the spray characteristics were investigated for diesel fuel, HVO, and five HVO-diesel blends under the non-vaporize condition in constant volume combustion chamber. The testing conditions included ambient gas pressure, injection pressure. The analysis focused on temporal spray tip penetration, spray tip velocity, spray cone angle, and spray volume. The observations and findings can be summarized as follows:

(1) The general spray penetration trend of the test fuels was the longer length along with time until wall impingement. The use of neat HVO contributed to the shorter spray tip penetration, wider spray angle, larger spray volume as compared to the others test fuels. Notably, diesel obtained slightly 12-18m/s higher in maximum spray tip velocity. The smaller value with HVO than B7 was about 5.1% in penetration, 0.2-1.1 degrees wider in spray angle averagely at typical quasi steady period of 1.0ms-1.5ms.

(2) Fuel blends exhibited the similar spray tip penetration, spray cone angle and spray tip velocity while the distribution in spray volume followed the larger trend as increasing HVO fraction in mixture.

(3) A significant shorter spray tip penetration and larger spray volume in fully developing time of fuel spray as well as wider spray angle at quasi-steady state of spray and smaller maximum spray tip velocity could be obtained by increasing ambient gas pressure owing to aerodynamic effect. Besides, the fuel spray quickly reached the chamber wall under low ambient gas pressure.

(4) From shadowgraph images, the applying high injection pressure caused the increase of the turbulence level surrounding fuel spray tip and the dispersion on spray at the exit of the injector that contributed to wider spray angle and larger spray volume. In addition, the higher injection pressure differential induced the longer spray tip penetration and faster spray tip velocity due to higher spray momentum.

CHAPTER 4
SPRAY COMBUSTION AND EMISSION CHARACTERISTICS OF HYDROTREATED VEGETABLE OIL IN RCEM

4.1. Introduction

Fossil fuels have been the essential source of energy in the global development for centuries. However, along with the continual rise in the fossil fuels consumption come the pollution and the environmental degradation. Thus, attempts have been made to mitigate the fossil fuels-related environmental impacts through the renewable and more environmentally-friendly energy alternatives as well as the deployment of modern technologies. Specifically, for diesel fuel, biodiesel has been successfully formulated and adopted by a number of countries, including Thailand where the commercial diesel fuel is legally required to contain a minimum of 7% palm methyl ester. Despite its low emissions and good lubricity, biodiesel nevertheless suffers from the poor oxidation stability, high NO_x emission, high density and viscosity, and low heating value (Masjuki *et al.*, [91]). Thus, additional research studies have been carried out to further improve the performance and emissions of the biodiesel, for instance, modifying bio-base fuels properties by using different production processes such trans-esterification, pyrolysis, dilution, and micro-emulsion (Ali *et al.*, [92]); or employing various feedstocks such soybean (Liu *et al.*, [93]), rapeseed oil (Nwafor *et al.*, [94]), palm oil (Zainal *et al.*, [95]; Hashimoto *et al.*, [96]), jatrophas curcas oil (Reksowardojo *et al.*, [97]; Tapanes *et al.*, [98]), waste cooking oil (Meng *et al.*, [99]), and animal fat (Bhatti *et al.*, [100]). Moreover, in order to diversify alternative fuel resources and upgrade biofuel generations with many dominant properties, the advanced alternative fuels consisting of biomass to liquid (BTL), gas to liquid (GTL), coal to liquid (CTL), hydrotreated vegetable oil (HVO), hydrogen, ethanol, fuel cell, etc. are strongly considered and initially applied in small-scale production (Schablitzky *et al.*, [101]; Schablitzky *et al.*, [102]; Unruh *et a*l., [103]; Gill *et al.*, [104]; Zhang, [105]; Leckel, [106]; Oguma *et al.*, [107]; Moon, [108]). In fact, as previous mentioned in this study, the HVO used is the one of the second generation biofuels which could address the problems associated with the conventional biodiesel (Knothe, [14]). Contemporarily, HVO possesses high cetane number and heating value, narrow distillation, no aromatics, ultra-low sulfur content, and excellent oxidation stability that collectively contribute to low emission and better engine performance (Soo-Young No, [11]; Caprotti et al., [17]; Koyama *et al.*, [21]; Hartikka *et al.*, [22]).

Direct injection diesel engines are widely used in many fields due to high thermal efficiency, and lower fuel costs. However, diesel engine emissions are a significant

contributor to environmental pollution, especially NO_x and soot which are the most strictly regulated emissions from diesel engines. To satisfy the increasing regulation of emission standards being applied by many countries, reducing diesel engine emissions is currently considered a top priority in diesel engine research. Accordingly, existing research has investigated the effects of exhaust gas recirculation (EGR) on the NO_x and soot formation and reported that a decrease in the oxygen concentration under the ambient condition contributed to the lower flame temperature and the subsequent lower NO_x emission (Lehto *et al.*, [109]; Ladommatos *et al*., [110]). However, the lower oxygen concentration would suppress the soot oxidation and thus elevates the soot concentration (Shi *et al*., [111]). Furthermore, under the EGR, the heat capacity of the ambient gas increases while the heat release declines (Zhang *et al*., [112]). In fact, the soot level could be lowered by raising the injection pressure (using common-rail injection system with electronic control) as the faster spray breakup, the higher injection velocity, the better fuel atomization and vaporization, the shorter mixing time collectively contribute to a more complete combustion (Heywood, [7]; Pickett *et al.*, [113]; Wang *et al.*, [114]). The simultaneous application of supercharger condition, high pressure common rail system and EGR could obtain lower the final NO_x mass per released heat (Kitamura *et al.,* [115]). On the other hand, the use of after-treatment systems for modern diesel engine helps reduce emissions (Soltic *et al.*, [116]). The development of new modes of combustion has given the opportunities and challenges to optimize the low fuel consumption and high engine performance (Shi *et al*., [117]; Ganesh *et al.,* [118]). Remarkable in-cylinder NO_x and soot reduction is achievable using the optimized combustion chamber geometry and various key engine parameters (Raeie *et al*., [119]; Deqing *et al*., [120]; Buyukkaya *et al*., [121]).

Obviously, the combination of bio-base fuels and the progressive technologies in diesel engine will be the effective solution to achieve lower emissions. Aforementioned in literature review's part (1.2), the existing researches of HVO did not provide sufficient data for analyzing the effects of physical and chemical properties on combustion and emission characteristics, importantly, the understanding of NO_x and soot formation of the HVO, given the variable oxygen concentrations and injection pressures has very limited. Therefore, the aim of this study is to clarify the effects of variable oxygen concentrations, injection pressures, typical HVO's properties on the combustion and emission characteristics under the simulated diesel condition by using high pressure common rail injection system and rapid compression-expansion machine (RCEM). Five experimental fuels were the B7 diesel fuel (7% PME), the neat HVO, the 20%, 50% and 80% HVO by mass fraction blended with the B7. In the study, there were two injection pressures: 80MPa and 120MPa, given the identical amount of injection; and three oxygen (O_2) concentrations: 21%, 15% and 10%. In this research,

the combustion characteristics include the ignition delay, the heat release rate, and the integral heat release, while the emissions characteristics focus on NO_x and soot. The analysis was carried out using the two-color method (the flame temperature and the KL factor).

4.2. Research methodology-Two color method

The thermal radiation in the diesel combustion could be largely attributed to the soot particles. Meanwhile, the two-color method is a measurement technique based on the intensity of thermal radiation from the incandescent soot particles at two different visible wavelengths. In fact, the two-color method has been discussed in many studies (Munsin *et al*., [65]; Shi *et al*., [111]; Ito *et al*., [122]; Zhang *et al*., [123]; Kamimoto *et al*., [124]) and could be summarized as follows:

Let $I_{b(\lambda, T)}$ be the monochromatic radiant intensity of the black-body. According to Wien's law, the monochromatic radiant intensity of a soot particle is expressed as

$$I_{(\lambda, T)} = \varepsilon_\lambda I_{b(\lambda, T)} = \varepsilon_\lambda (C_1/(\pi^5))\exp[-C_2/(\lambda T)] \quad (8)$$

Assuming T_a an apparent temperature of a black-body with the same radiant intensity of soot as at the temperature T, Eq. (8) is rewritten as

$$I_{b(\lambda, Ta)} = I_{(\lambda, T)} = (C_1/(\pi\lambda^5))\exp[-C_2/(\lambda T_a)] \quad (9)$$

According to Hottel and Broughton [125], the monochromatic emissivity of a soot particle can be expressed as

$$\varepsilon_\lambda = 1 - e^{(-KL/\lambda^\alpha)} \quad (10)$$

Then, the KL value could be extracted from the combination of Eqs. (8), (9) and (10) and shown in Eq. (11)

$$KL = -\lambda^\alpha \ln\left[1 - \exp\left\{-\frac{C_2}{\lambda}\left(\frac{1}{T_a} - \frac{1}{T}\right)\right\}\right] \quad (11)$$

Given the apparent temperatures of T_{a1} and T_{a2}, which are measured at the two wavelengths λ_1 and λ_2, the true flame temperature (T) and the KL factor can be determined from Eq. (11).

Meanwhile, the rate of heat release is calculated from the first law of thermodynamics (Heywood, [7]), as shown in Eq. (12)

$$dQ/dt = (\gamma/(\gamma-1))P(dV/dt)+(1/(\gamma-1))V(dP/dt) \quad (12)$$

4.3. Experimental setup and test procedure

4.3.1. Experimental apparatus and conditions

Fig. 4.1 is a photograph of the two color method setup and Fig. 4.2 illustrates the streamlined layout of the experimental system. The experiments were carried out using a rapid compression-expansion machine (RCEM) (Kobori *et al.*, [10]) of the electrically controlled and hydraulically actuated driving cycle type. The RCEM piston was of the flat type with 86mm, 151.5mm and 16.5mm for the bore, stroke and clearance height. To simulate a diesel engine environment, the synthetic air composed of 79% N_2 and 21% O_2 was generated in the mixing tank at 453K ± 1K and then entrained into the cylinder at the bottom dead center (BDC). The charged gas was then compressed by the piston for 30ms to increase the temperature and pressure. The piston was subsequently held motionless at the top dead center (TDC) for 150ms to generate the constant volume combustion chamber (CVCC) condition. The pressurized fuel in the solenoid-single hole injector (0.2mm in the orifice diameter) connected to the common rail system was injected into the chamber at a constant injection pressure. The pressure in the combustion chamber was measured by a piezoelectric transducer sensor (AVL-GU22CK) and amplified by a charge amplifier (Kistler type 5010). In addition, a cooling-water system was applied to the injector to maintain the nozzle and fuel temperatures at 325K±1K. During the combustion, the spray flame images were captured by a high speed camera (NAC Memrecam GX-1) at 10,000fps (frame per second) through the quartz window in front of the chamber. The high speed camera was coupled with a micro-Nikkor 55mm f/2.8 lens using aperture f/8 and an infrared

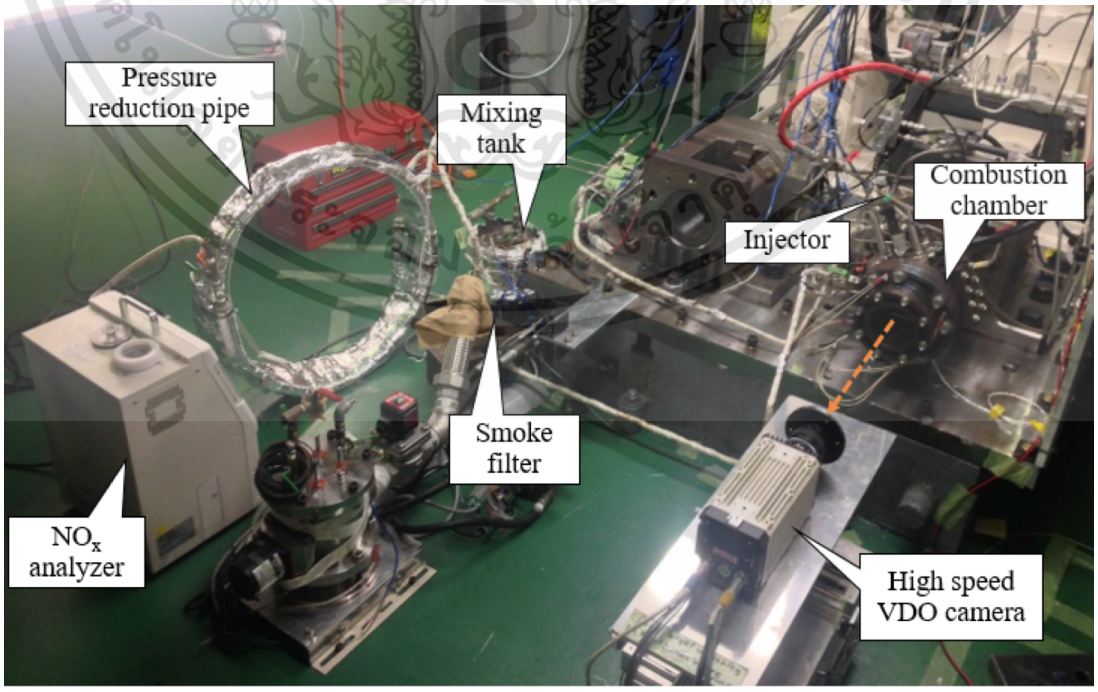

Fig. 4.1. Photograph of the two color method setup

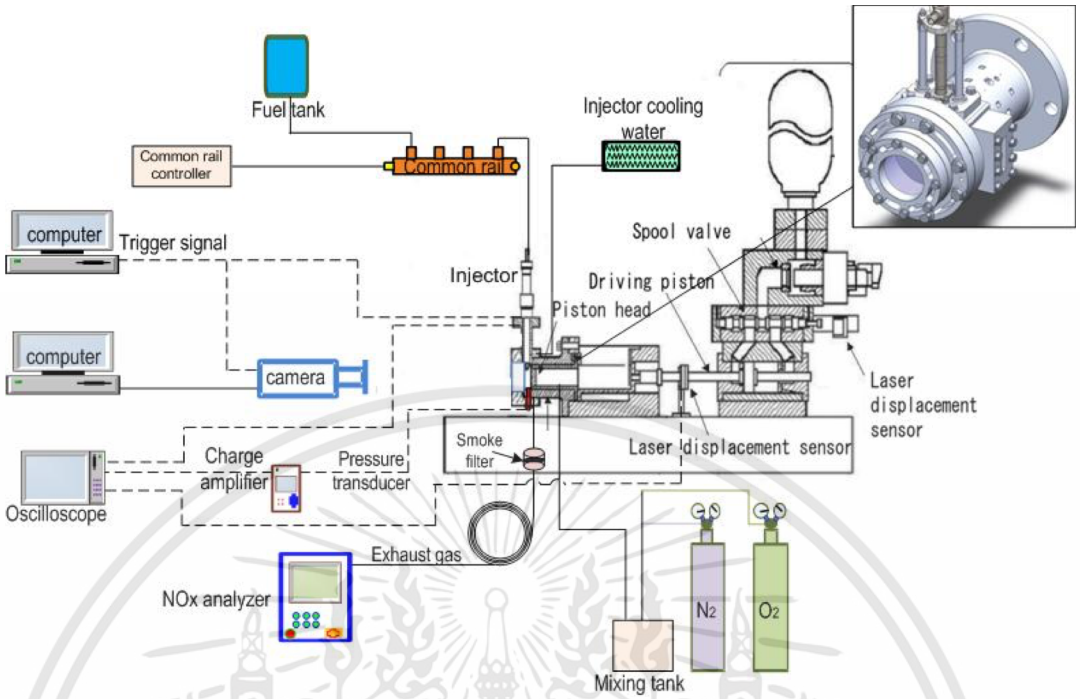

Fig. 4.2. Schematic representation of experimental apparatus

filter (SIGMA KOKI-HAF-50S-15H) to transmit only the visible wavelengths. The signals from the injector, camera trigger and RCEM were synchronized and recorded by an oscilloscope (YOKOGAWA DL 750) with 1x106 sampling/sec. Moreover, the smoke particulates were trapped by filter paper. After flowing out of filter paper, exhaust emissions were led to a pressure reduction pipe to drop gas pressure to 0.1MPa, then sucked to NO_x gas analyzer (NOA-7000, Fig. 4.3). The soot particles trapped by filter paper were measured by a smoke meter (SOKKEN-GSM3, Fig. 4.5). The soot contamination on paper filter for all fuels was illustrated in Fig. 4.4.

Measuring range	25-4000ppm in 8 steps
Linearity	Within ±2% of full scale
Response time	NOx (20s-60s)

Fig. 4.3. NO_x emission analyzer-NOA7000

Display range	0-100% filter blackening
Accuracy	±3%
Standard calibration papers: JIS % filter blackening: 0, 5, 10, 15, 20, 25, 30, 40, 50, 60, 70, 80	

Fig. 4.5. Smoke meter-Sokken (GSM3)

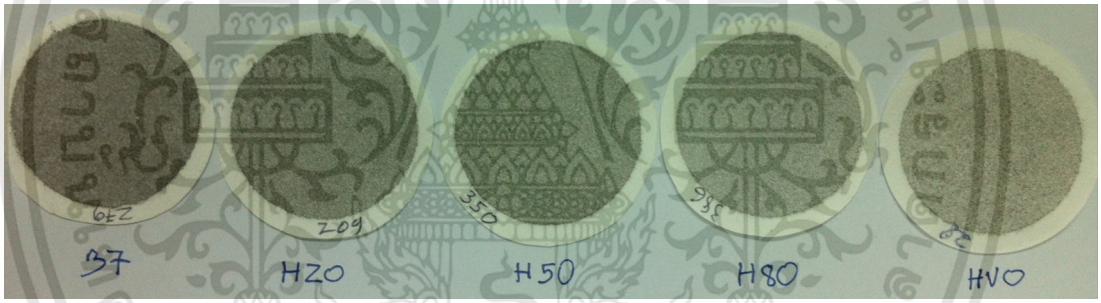

Fig. 4.4. The degree of soot contamination in filler

Table 4.1 tabulates the experimental conditions, in which the ambient pressure was 4.0MPa at TDC after compression, and the injection pressures were 80MPa and 120MPa, given the same amounts of injection for all five experimental fuels (the B7, the neat HVO, the 20%, 50% and 80% blended HVO fuels) by varying the injection duration. The O_2 concentrations of the intake gas were varied between 21% (the base condition), 15% and 10% to simulate the EGR condition. The chamber wall temperature remained constant at 453K±1K. The measurements were taken 10 times under each experimental conditions to verify the repeatability. Prior to each experiment, the fuel filters were replaced and the gas emissions devices were calibrated.

Table 4.1. Experimental combustion conditions

Parameters	Value	Unit
Fuels	B7, H10, H20, H50, H80, HVO	
Ambient pressure (P_a)	4.0	MPa
Rail Pressures (P_{inj})	80, 120	MPa
Amount of injection (m_{inj})	29.73	mg
O_2 concentrations (%O_2)	21, 15, 10	%
Ambient gas density	19.23; 19.07; 18.94	Kg/m^3
Single hole nozzle diameter (D_{inj})	0.2	mm
Wall temperature (T_w)	453	K

4.3.2. High-speed camera setup and temperature calibration

In this study, the high speed camera (NAC Memrecam Gx-1) was applied for two color method at 10,000fps as seen in Fig. 4.1. An aperture of f8.0 and shutter time of 3.0us were selected for camera setup. The high speed camera was coupled with a micro-Nikkor 55mm f/2.8 lens using an infrared filter (SIGMA KOKI-HAF-50S-15H) to transmit only the visible wavelengths. The optimal visuals of the luminous flames were realized by adjusting the camera-combustion chamber distance which was subsequently used in the calibration of the camera against the blackbody. The

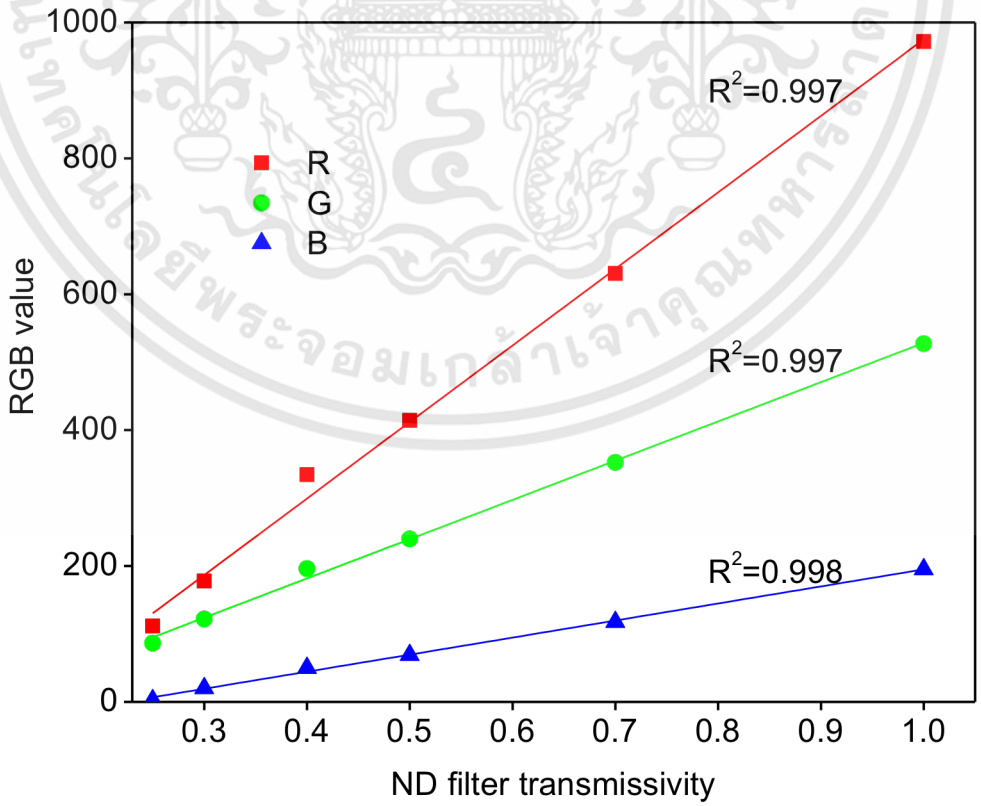

Fig. 4.6. Linearity between RGB value and ND filter transmissivity.

blackbody furnace was used as a calibration light source. An interval of 100^{0}C was applied as the rising step for blackbody furnace calibration from 900^{0}C to 2200^{0}C. Both blackbody furnace and pyrometer were used to accurately determine the reference temperatures. The visible light can be converted by CCD-detector in camera into three color band (Red-Green-Blue). With two in three color band, it is possible to calculate flame temperature and KL factor. In addition, the neutral density (ND) filters were utilized to reduce the light intensity of the flames and enhance the visuals. Fig. 4.6 shows the linearity between RGB value and ND filters transmissivity with R^2 value greater than 0.99. Two wavelengths used in this study are blue color (529nm) and red color (603nm). The flame temperature and KL factor can be determined by using Matlab code built from on Eq. (11).

4.3.3. Experimental fuels

In this research, there were five experimental fuel types: the commercial diesel fuel (B7) as the reference fuel, the neat HVO (HVO), the 20% (H20), 50% (H50) and 80% (H80) HVO by mass fraction blended with the B7 (Lapuerta *et al.*, [16]). Specifically, the fuels were experimented under the three O_2 concentrations (21%, 15%, 10%) except for the H80 whose experiments were carried out solely under the 21% O_2 environment to track the developing propensity of result. The fuels were supplied by Thailand's PTT Research and Technology Institute. Table 4.2 tabulates the properties of the experimental fuels. By comparison, the viscosity, density, surface tension, and distillation temperatures (T50, T90) of the HVO-based fuels are lower than those of

Table 4.2. The properties of the experimental fuels

Fuel	B7	H20	H50	H80	HVO
Derived cetane index	60.43	63.37	68.32	73.44	76.89
Viscosity @ 40^{0}C(mm^2/s)	3.235	3.088	2.901	2.740	2.637
Density @ 15^{0}C(Kg/m^3)	823.5	814	799.9	786.5	778
Surface tension (mN/m)	26.38	25.89	25.56	24.91	24.84
Heating value (Mj/kg)	45.86	46.04	46.38	46.55	46.86
Initial boiling point (^{0}C)	157.2	158.8	160.4	159.8	160.8
Distillation T10 (^{0}C)	207.7	210.7	216.3	223.1	227.4
Distillation T50 (^{0}C)	287.9	284.5	281.4	279.2	278.2
Distillation T90 (^{0}C)	352.3	345.2	327.4	303.5	293.2
Sulfur content (%)	0.018	0.0014	-	-	0.0001
Flash point (^{0}C)	61.3	63	65.8	67.8	69
Pour point (^{0}C)	-2	-5	-	-	-6
Formula	$C_{14.28}H_{26.43}$	$C_{14.23}H_{27.17}$	$C_{14.16}H_{28.27}$	$C_{14.09}H_{29.36}$	$C_{14.03}H_{30.1}$

the B7. These properties influence the friction flow in the injector, the fuel droplet size, the spray angle, penetration, breakup, atomization and vaporization (Borhanipour *et al*., [66]; Pandey *et al*., [67]). Meanwhile, the heating value and the cetane index of the HVO-based fuels are higher than those of the B7, indicating the fuel consumption and combustion efficiency. In fact, the compositional disparities between the diesel and HVO-based fuels could be attributed to the latter's branched-chain paraffin and higher ratios of hydrogen and carbon.

4.4. Results and discussion

4.4.1. Combustion Characteristics

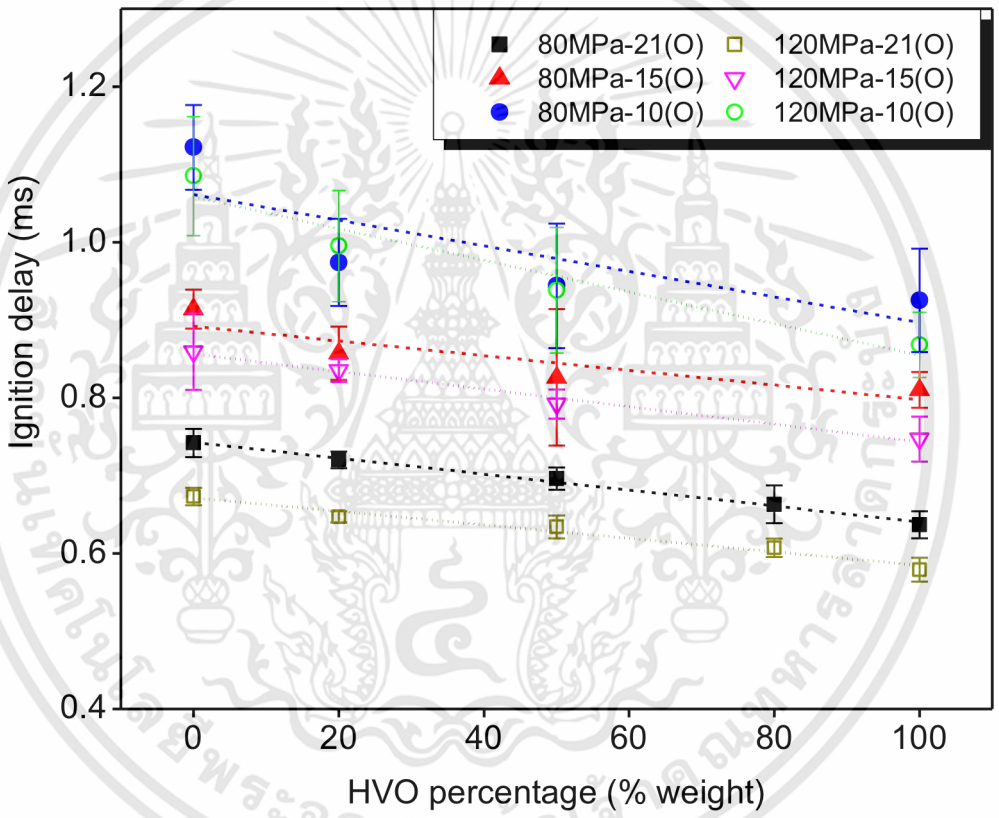

Fig. 4.7. Ignition delay of the experimental fuels under variable injection pressures (80 and 120MPa) and oxygen concentrations (21%, 15%, 10%).

In this research, the combustion characteristics focus on the ignition delay, the heat release rate, and the integral heat release. The ignition delay refers to the interval time between the start of injection signal and the start of heat release. It plays a crucial role in the combustion process of the DI engines. Fig. 4.7 compares the ignition delays of the experimental fuels, given the same injection quantity, under the 80MPa and 120 MPa injection pressures and the 21%, 15% and 10% O_2 concentrations. In the figure, the higher HVO fraction contributed to the shorter ignition delay under all experimental conditions, a phenomenon attributable to the high cetane value of the HVO (Dale *et*

al., [126]; Nishiumi *et al*., [127]). In addition, the higher injection pressure (120MPa) led to the shorter ignition delay due to the higher injection velocity and faster breakup, which facilitated the spray atomization and vaporization (Dodge *et al*., [89]). However, the lower O_2 level prolonged the auto-ignition timing due to the lower air entrainment in the fuel spray, resulting in the lower reaction rate (Xiaojie *et al*., [128]; Haifeng *et al*., [129]). By comparison, the HVO's cetane value, surface tension and viscosity were respectively 27.2% higher, 5.8% lower, 18.48% smaller than those of the B7 fuel. This led to the HVO's shorter ignition delays of about 14.1%, 11.3% and 17.5% (at the 80MPa injection pressure) and 13.9%, 13.03% and 20% (at the 120MPa injection pressure), given the 21%, 15% and 10% O_2 concentrations, respectively, in comparison with the diesel fuel. Nevertheless, the impact of different injection pressures on the ignition delay was smaller than that of different O_2 concentrations.

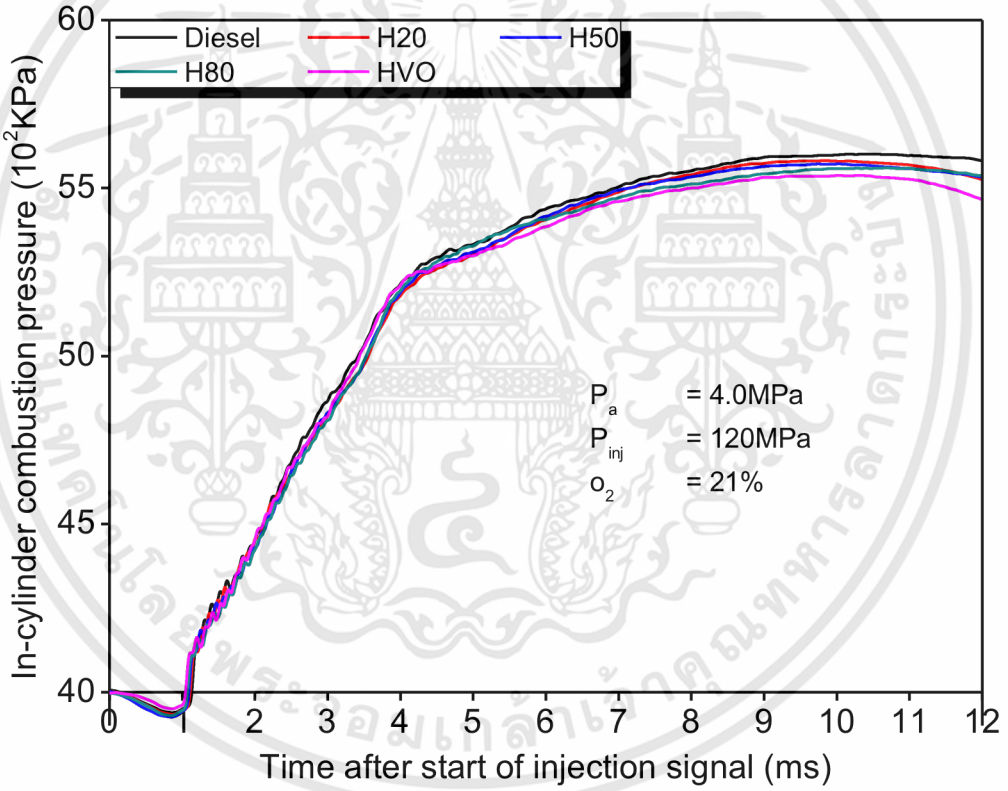

Fig. 4.8. In-cylinder combustion pressure for test fuels at the base condition (21% O_2), given at 120MPa of injection pressure.

Fig. 4.8, Fig. 4.9, and Fig. 4.10 show the pressure in the combustion chamber corresponding to the the change of HVO mixed percentages in blend, the various oxygen concentrations in the charged gas, and the different injection pressures, respectively. The results indicated that all the test fuels have quite similar pressure evolution. However, it is clearly seen that HVO has lower pressure rise than diesel due

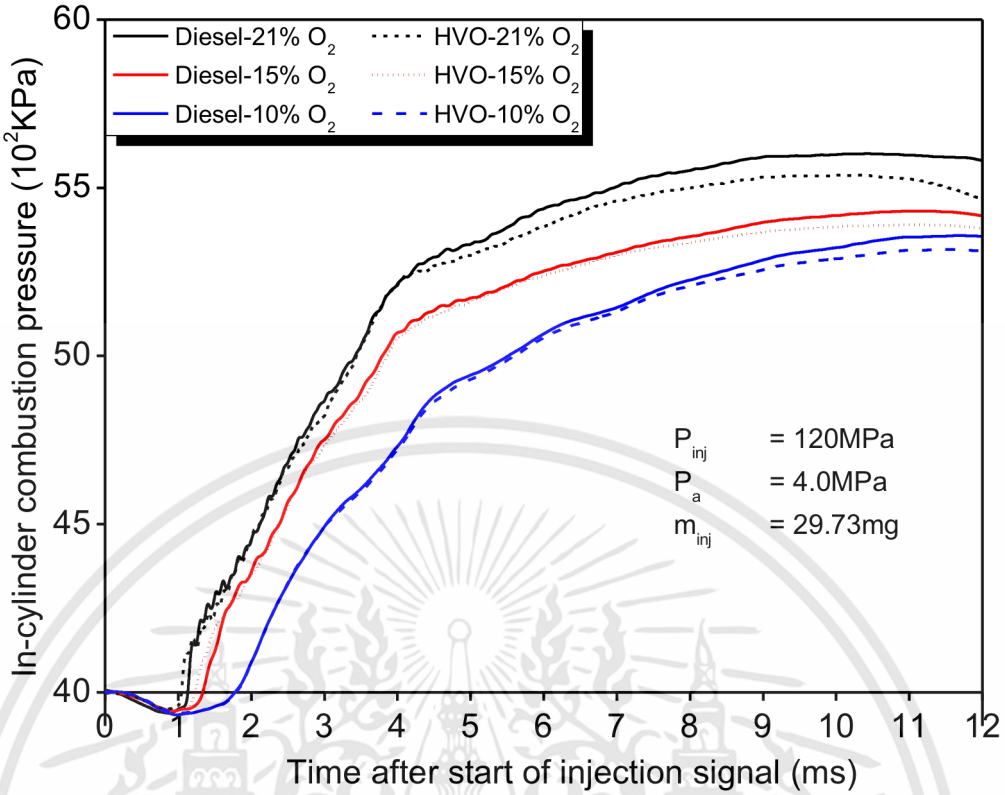

Fig. 4.9. In-cylinder combustion pressure of diesel and HVO at 120MPa of injection pressure, under various EGR conditions.

to smaller ignition delay. It means that different fuel properties have the different ignition delay which results in different accumulative fuel in the premixed-combustion phase. In other words, the longer ignition delay provides longer residence time for air-fuel mixing. Therefore, it is possible to provide more combustible mixure resulting in a rapid pressure rise when combustion starts. In addition, in Fig. 4.9, the pressure rise significantly reduced because the mixing rate between fuel vapor and surrounding air in the chamber was poorer under higher EGR conditions. This causes less combustible mixture and slower reaction rate. In the comparison between HVO and diesel under 21% O_2 (Fig. 4.10), given at two injection pressures (80MPa and 120MPa) under constant injection quantity, it is shown that higher pressure rise corresponds to higher injection pressure. This can be explained by more air into the fuel spray leading to better fuel mixing.

Fig. 4.11 indicates the heat release rate of test fuels at base condition (21% O_2), given at 120MPa injection pressure, as representative. The result shows that all fuels have similar rate of heat release trend. Although B7 has the slightly higher heat release rate, the compensative influence of narrow distillation and higher heating value of HVO

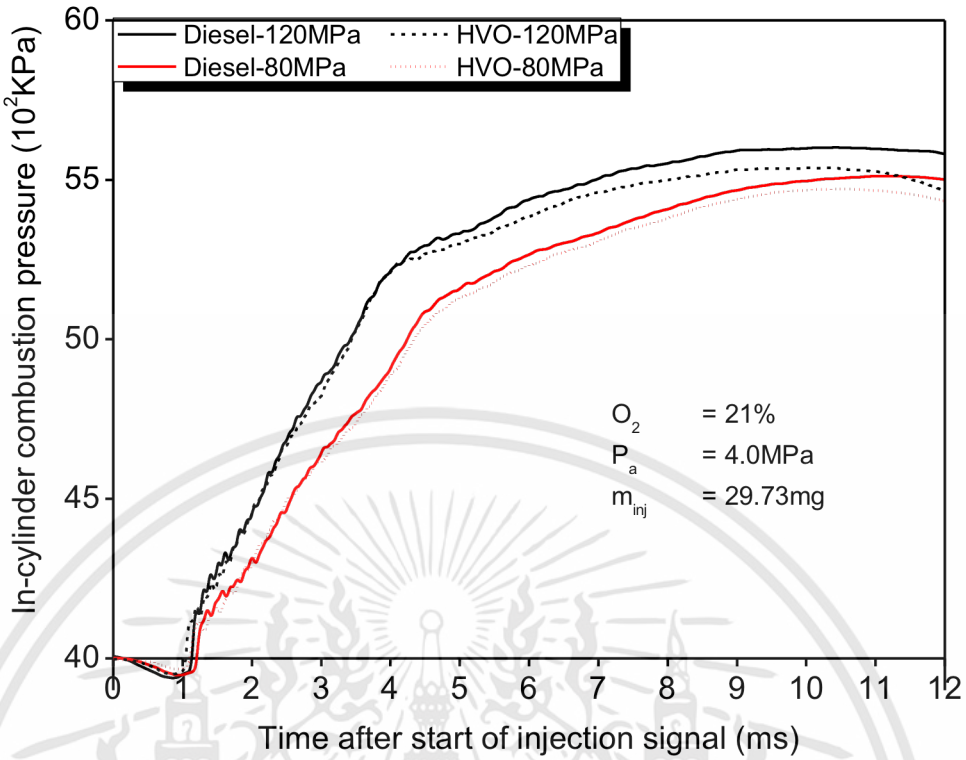

Fig. 4.10. In-cylinder combustion pressure of diesel and HVO at the base condition (21% O_2), under different injection pressures.

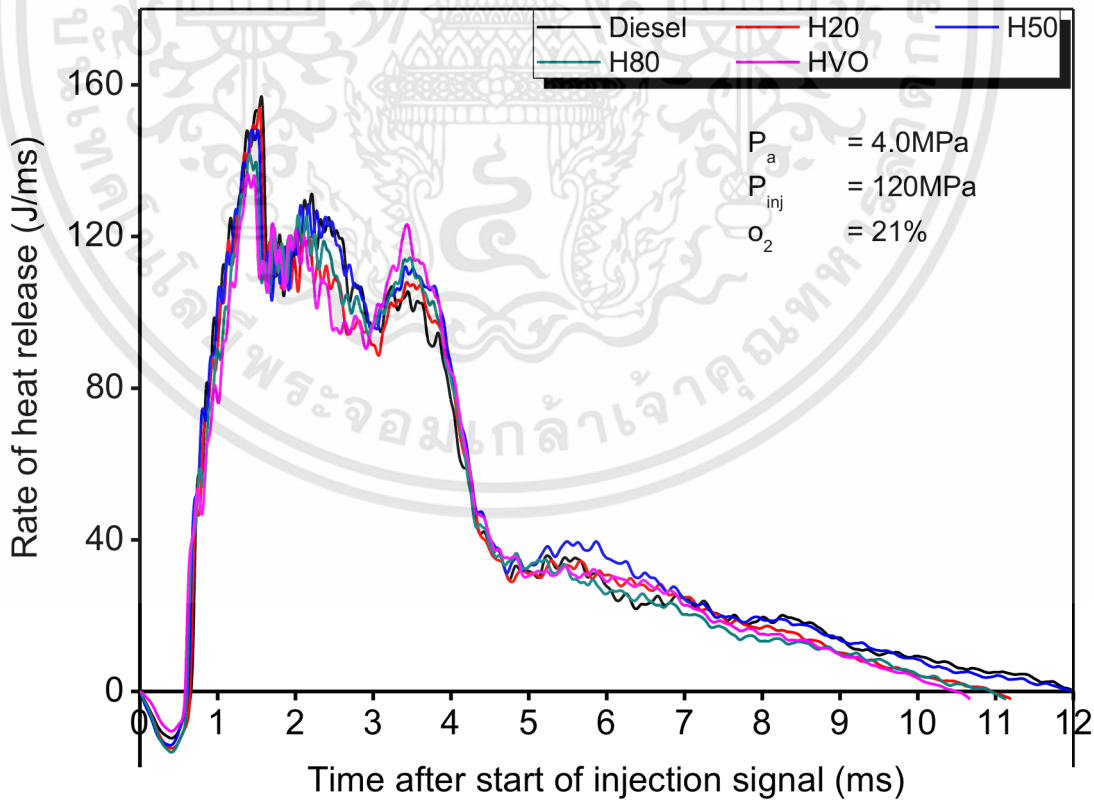

Fig. 4.11. ROHR for test fuels at the base condition (21% O_2), given at 120MPa.

causes the difficult distinguish of the heat release rate of HVO and blend clearly.

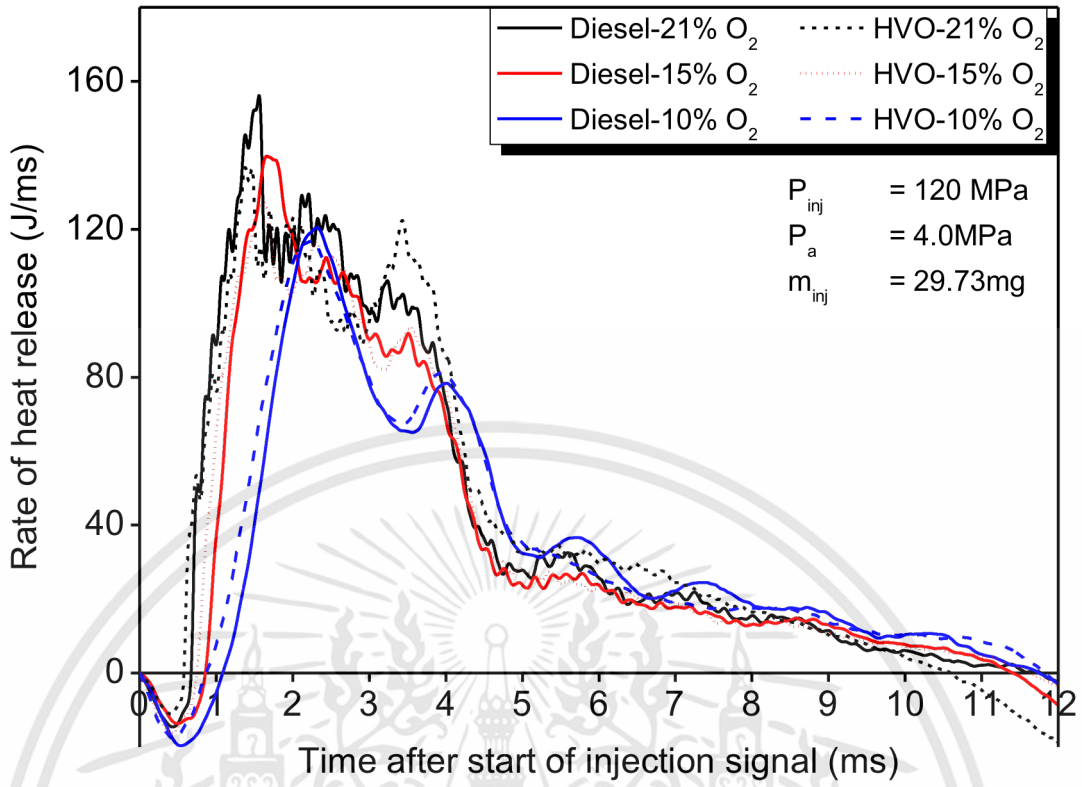

Fig. 4.12. Heat release rate of diesel and HVO at injection pressure of 120MPa under various EGR conditions.

Besides, due to the similarity in the heat release rates between the experimental fuels, this research deliberately discussed only the findings associated with the neat HVO (i.e.

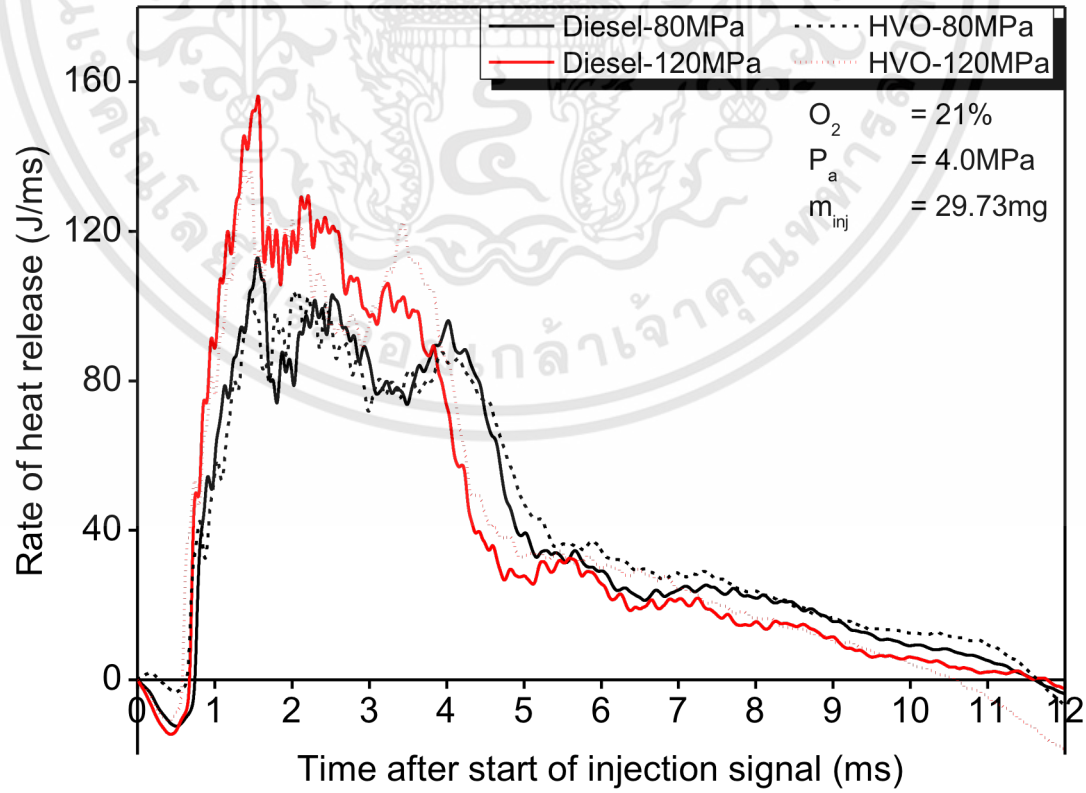

Fig. 4.13. ROHR of diesel and HVO at 21% O_2 under different injection pressures.

the HVO) and B7 diesel fuels under the three O_2 concentrations, given the 120MPa injection pressure (Fig. 4.12); and the two injection pressures, given the 21% O_2 concentration (Fig. 4.13). Since the longer ignition delay affords a longer residence time for the air-fuel mixing, the diesel fuel thus exhibited a slightly higher heat release rate than the HVO. In Fig. 4.12, the premixed combustion phase became longer and the heat release weaker as the O_2 concentration decreased. The findings are attributable to the less effective collisions between oxygen and the fuel vapor, resulting in the low combustion efficiency (Fujimoto *et al.*, [130]). Meanwhile, the reaction rate increased and the diffusion phase became shorter as the injection pressure rose from 80MPa to 120MPa (Fig. 4.13), giving rise to the improved air-fuel mixing (Heywood, [7]).

The effects of variable oxygen concentrations on the integral heat release of the experimental fuels, given the 120MPa injection pressure calculated by Simpson's 3/8 rule is illustrated in Fig. 4.14. In the figure, the higher HVO fraction in the blend minimally influenced the integral heat release, due to the balancing effect between the shorter ignition delay and the higher heating value of the HVO. In addition, the lower oxygen concentration contributed to the lower integral heat release, as a result of the lower reaction rate (Xiaojie *et al.*, [128]). On average, the integral heat release rates under the 10% and 15% O_2 concentrations declined by 17.3% and 11.5%, respectively, vis-à-vis under the 21% O_2.

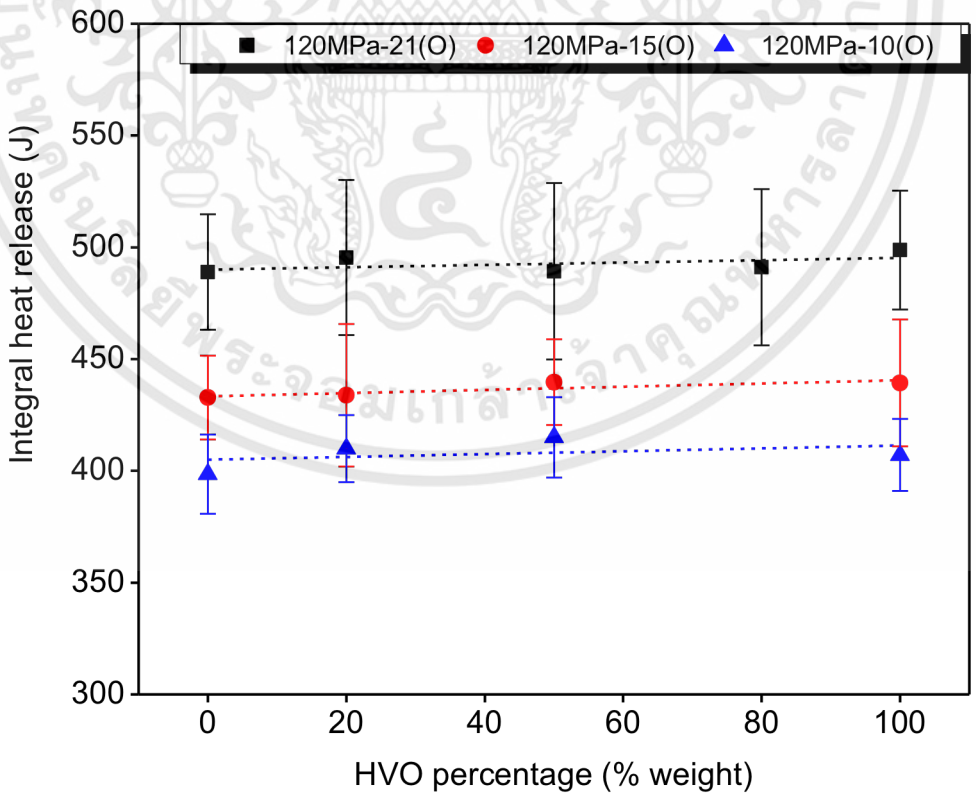

Fig. 4.14. Integral heat release of the experimental fuels under variable O_2 concentrations given the 120MPa injection pressure.

Fig. 4.15 compares the integral heat release of the HVO and diesel fuels (B7) under variable O_2 concentrations and injection pressures. Generally, the higher injection pressure contributes to the better air-fuel mixing and the subsequent higher heat release. The increase in the injection pressure from 80MPa to 120MPa increased the integral heat release, on average, by 4.2%, 5.5% and 14.5%, under the 21%, 15%, and 10% O_2 concentrations, respectively. Importantly, the significant difference between the total heat release under the 80MPa and 120MPa injection pressures, given the 10% O_2 concentration, validates the essential role of the high injection pressure in the combustion efficiency. The enhanced combustion efficiency under the higher injection pressure was largely attributable to the improved air entrainment, higher spray velocity, smaller droplet size, wider spray angle and faster breakup (Hulkkonen *et al.*, [33]; Dodge *et al.*, [89]; Wang *et al.*, [114]).

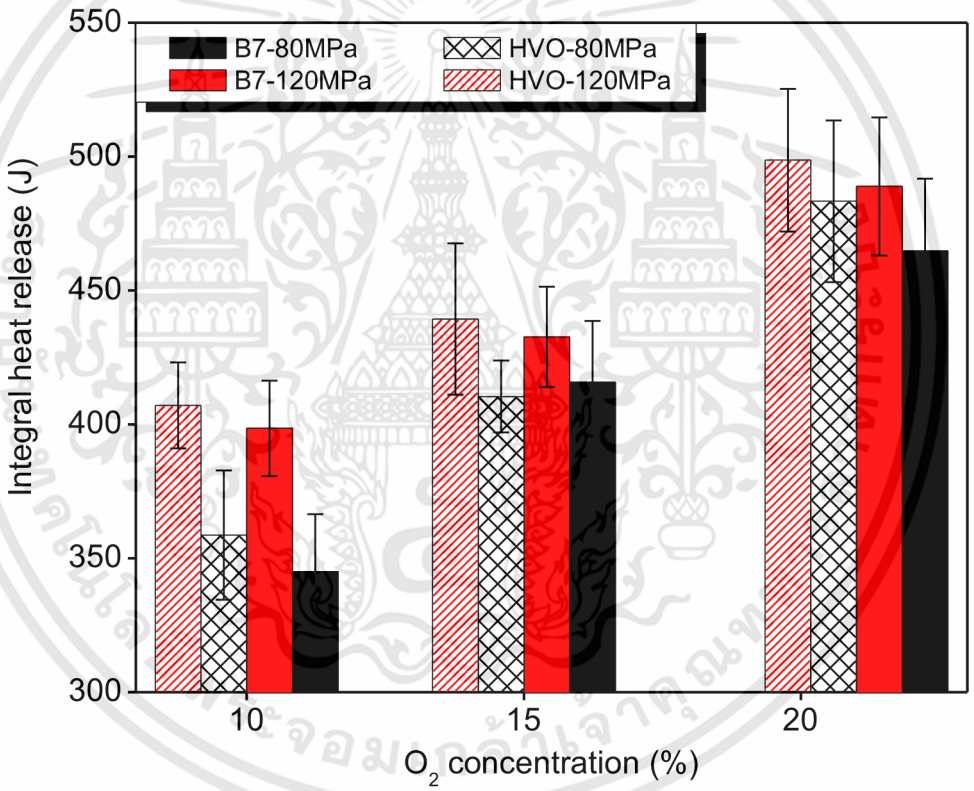

Fig. 4.15. Integral heat release of the HVO and diesel fuels under variable O_2 concentrations and injection pressures.

Fig. 4.16 shows the apparent heat release fraction efficiency of test fuels under 120MPa injection pressure and different ambient oxygen concentrations. The apparent heat release fraction efficiency is the ratio of total heat release due to combustion and the heat input from injection fuel. The results show that the value of the apparent heat release fraction efficiencies of HVO and blends are equivalence to B7. This tendency is similar to the result of Fig. 4.14.

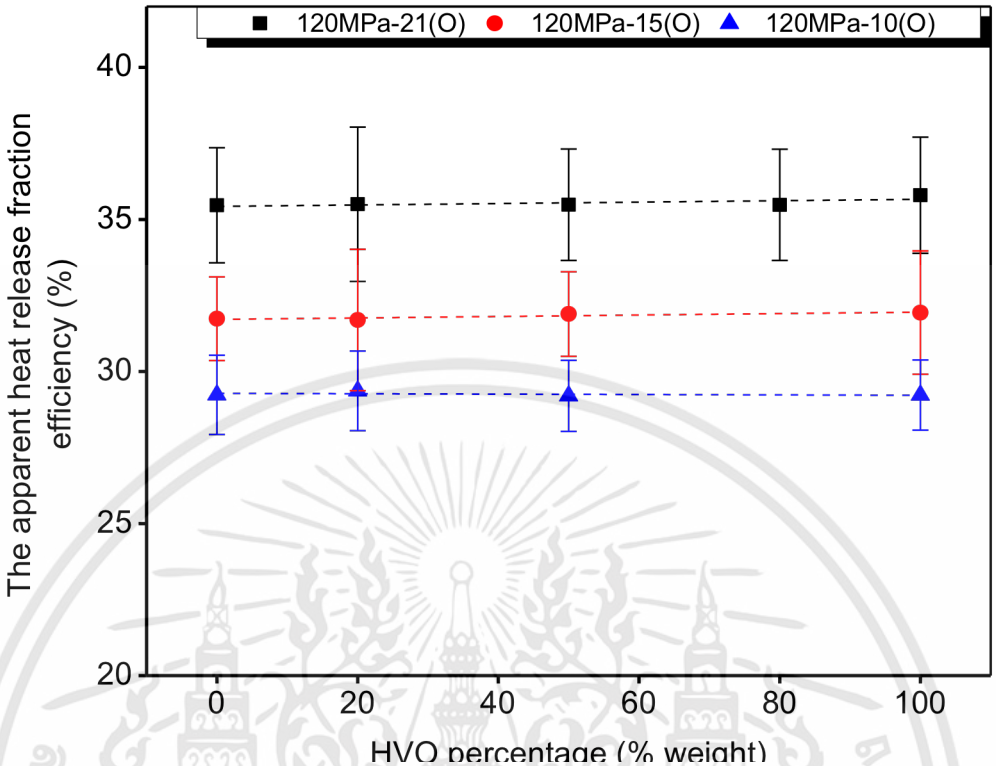

4.4.2. Spatial and temporal distributions of the flame temperature and soot density-KL factor

Fig. 4.17 illustrates, as representative, the spatial distribution of the in-chamber flame temperatures of the HVO and B7 fuels under the experimental oxygen concentrations and injection pressures. In the figure, the first flame image could be clearly captured at 1.1ms after the start of injection signal for the HVO under the higher injection pressure (120MPa) and 21% O_2 concentration. The finding verifies the essential role of the high injection pressure and the HVO's high cetane number and narrow distillation in the rapid realization of the mixture homogeneity and the subsequent early premixed combustion phase. Meanwhile, the slow emergence of the flame intensity and the weak flame luminosity were observed under the 15% and 10% O_2 concentrations, respectively. This could be attributed to the lower air entrainment under the low O_2 concentrations, which subsequently led to the less formed combustible mixture and lower combustion temperature (Zhang *et al.*, [112]; Haifeng *et al.*, [129]). Thus, the NO_x production is eliminated and the soot oxidation is suppressed. Moreover, in Fig. 4.17, the higher injection pressure also contributed to the wider combustion area and slightly darker flame color, due to the larger spray

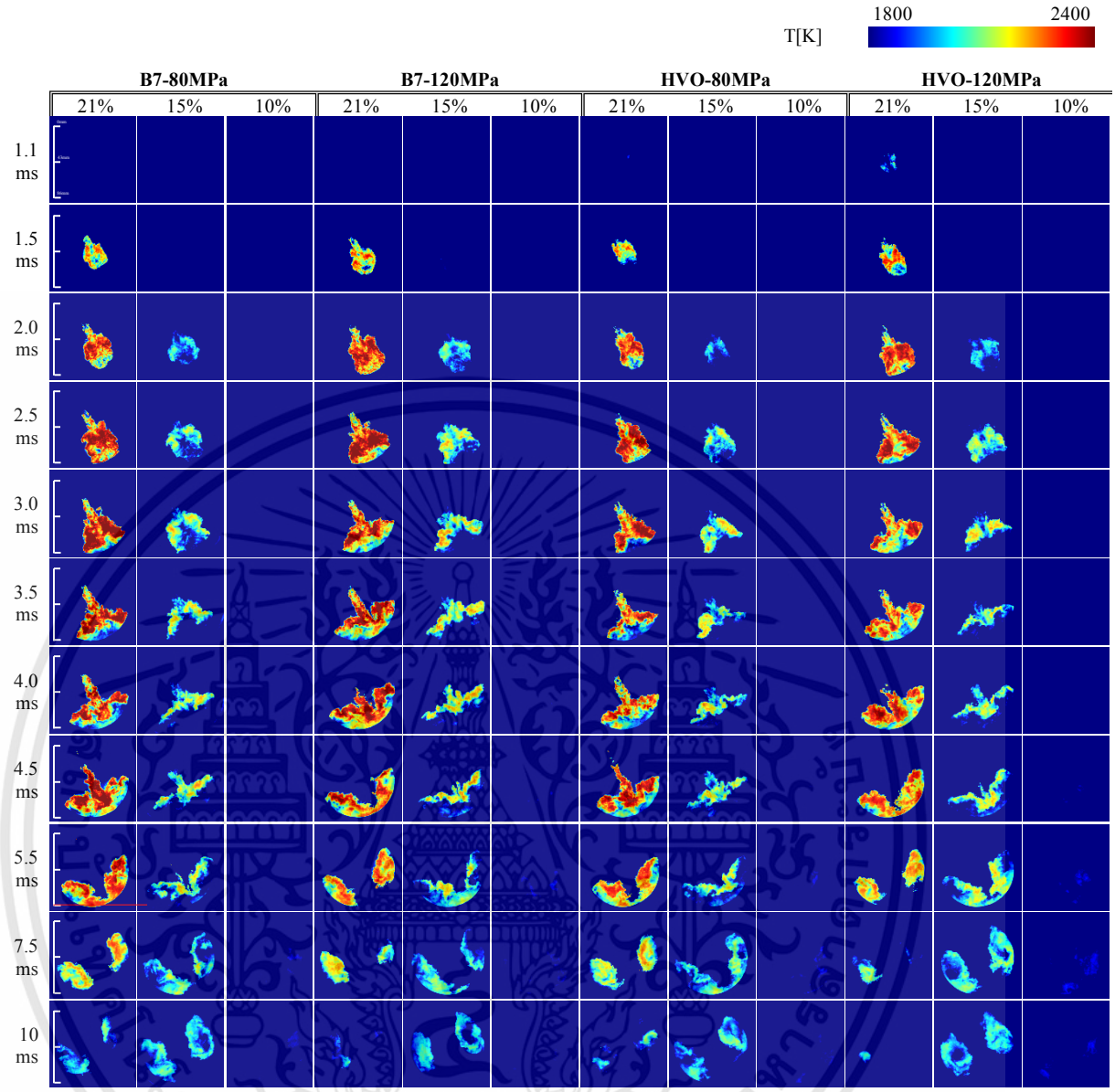

Fig. 4.17. The spatial distribution of the flame temperature of the HVO and diesel (B7) fuels under variable injection pressures and O_2 concentrations.

angle, longer lift-off length and faster evaporation (Hulkkonen *et al.*, [33]; Dernotte *et al.*, [71]; Pickett *et al.*, [113]). In addition, since the longer ignition delay induces more accumulative fuel in the premixed combustion phase, the flame of the diesel fuel was darker than that of the HVO. The flame images were subsequently used to predict the NO_x-forming propensity.

In the combustion, the injected fuel first atomizes and mixes with the surrounding air near the nozzle, where the combustion occurs. The flames then move along the chamber wall following the direction of the nozzle exit. This observation has contrary trend with Heifeng's study [131] which reported that the main combustion occurred at near wall region and followed by flame propagating towards the nozzle. In Fig. 4.17, the larger areas of the high flame temperature were captured between 2.0ms and

4.5ms after the start of injection signal, which was the diffusion combustion phase. Furthermore, the high flame temperature regions were concentrated around the upstream spray flame, due to the higher fuel-vapor concentration in the upstream regions which enhanced the local flame temperature (Wang *et al.*, [114]). The spray flame tail trailed off once the injection was terminated (around 4.0ms). Toward the end of the combustion, the flame split into two parts as a result of the impinging on and rebounding off the wall chamber.

Fig. 4.18 illustrates, as representative, the spatial distribution of the soot density-KL factor of the HVO and diesel (B7) fuels under the experimental oxygen concentrations and injection pressures. In the figure, the soot formation was initially accelerated during the premixed combustion phase under both the 21% and 15% O_2 concentrations. Similar to the flame evolution, the higher soot density regions

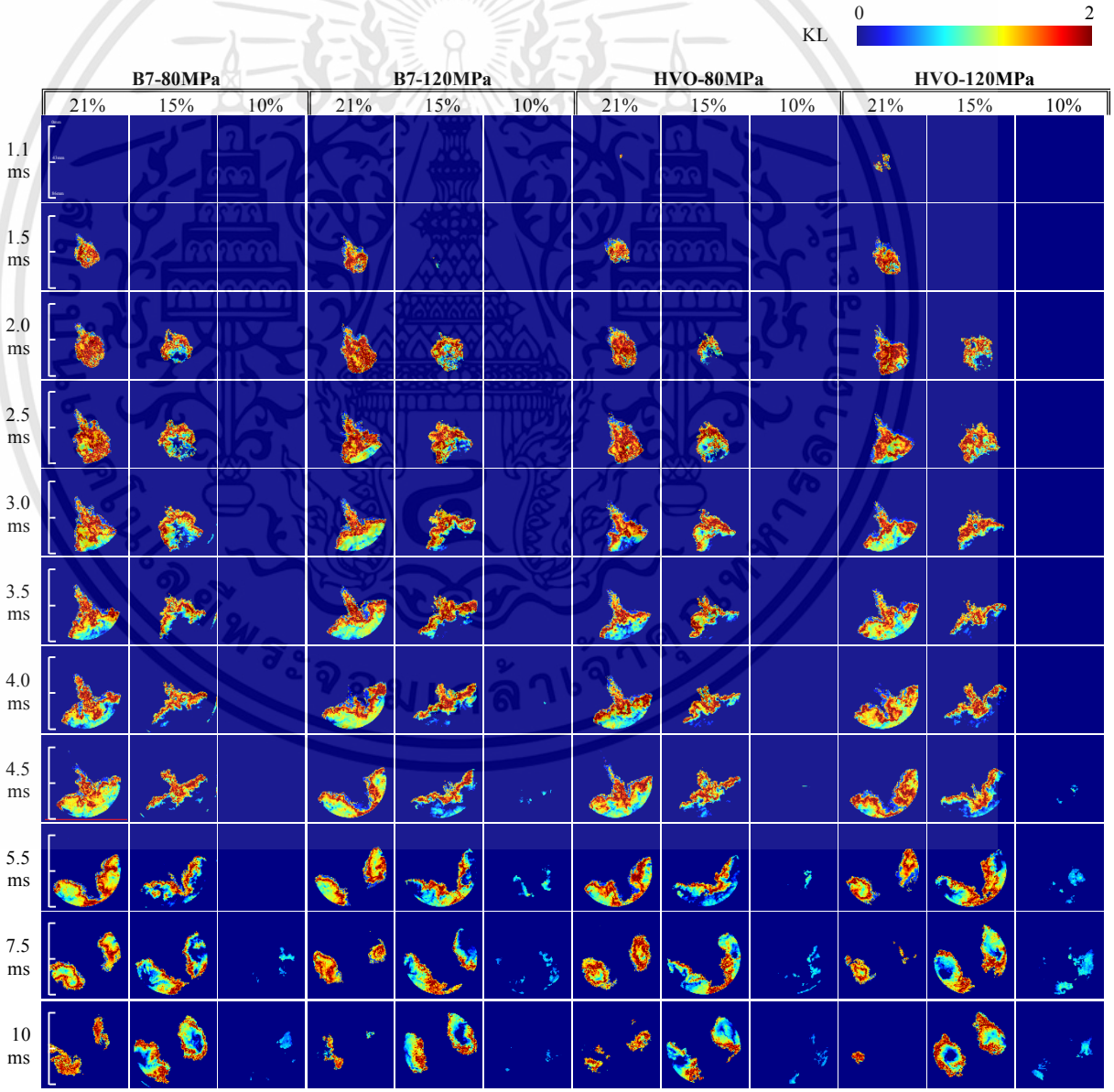

Fig. 4.18. The spatial distribution of the KL factor of the HVO and diesel (B7) fuels under variable injection pressures and O_2 concentrations.

appeared on the upper section of the spray flame because of the high fuel concentration and low oxygen. In addition, the findings suggested that the soot formation was influenced by the flame temperature (Idicheria *et al*., [132]). In the figure, the decrease in the KL light intensity and the slow emergence of soot were observed under the lower O_2 concentrations, especially under the 10% O_2 condition. The findings could be attributed to the poor combustible mixture, low flame luminosity and stagnant auto-ignition timing. Interestingly, given the 21% O_2 concentration, the soot density under the 120MPa injection pressure minimally differed from that under the 80MPa injection pressure, regardless of the fuel. However, the soot formation and oxidation rates under the 120MPa were considerably faster than under the 80MPa, due to the former's higher injection velocity and the subsequent more turbulent spray (Dodge *et al*., [89]; Wang *et al*., [114]). Specifically, under the 21% O_2 concentration, the soot formation appeared earlier and more noticeable under the higher injection pressure (120MPa) for the HVO than for the diesel fuel, a phenomenon that resembles the flame temperature. The result suggested that the early soot formation was related to the shorter ignition delay.

Fig. 4.19 (a)-(b) respectively illustrate the temporal flame temperatures of the HVO and diesel (B7) fuels under the experimental O_2 concentrations and injection pressures. In Fig. 4.19(a), the maximum flame temperatures (above 2200K) were observed at around 2.2ms after the start of injection signal for both fuels under the 21% O_2 condition. By comparison, the flame temperatures associated with the diesel fuel were higher under all experimental O_2 concentrations, due to the lengthened ignition delay. However, this could lead to higher NO_x emissions for the diesel fuel (Gomes *et al*., [133]). In addition, the lower O_2 concentration significantly reduced the flame temperature (Fig. 4.17) as the low oxygen entrainment resulted in the poor combustible reaction. Furthermore, the maximum flame temperatures under the 15% and 10% O_2 concentrations were approximately 230K and 424K lower, compared to

that under the 21% O_2 concentration, indicating the significant reduction in the NO_x

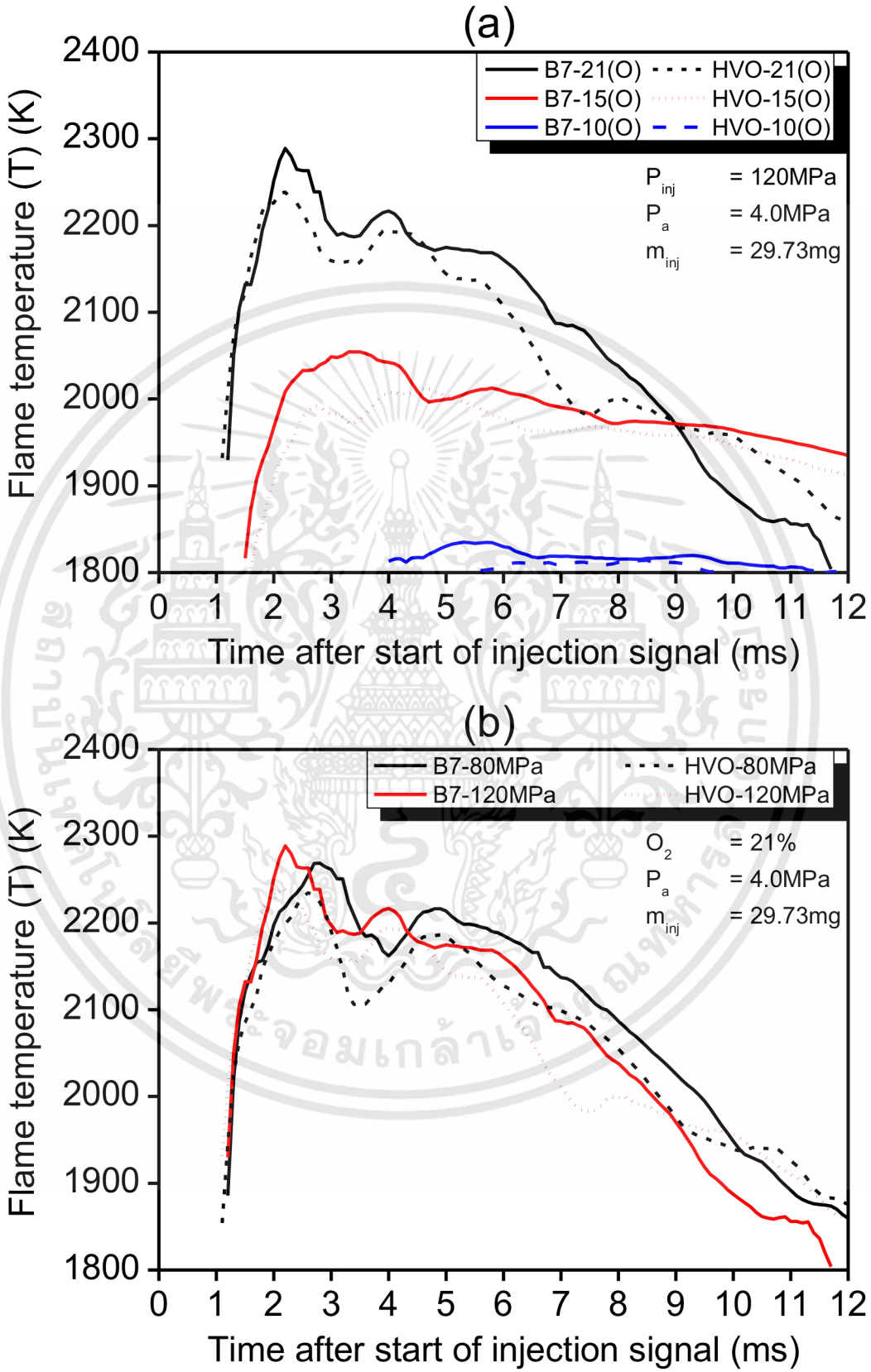

Fig. 4.19. The temporal flame temperatures of the HVO and diesel fuels under variable: (a) O_2 conditions, (b) injection pressures.

emissions under the lower O_2 environment. Meanwhile, in Fig. 4.19(b), the difference

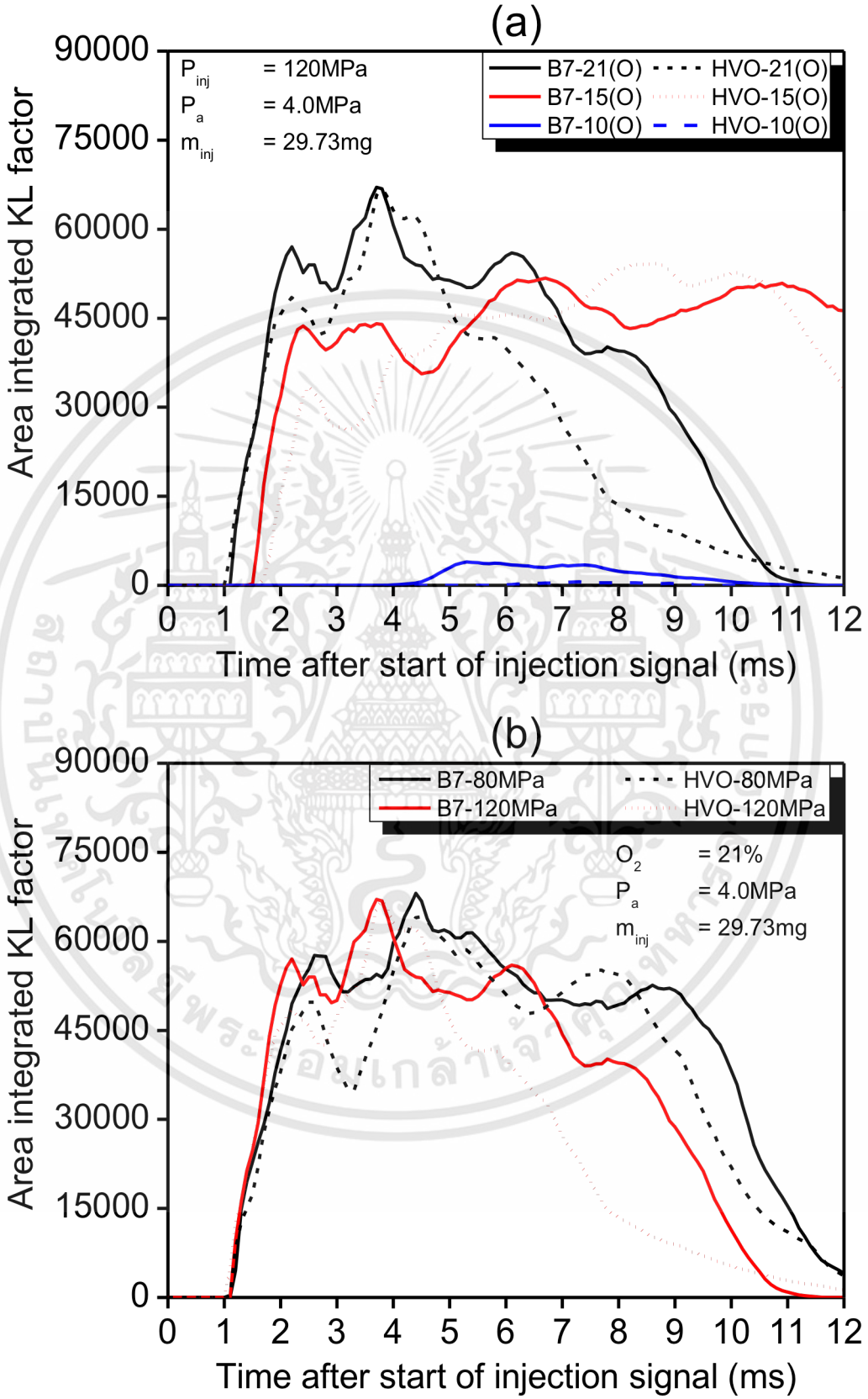

Fig. 4.20. The temporal variation of the integrated KL factor of the HVO and diesel fuels under variable: (a) O_2 concentrations, (b) injection pressures.

in the flame temperatures between both injection pressures under same fuel type was negligible. The higher injection pressure (120MPa) nevertheless contributed to the early peak of the flame temperature, which subsequently resulted in the high NO_x emissions. This is consistent with the heat release rate results.

Fig. 4.20 (a)-(b) respectively depict the evolution of the area integrated KL factor of the HVO and diesel fuels under the experimental O_2 concentrations and injection pressures. In Fig. 4.20(a), under the 21% O_2 environment, the soot formation appeared in the premixed combustion phase. The initial peak of the KL factor was attributed to the higher soot formation rate in relation to the soot oxidation rate. The soot formation continued in the diffusion phase until the highest peak was reached, indicating the soot formation-soot oxidation equilibrium, which in turn was influenced by the flame temperature and oxygen entrainment. Nevertheless, the KL summation decreased due to the dominance of the soot oxidation as the flame spread and more air was entrained. The soot evolution of this current research is consistent with (Pickett *et al*., [113]; Fujimoto *et al*., [130]). The soot formation and oxidation rates of the diesel fuel were respectively higher and slower than those of the HVO under all experimental conditions. Specifically, under the 15% O_2 concentration, the soot formation rate decreased due to the lower flame temperature and lower reaction rate than under the 21% O_2, but the process was prolonged due to the increased residence time, consistent with (Xiaojie *et al*., [128]; Idicheria *et al*., [132]). Meanwhile, under the 10% O_2, the soot density was barely detectable due to the weak flame luminosity. Interestingly, the improved spray atomization and combustible mixture under the 120MPa injection pressure accelerated the appearance of the first peak of the soot and the soot oxidation rate, in relation to under the 80MPa (Fig. 4.20(b)). The substantially shorter soot oxidization process of the HVO under the 120MPa injection pressure was attributable to the enhanced injection velocity and beneficial vaporization characteristics of the HVO. Furthermore, the shorter period of the soot oxidation implies that the soot-out was lower under the higher injection pressure.

4.4.3. Soot and NO_x concentrations

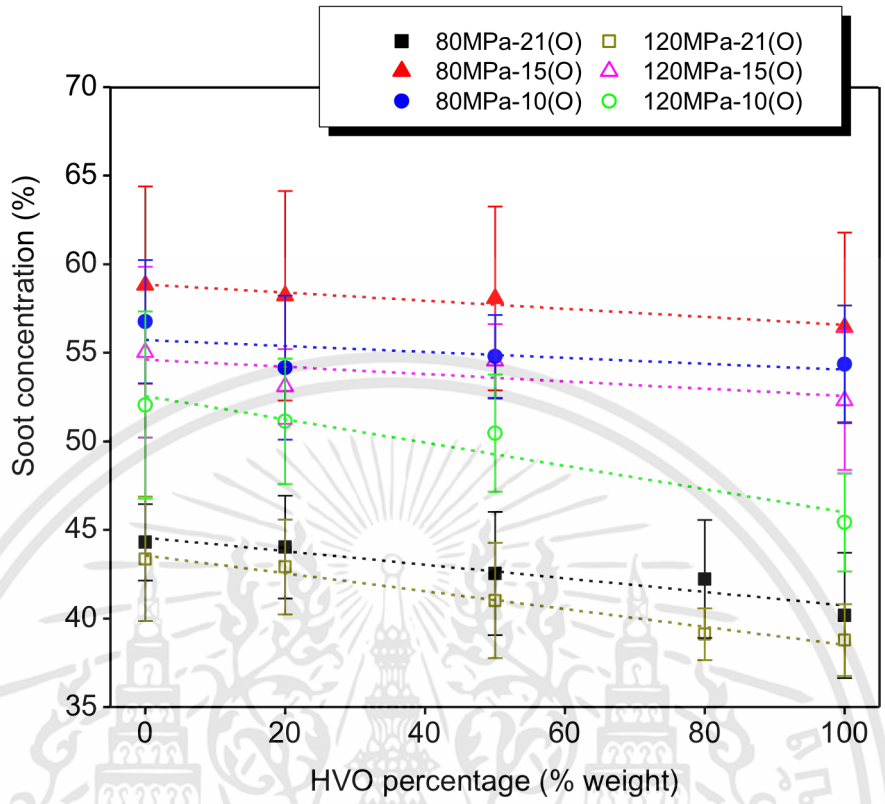

Fig. 4.21. Soot concentrations of the HVO and diesel fuels under variable O_2 concentrations and injection pressures.

Fig. 4.21 illustrates the soot concentrations of the experimental fuels under the various O_2 concentrations and injection pressures. In the figure, the soot level and the HVO percentage were inversely correlated under all experimental conditions. Specifically, given the 21% O_2 concentration, the HVO lowered the soot concentrations by 9.3% and 10.5% under the 80MPa and 120MPa injection pressures, in comparison with the diesel fuel. This could be attributed to the higher cetane number and lower distillation of the HVO. The improved fuel properties resulted in the less unburned fractions and better evaporation in the combustion chamber (Jaroonjitsathian *et al.*, [34]; Nishiumi *et al.*, [127]). In addition, at the 21% O_2, the soot levels under the two injection pressures were minimally different (approximately 3%). In fact, the lower oxygen concentration and the subsequent lower air entrainment were largely responsible for the significant rise in the soot-out concentration (Idicheria *et al.*, [132]). This obtained result has different trend with Haifeng's finding which reported that total soot mass for oxygenated biofuels was reduced as declining ambient oxygen concentration (21%, 16%, and 10.5%) under 800K ambient temperature condition (Haifeng *et al.*, [134]). Moreover, under the 120MPa injection pressure, the soot levels increased by 26.9% and 15.13% for the diesel fuel; and 34.9% and 13.5% for the HVO, given the 15% and 10% O_2 concentrations, respectively, relative to under the 21% O_2.

Interestingly, the highest soot concentration was observed under the 15% O_2 concentration as the lower oxygen concentration induced the incomplete combustion, the low flame temperature and the longer residence time in the soot forming regions (Xiaojie *et al.*, [128]; Haifeng *et al.*, [129]; Idicheria *et al.*, [132]). More importantly, the lower soot concentration as the HVO percentage increased resembles the results on the spatial and temporal distributions of the flame temperature and the KL density. Moreover, under the low oxygen concentration, the higher pressure differential increased the air entrainment and enhanced the soot oxidization process. Therefore, the difference in soot reduction was clearly seen between both injection pressures under low O_2 concentration.

Fig. 4.22 illustrates the NO_x concentrations of the experimental fuels under the various O_2 concentrations and injection pressures. In the figure, the NO_x concentrations were inversely correlated to the HVO percentage in the blend. In comparison with the diesel fuel, the neat HVO reduced the NO_x concentration by 35% and 25% under the 80MPa and 120MPa injection pressures, respectively, given the 21% O_2 concentration. On the other hand, the NO_x concentration was positively correlated to the O_2 concentration. By comparison, the NO_x concentrations under the 10% and 15% O_2 environments were noticeably lower than that under the 21% O_2, given the identical

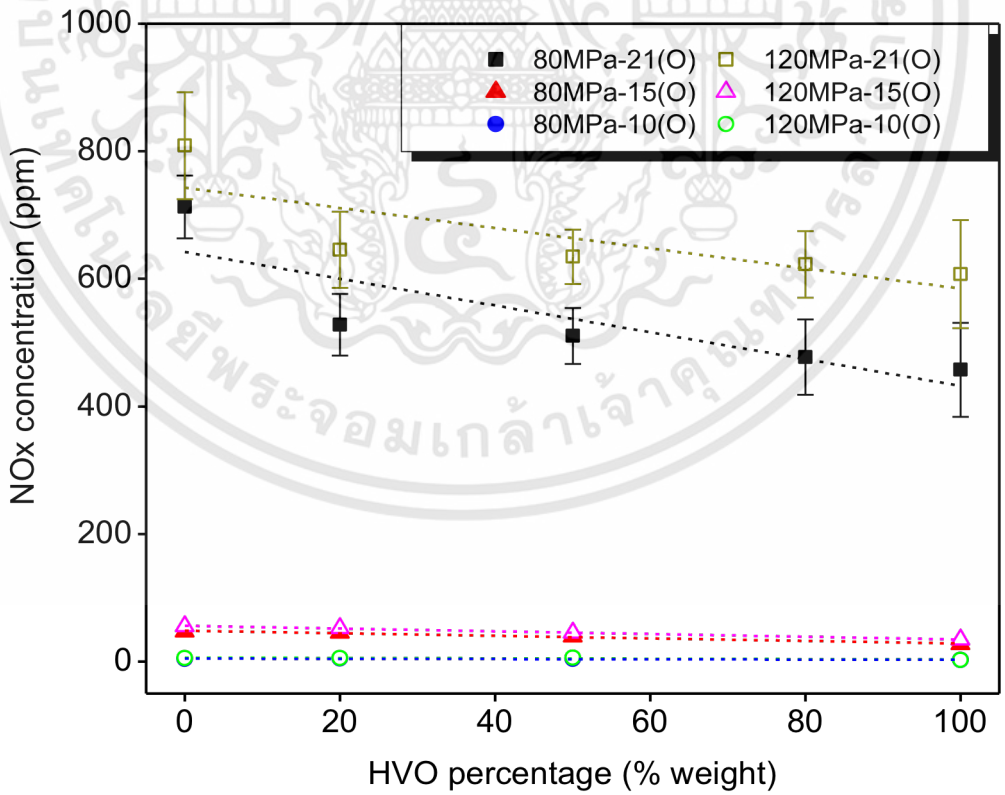

Fig. 4.22. NO_x concentrations of the experimental fuels under variable O_2 concentrations and injection pressures.

fuels and injection pressures. In fact, the higher HVO fraction in the mixture and the lower oxygen concentration contributed to the lower flame temperature and the subsequent lower NO_x formation (Heywood, [7]; Gomes *et al*., [133]; Haifeng *et al.*, [135]). However, the NO_x concentration increased as the injection pressure increased (Fig. 4.22). Despite the minimal difference in the flame temperatures (Fig. 4.19(b)), the early peak of the flame temperature as the differential between the injection pressure and the ambient pressure (i.e. the pressure differential) raised the NO_x emissions by 13.5% and 32.7% for the diesel and HVO fuels, respectively. Importantly, the findings revealed the relationship between the rapid increase in the heat release rate and the NO_x production (Fig. 4.13).

4.5. Conclusion

This research has investigated the effects of variable O_2 concentrations (21%, 15%, 10% O_2) and injection pressures (80 and 120MPa) on the combustion and emissions characteristics of the five experimental fuels: the diesel fuel (B7), the neat hydrotreated vegetable oil (HVO), the 20%, 50% and 80% by mass fraction HVO blended with the diesel. The experiments were carried out in the rapid compression-expansion machine (RCEM) under the direct injection (DI) diesel combustion condition. The analysis was undertaken using the two-color method and the experimental results are as follows:

(1) The higher HVO fraction contributed to the shorter ignition delay, lower heat release rate. Interestingly, the variation in the HVO blend minimally influenced the integral heat release.

(2) The lower ambient oxygen concentration induced the longer ignition delay and premixed combustion phase as well as the lower heat release rate and the smaller integral heat release.

(3) As the differential between the injection pressure and the ambient pressure (i.e. the pressure differential) increased, the ignition delay became shorter, the integral heat release larger, in addition to the early premixed combustion phase.

(4) The flame profile of the HVO resembled that of the diesel fuel in which the higher flame temperature region and the darker KL density were concentrated around the spray flame upstream, regardless of the HVO mixing ratio, in addition to the early appearance of the flame and the KL factor.

(5) Under the lower oxygen concentration, the flame became less luminous and emerged slowly, the flame luminosity was barely detectable under the 10% O_2 concentration. Meanwhile, the greater pressure differential contributed to the wider combustion area, darker flame color, minimal differences between the KL images, and the increased soot formation and oxidation rates.

(6) HVO displayed the lower temporal distributions of the flame temperature and integral KL factor, in comparison with the diesel fuel. In addition, the lower O_2 concentration significantly lowered the flame temperature and the soot formation rate. Meanwhile, the greater pressure differential minimally influenced the flame temperature but accelerated the flame temperature peak and the soot oxidation.

(7) The soot contamination and the HVO percentage in the blend were inversely correlated. The absence of the soot precursors in the HVO, e.g. the poly aromatics hydrocarbons and sulfur, also contributed to the lower soot formation. However, the lower O_2 environment resulted in the higher soot concentrations, especially under the 15% O_2 where the soot concentration was highest. Interestingly, an extremely low O_2 concentration resulted in excessive unburned fractions and the subsequent soot-out reduction at the expense of poor fuel efficiency. Furthermore, the soot levels under injection pressure differential, given the 21% O_2 concentration, were minimally different. On the other hand, the difference was obvious under the lower O_2 concentrations.

(8) The NO_x concentration was inversely correlated to the HVO fraction in the blend. Under the low O_2 concentration, the great NO_x reduction were achieved. In addition, the higher pressure differential induced the increase in the NO_x formation.

CHAPTER 5
CONCLUSIONS

The second generation biofuel of hydrotreated vegetable oil (HVO) was fundamentally studied the fuel injection rate, spray flow, the combustion and exhaust gas emissions by using injection rate-Zeuch measurement system, constant volume combustion chamber, and rapid compression expansion machine, respectively. HVO and its blends with diesel were used throughout whole sequence of experiments in order to provide continual fundamental data on the influences of HVO's properties on injection flow characteristics, spray formation in chamber and subsequent on combustion and emissions characteristics and compare these with those of commercial diesel fuel. Furthermore, the key parameters of engine control were concurrently applied in this work to investigate their effects to the developing trend and effectiveness when combining with HVO.

5.1. Conclusions for injection rate characteristics of HVO and its blends by using high pressure fuel injection system

HVO possess lower density which causes 7.57% smaller bulk modulus of compressibility as compared to diesel. An increase of back pressure indicates the linear increase trend of bulk modulus for HVO and its blends as same as B7. Shorter hydraulic injection delay is clearly recognized with higher injection pressure as well as with higher HVO fraction under low injection pressure due to the effect of small viscosity. The mixing ratios of HVO in mixture, being not up to 50%, hardly causes the change in hydraulic injection delay. In addition, the effective injection duration of all test fuels is longer than the injection duration signal. Interestingly, the effective injection duration of test fuels is equally regardless mixing ratio. However, a higher injection pressure causes a shorter the effective injection duration. The averaged value of injection rate and injection quantity is slightly smaller for HVO due to mainly smaller density. Approximately 5.85% lower in injection quantity under constant injection duration is for HVO as compared to B7. An increase of injection pressure synonymizes higher mass flow rate. The various energizing times barely impact to the hydraulic injection delay and the averaged value of injection rate but affect to the opening and closing needle timing as well as the steady phase of injection process. In this work, the impact of back pressure on the averaged value of the injection rate is negligible. Importantly, an increasing trend of discharge coefficient is observed with higher HVO fraction in mixture, higher injection pressure and back pressure.

In conclusion, HVO and its blends have similar trend of injection process to B7. However, the effect of different density and viscosity of HVO shows the different impact on injection process which subsequently influences on combustion.

5.2. Conclusions for fuel spray characteristics of HVO and its blends by using constant volume combustion chamber

The difference in chemical composition and physical properties of HVO helps resolve ongoing concerns about evironmental issues and sustainable energy due to its improving in mixture formation and subsequently complete combustion. The experimental results show a great effect of density, viscosity, and surface tension on spray characteristics. It is recognized that the spray tip penetration are inversely correlated while spray cone angle and spray volume are directly proportional to HVO fraction in mixture. In addition, spray velocity is not clearly different in the deceleration phase. Notably, HVO displays 5.1% shorter in spray tip penetration, 0.2-1.1 degrees wider in spray angle, and 12-18m/s slower in maximum spray tip velocity at typical quasi steady period of 1.0ms-1.5ms, 80MPa injection pressure, and 4.0MPa ambient gas condition than that of B7. An increase in gas density in range from 11.16kg/m^3 to 44.75kg/m^3 under constant 100MPa injection pressure induces the longer full development time of fuel spray, wider up to 6 degrees in spray cone angle, and smaller 37m/s for B7 and 20m/s for HVO in maximum spray tip velocity. These are correlated with an increase of spray volume in full development time. A variation in injection pressure from 40MPa to 160MPa under constant ambient gas pressure (4.0MPa) shows the increase of spray penetration, spray velocity (60m/s for B7 and 46m/s for HVO) and angle (2.4deg wider in steady state). Furthermore, it is observed that higher pressure differential induces the increase of the turbulence level surrounding fuel spray tip which results in larger gas entrainment.

In general, spray characteristics of HVO validate that the improved its air utilization and fuel impingement decrease as well as the combination of high injection pressure and ambient gas density has promoted to be well mixed with air and subsequently contribute to better combustion.

5.3. Conclusions for spray combustion and emission characteristics of HVO and its blends by using rapid compression and expansion machine

A single hole-solenoid injector with 0.2mm in nozzle diameter, same ambient gas condition and injection pressure were applied thoughout for whole experiements. An investigation on combustion characteristics of HVO and its blends was considered as

the last part for this work. The results exhibited that the higher HVO fraction contributed to the shorter ignition delay under all experimental conditions due to the higher cetane number, smaller surface tension and narrower distillation of the HVO. In addition, the HVO fuels indicated the lower heat release rate than the diesel fuel. Interestingly, the variation in the HVO blend minimally influenced the integral heat release. The lower oxygen concentration induced the longer ignition delay, the longer premixed combustion phase, the lower heat release rate, and the smaller integral heat release. This is because less oxygen was entrained into the fuel spray, resulting in the low reaction rate. As the differential between the injection pressure and the ambient pressure increased, the ignition delay became shorter, the integral heat release larger, in addition to the early premixed combustion phase. This could be attributed to the higher injection velocity, the longer lift-off length and the subsequent more air entrainment.

The higher flame temperature and the darker soot density-KL factor were concentrated around the upstream spray flame, the phenomena which could be attributed to the higher fuel concentration in the upper region. The flame profile of the HVO resembled that of the diesel fuel, in addition to the early appearance of the flame and the KL factor. Under the lower oxygen concentration, the flame became less luminous and emerged slowly. Meanwhile, the greater pressure differential contributed to the wider combustion area, darker flame color, and minimal differences between the KL images. In addition, the soot formation and oxidation rates increased with increase in the pressure differential. However, the flame luminosity was barely detectable under the 10% O_2 concentration. The HVO's shorter ignition delay and narrower distillation contributed to the lower temporal distributions of the flame temperature and integral KL factor, in comparison with the diesel fuel. In addition, the lower O_2 concentration significantly lowered the flame temperature and the soot formation rate. Interestingly, under the 15% O_2 condition, the soot formation was prolonged due to the increased residence time. Meanwhile, the greater pressure differential minimally influenced the flame temperature but accelerated the flame temperature peak and the soot oxidation.

The soot contamination and the HVO percentage in the blend were inversely correlated. This was due to the higher cetane number and lower distillation of the HVO, which resulted in less unburned fractions. The absence of the soot precursors in the HVO, e.g. the poly aromatics hydrocarbons and sulfur, also contributed to the lower soot formation. However, the lower O_2 environment resulted in the higher soot concentrations, especially under the 15% O_2 where the soot concentration was highest. Interestingly, an extremely low O_2 concentration resulted in excessive unburned fractions and the subsequent soot-out reduction at the expense of poor

fuel efficiency. Furthermore, the soot levels under the 80MPa and 120MPa injection pressures, given the 21% O_2 concentration, were minimally different. On the other hand, the difference was obvious under the lower O_2 concentrations as the higher injection velocity enhanced the soot oxidization process. The NO_x concentration was inversely correlated to the HVO fraction in the blend due to the shorter ignition delay and the subsequent lower flame temperature as the HVO fractions increased. Under the low O_2 concentration, the NO_x emissions were suppressed, indicating that the NO_x reduction could be achieved by lowering the flame temperature. In addition, the greater pressure differential induced the increase in the NO_x formation due to the early premixed combustion phase.

5.4. Recommendations for future wok

This research presented the effects of variable O_2 concentrations and injection pressures on the combustion and emissions characteristics of the commercial diesel fuel (B7) and hydrotreated vegetable oil-based fuels (HVO) on rapid compression expansion machine (RCEM). Two color method was used to measure the combustion temperature and KL factor. The study work is significant to understand the combustion and emissions of HVO fuel. The continuous works are suggested as follows:

- Ignition delay value of HVO is 14% shorter than B7. The reason may mainly from high cetance number and distillation value. The use of HVO fuel in the conventional diesel engine without adjusting parameters of electronic injection system may be harmful for engine performance. It is suggested to perform more experiments with the change of injection timing.
- During conducting experiments, the SCV valve of common rail system was often broken. The reason may be that HVO possesses poor lubricity property. This may causes the reduction of engine lifetime when usually running HVO fuel. It is suggested to carry out the engine endurance test or use the additives to improve the lubricity property of HVO.
- The use of catalytic converter is one of the additional option for HVO's studies.

APPENDIX A
FUEL DISTILLATION

PTT PUBLIC COMPANY LIMITED
QUALITY ANALYSIS DEPARTMENT, SUPPLY AND TERMINAL OPERATIONS, OIL BUSINESS
555 ARDNARONG RD., KLONGTOEY, BANGKOK 10260, THAILAND
TEL. +66(0)2239-7148 FAX. +66(0)2239-7149 WWW.PTTPLC.COM

Certificate of Analysis

Product : Diesel

Certificate No. : T-15/12601
Sample Lab No. : OP-HSD-1512973
Customer/Supplier : สถาบันเทคโนโลยีพระจอมเกล้าเจ้าคุณทหารลาดกระบัง
เลขที่ 1 ซอยฉลองกรุง 1 เขตลาดกระบัง กทม. 10520
Sample Location : ---
Batch No. : -
Product Source : หนังสือขอความอนุเคราะห์ที่ ศธ.0524.22/349

Received Date : 02 Jun 2015
Date of Test : 02 Jun 2015
Date of Sampling : 29 May 2015
Sample Condition : Normal

Test Item	Test Method	Limit	Result
1. Density @ 15°C,g/cm3	ASTM D 4052-11	-	0.8235
2. Distillation :Initial Boiling Point,°C	ASTM D 86-11b	-	157.2
3. Distillation :10 %vol. Recovered,°C	ASTM D 86-11b	-	207.7
4. Distillation :50 %vol. Recovered,°C	ASTM D 86-11b	-	287.9
5. Distillation :90 %vol. Recovered,°C	ASTM D 86-11b	-	352.3
6. Calculated Cetane Index	ASTM D 976-06	-	60.43

Approved by :
(Wipawee Chuntaruchi)
Position Title : Product Quality Control Officer
Date of Issue : 04 Jun 2015

(This certificate relates only to the sample tested. Reproduction of it or any of its constituent part is not permitted without the consent of Vice President, Quality Analysis Department.)

PTT PUBLIC COMPANY LIMITED
QUALITY ANALYSIS DEPARTMENT, SUPPLY AND TERMINAL OPERATIONS, OIL BUSINESS
555 ARDNARONG RD., KLONGTOEY, BANGKOK 10260, THAILAND
TEL. +66(0)2239-7148 FAX. +66(0)2239-7149 WWW.PTTPLC.COM

Certificate of Analysis

Product : H10

Certificate No. : T-15/12602
Sample Lab No. : OP-HSD-1513012
Customer/Supplier : สถาบันเทคโนโลยีพระจอมเกล้าเจ้าคุณทหารลาดกระบัง เลขที่ 1 ซอยฉลองกรุง 1 เขตลาดกระบัง กทม. 10520
Sample Location : ---
Batch No. : -
Product Source : หนังสือขอความอนุเคราะห์ที่ ศธ.0524.22/349

Received Date : 02 Jun 2015
Date of Test : 02 Jun 2015
Date of Sampling : 29 May 2015
Sample Condition : Normal

Test Item	Test Method	Limit	Result
1. Density @ 15°C,g/cm3	ASTM D 4052-11	-	0.8188
2. Distillation :Initial Boiling Point,°C	ASTM D 86-11b	-	158.2
3. Distillation :10 %vol. Recovered,°C	ASTM D 86-11b	-	209.2
4. Distillation :50 %vol. Recovered,°C	ASTM D 86-11b	-	286.7
5. Distillation :90 %vol. Recovered,°C	ASTM D 86-11b	-	350.4
6. Calculated Cetane Index	ASTM D 976-06	-	61.96

Approved by :
(Wipawee Chuntaruchi)
Position Title : Product Quality Control Officer
Date of Issue : 04 Jun 2015

(This certificate relates only to the sample tested. Reproduction of it or any of its constituent part is not permitted without the consent of Vice President, Quality Analysis Department.)

PTT PUBLIC COMPANY LIMITED
QUALITY ANALYSIS DEPARTMENT, SUPPLY AND TERMINAL OPERATIONS, OIL BUSINESS
555 ARDNARONG RD., KLONGTOEY, BANGKOK 10260, THAILAND
TEL. +66(0)2239-7148 FAX. +66(0)2239-7149 WWW.PTTPLC.COM

Certificate of Analysis

Product : H20

Certificate No. : T-15/12603
Sample Lab No. : OP-HSD-1513013
Customer/Supplier : สถาบันเทคโนโลยีพระจอมเกล้าเจ้าคุณทหารลาดกระบัง เลขที่ 1 ซอยฉลองกรุง 1 เขตลาดกระบัง กทม. 10520
Sample Location : ---
Batch No. : -
Product Source : หนังสือขอความอนุเคราะห์ที่ ศธ.0524.22/349

Received Date : 02 Jun 2015
Date of Test : 02 Jun 2015
Date of Sampling : 29 May 2015
Sample Condition : Normal

Test Item	Test Method	Limit	Result
1. Density @ 15°C,g/cm3	ASTM D 4052-11	-	0.8140
2. Distillation :Initial Boiling Point,°C	ASTM D 86-11b	-	158.8
3. Distillation :10 %vol. Recovered,°C	ASTM D 86-11b	-	210.7
4. Distillation :50 %vol. Recovered,°C	ASTM D 86-11b	-	284.5
5. Distillation :90 %vol. Recovered,°C	ASTM D 86-11b	-	345.2
6. Calculated Cetane Index	ASTM D 976-06	-	63.37

Approved by : Wipawee
(Wipawee Chuntaruchi)
Position Title : Product Quality Control Officer
Date of Issue : 04 Jun 2015

PTT PUBLIC COMPANY LIMITED
QUALITY ANALYSIS DEPARTMENT, SUPPLY AND TERMINAL OPERATIONS, OIL BUSINESS
555 ARDNARONG RD., KLONGTOEY, BANGKOK 10260, THAILAND
TEL. +66(0)2239-7148 FAX. +66(0)2239-7149 WWW.PTTPLC.COM

Certificate of Analysis

Product : H30

Certificate No. : T-15/12604
Sample Lab No. : OP-HSD-1513014
Customer/Supplier : สถาบันเทคโนโลยีพระจอมเกล้าเจ้าคุณทหารลาดกระบัง เลขที่ 1 ซอยฉลองกรุง 1 เขตลาดกระบัง กทม. 10520
Sample Location : ---
Batch No. : -
Product Source : หนังสือขอความอนุเคราะห์ที่ ศธ.0524.22/349

Received Date : 02 Jun 2015
Date of Test : 02 Jun 2015
Date of Sampling : 29 May 2015
Sample Condition : Normal

Test Item	Test Method	Limit	Result
1. Density @ 15°C,g/cm3	ASTM D 4052-11	-	0.8075
2. Distillation :Initial Boiling Point,°C	ASTM D 86-11b	-	160.5
3. Distillation :10 %vol. Recovered,°C	ASTM D 86-11b	-	212.4
4. Distillation :50 %vol. Recovered,°C	ASTM D 86-11b	-	282.9
5. Distillation :90 %vol. Recovered,°C	ASTM D 86-11b	-	338.9
6. Calculated Cetane Index	ASTM D 976-06	-	65.59

Approved by : Wipawee
(Wipawee Chuntaruchi)
Position Title : Product Quality Control Officer
Date of Issue : 04 Jun 2015

PTT PUBLIC COMPANY LIMITED
QUALITY ANALYSIS DEPARTMENT, SUPPLY AND TERMINAL OPERATIONS, OIL BUSINESS
555 ARDNARONG RD., KLONGTOEY, BANGKOK 10260, THAILAND
TEL. +66(0)2239-7148 FAX. +66(0)2239-7149 WWW.PTTPLC.COM

Certificate of Analysis

Product : H50

Certificate No. : T-15/12605
Sample Lab No. : OP-HSD-1513015
Customer/Supplier : สถาบันเทคโนโลยีพระจอมเกล้าเจ้าคุณทหารลาดกระบัง
เลขที่ 1 ซอยฉลองกรุง 1 เขตลาดกระบัง กทม. 10520
Sample Location : ---
Batch No. : -
Product Source : หนังสือขอความอนุเคราะห์ที่ ศธ.0524.22/349

Received Date : 02 Jun 2015
Date of Test : 02 Jun 2015
Date of Sampling : 29 May 2015
Sample Condition : Normal

Test Item	Test Method	Limit	Result
1. Density @ 15°C,g/cm3	ASTM D 4052-11	-	0.7999
2. Distillation :Initial Boiling Point,°C	ASTM D 86-11b	-	160.4
3. Distillation :10 %vol. Recovered,°C	ASTM D 86-11b	-	216.3
4. Distillation :50 %vol. Recovered,°C	ASTM D 86-11b	-	281.4
5. Distillation :90 %vol. Recovered,°C	ASTM D 86-11b	-	327.4
6. Calculated Cetane Index	ASTM D 976-06	-	68.32

Approved by :
(Wipawee Chuntaruchi)
Position Title : Product Quality Control Officer
Date of Issue : 04 Jun 2015

PTT PUBLIC COMPANY LIMITED
QUALITY ANALYSIS DEPARTMENT, SUPPLY AND TERMINAL OPERATIONS, OIL BUSINESS
555 ARDNARONG RD., KLONGTOEY, BANGKOK 10260, THAILAND
TEL. +66(0)2239-7148 FAX. +66(0)2239-7149 WWW.PTTPLC.COM

Certificate of Analysis

Product : H80

Certificate No. : T-15/12606
Sample Lab No. : OP-HSD-1513016
Customer/Supplier : สถาบันเทคโนโลยีพระจอมเกล้าเจ้าคุณทหารลาดกระบัง
เลขที่ 1 ซอยฉลองกรุง 1 เขตลาดกระบัง กทม. 10520
Sample Location : ---
Batch No. : -
Product Source : หนังสือขอความอนุเคราะห์ที่ ศธ.0524.22/349

Received Date : 02 Jun 2015
Date of Test : 02 Jun 2015
Date of Sampling : 29 May 2015
Sample Condition : Normal

Test Item	Test Method	Limit	Result
1. Density @ 15°C,g/cm3	ASTM D 4052-11	-	0.7865
2. Distillation :Initial Boiling Point,°C	ASTM D 86-11b	-	159.8
3. Distillation :10 %vol. Recovered,°C	ASTM D 86-11b	-	223.1
4. Distillation :50 %vol. Recovered,°C	ASTM D 86-11b	-	279.2
5. Distillation :90 %vol. Recovered,°C	ASTM D 86-11b	-	303.5
6. Calculated Cetane Index	ASTM D 976-06	-	73.44

Approved by : (Wipawee Chuntaruchi)
Position Title : Product Quality Control Officer
Date of Issue : 04 Jun 2015

PTT PUBLIC COMPANY LIMITED
QUALITY ANALYSIS DEPARTMENT, SUPPLY AND TERMINAL OPERATIONS, OIL BUSINESS
555 ARDNARONG RD., KLONGTOEY, BANGKOK 10260, THAILAND
TEL. +66(0)2239-7148 FAX. +66(0)2239-7149 WWW.PTTPLC.COM

Certificate of Analysis

Product : HVO

Certificate No. : T-15/12607
Sample Lab No. : OP-HSD-1513017
Customer/Supplier : สถาบันเทคโนโลยีพระจอมเกล้าเจ้าคุณทหารลาดกระบัง เลขที่ 1 ซอยฉลองกรุง 1 เขตลาดกระบัง กทม. 10520
Sample Location : ---
Batch No. : -
Product Source : หนังสือขอความอนุเคราะห์ที่ ศธ.0524.22/349

Received Date : 02 Jun 2015
Date of Test : 02 Jun 2015
Date of Sampling : 29 May 2015
Sample Condition : Normal

Test Item	Test Method	Limit	Result
1. Density @ 15°C,g/cm3	ASTM D 4052-11	-	0.7780
2. Distillation :Initial Boiling Point,°C	ASTM D 86-11b	-	160.8
3. Distillation :10 %vol. Recovered,°C	ASTM D 86-11b	-	227.4
4. Distillation :50 %vol. Recovered,°C	ASTM D 86-11b	-	278.2
5. Distillation :90 %vol. Recovered,°C	ASTM D 86-11b	-	293.2
6. Calculated Cetane Index	ASTM D 976-06	-	76.89

Approved by : Wipawee
(Wipawee Chuntaruchi)
Position Title : Product Quality Control Officer
Date of Issue : 04 Jun 2015

(This certificate relates only to the sample tested. Reproduction of it or any of its constituent part is not permitted without the consent of Vice President, Quality Analysis Department.)

APPENDIX B
PUBLICATIONS

1. Vo Tan Chau, Charoenphonphanich Chinda, Karin Preechar, Susumu Sato, and Hidenori Kosaka. Optical study on combustion characteristics of hydrotreated vegetable oil and blends under simulated CI engine conditions and various EGR, Journal of mechanical science and technology, Vol. 31, No. 9, 2017, doi: 10.1007/s12206-017-0913-y.
2. V. Chau, C. Chinda, K. Preechar, S. Sato, and H. Kosaka. Effects of variable O_2 concentrations and injection pressures on the combustion and emissions characteristics of the petro-diesel and hydrotreated vegetable oil-based fuels under the simulated diesel engine condition, Journal of the energy institute, 2017, doi: 10.1016/j.joei.2017.07.002.
3. Vo Tan Chau, Pop Paul Ewphun, Huynh Thanh Cong, Preechar Karin, Chinda Charoenphonphanich. Experimental study on injection characteristics of hydrotreated vegetable oil-diesel blends using common rail system, the 14th conference on science & Technology, 2015, Vietnam.

REFERENCES

[1] International Energy Agency (IEA), Energy and Air Pollution, World Energy Outlook, Special report 2016

[2] International Energy Agency (IEA), Energy and Climate Change World Energy Outlook, Special report 2015

[3] S.shafiee, E. Topal; When will fossil fuel reserves be diminished?, Energy Policy. Volume 37, Issue 1, January 2009, Pages 181–189, doi: 10.1016/j.enpol.2008.08.016

[4] World energy outlook 2007, International energy agency (IEA)-2007.

[5] Renewables 2016-Global status report, REN 21-Renewable energy policy network for 21st century.

[6] Chevron, 1998. Diesel Fuels Technical Review (FTR-2), Chevron Products Company, USA

[7] Heywood J. B., Internal combustion engine fundamentals. McGraw-Hill series in mechanical engineering, ISBN 13:9780071004992 (1988).

[8] Twarath Sutabutr, Alternative Energy Development Plan: AEDP 2012-2021, International Journal of Renewable Energy, Vol. 7, No. 1, January - June 2012.

[9] Naber, J. and Siebers, D., Effects of Gas Density and Vaporization on Penetration and Dispersion of Diesel Sprays, SAE Technical Paper 960034, 1996, doi:10.4271/960034.

[10] Kobori S, and Kamimoto T. Development of a rapid compression-expansion machine simulating diesel combustion. SAE no. 952514, 1995, doi: 10.4271/952514.

[11] Soo-Young No. Application of hydrotreated vegetable oil from triglyceride based biomass to CI engine-A review. Fuel, 115, 2014, 88-96, doi: 10.1016/j.fuel.2013.07.001

[12] Sunde Kathrin, Andreas Brekke, and Birger Solberg. Environmental impacts and Costs of Hydrotreated Vegetable Oils, Transesterfified Lipids and Woody BTL-A Revoew, Energies 2011, 4, 845-877, doi: 10.3390/en4060845.

[13] Rickard A, Sara P, Morgan F, Magdalena S. Life cycle assessment of hydrotreated vegetable oil from rape, oil palm and jatropha, Journal of cleaner production, 19 (2011), 129-137, doi: 10.1010/j.jclepro.2010.02.008.

[14] Knothe G. Biodiesel and renewable diesel: A comparison. Progress in Energy and Combustion Science, 36, 3, 2010, Pages 364–373, doi: 10.1016/j.pecs.2009.11.004

[15] Hoekman S. K., Gertler Alan, Broch Amber, Robbins Curt. Investigation of biodistillates as potential blendstocks for transportation fuel, CRC report No. AVFL-17; Coordinating Research Council, Imc.: Alpharetta, GA, USA, 2009.

[16] Lapuerta M, Villajos M, Agudelo JR, Boehman AI., Key properties and blending strategies of hydrotreated vegetable oil as biofuel for diesel engines. Fuel Process Technology 2011; 92:2406–11, doi: 10.1016/j.fuel.2013.07.001

[17] Caprotti R, Tanng T, Ishibe N, In-ochanon R, Tipdecho C, Silapakampeerapap S. Performance of diesel containing bio-hydrogenated component. SAE Technical paper, 2011-01-1953, doi: doi:10.4271/2011-01-1953.

[18] Westphal A. G, Krahl J, Munack A, Rosenkranz N, Schröder O, Schaak J, Pabst C, Brüning T, and Bünger J., Combustion of hydrotreated vegetable oil and jatropha methyl ester in a heavy duty engine: emissions and bacterial mutagenicity, Environ. Sci. Technol., 2013, 47 (11), pp 6038–6046, doi: 10.1021/es400518d.

[19] Jo-Han Ng, Hoon Kiat Ng, Suyin G. Advances in biodiesel fuel for application in compression ignition engines. Clean technologies and environment policy,12 (5), 459-493, 2009, doi: 10.1007/s10098-009-0268-6.

[20] Agarwal AK; Biofuels (alcohol and biodiesel) applications as fuels for internal combustion engines, Progress in Energy combust Sci 2007; 33:233-71, doi: 10.1016/j.pecs.2006.08.003

[21] Koyama A, Iki H, Iguchi Y, Tsurutani K., Vegetable Oil Hydrogenating Process for Automotive Fuel, SAE Technical Paper 2007-01-2030, doi:10.4271/2007-01-2030.

[22] Hartikka T, Kuronen M, and Kiiski U., Technical Performance of HVO (Hydrotreated Vegetable Oil) in Diesel Engines, SAE Technical Paper 2012-01-1585, 2012, doi:10.4271/2012-01-1585.

[23] Magin L, John R. A, Matthew P, Andre. Bulk modulus of compressibility of Diesel/Biodiesel/HVO blends, Energy & fuel, 2012, 26, 1336-1343, doi: 10.1021/ef201608g

[24] Sugiyama K, Goto I, Kitano K, Mogi K., Effects of Hydrotreated Vegetable Oil (HVO) as Renewable Diesel Fuel on Combustion and Exhaust Emissions in Diesel Engine, SAE Int. J. Fuels Lubr. 5(1), p.205-p.217, 2012, doi:10.4271/2011-01-1954.

[25] Pflaum H, Hofmann P, Geringer B, and Weissel W., Potential of Hydrogenated Vegetable Oil (HVO) in a Modern Diesel Engine, SAE Technical Paper 2010-32-0081, 2010, doi:10.4271/2010-32-0081.

[26] Kim D, Kim S, Oh S, No S. Y., Engine performance and emission characteristics of hydrotreated vegetable oil in light duty diesel engines, Fuel 125, 2014, p.36-p.43, doi: 10.1016/j.fuel.2014.01.089.

[27] Aatola H, Larmi M, Sarjovaara T, and Mikkonen S., Hydrotreated Vegetable Oil (HVO) as a Renewable Diesel Fuel: Trade-off between NOx, Particulate Emission,

and Fuel Consumption of a Heavy Duty Engine, SAE Int. J. Engines 1(1):1251-1262, 2009, doi:10.4271/2008-01-2500.

[28] Kuronen M, Mikkonen S, Aakko P, and Murtonen T., Hydrotreated Vegetable Oil as Fuel for Heavy Duty Diesel Engines, SAE Technical Paper 2007-01-4031, 2007, doi:10.4271/2007-01-4031.

[29] Murtonen T, Aakko-Saksa P, Kuronen M, Mikkonen S. et al., Emissions with Heavy-duty Diesel Engines and Vehicles using FAME, HVO and GTL Fuels with and without DOC+POC Aftertreatment, SAE Int. J. Fuels Lubr.2(2):147-166, 2010, doi:10.4271/2009-01-2693.

[30] Kopperoinen A, Kyto M, and Mikkonen S., Effect of Hydrotreated Vegetable Oil (HVO) on Particulate Filters of Diesel Cars, SAE Technical Paper 2011-01-2096, 2011, doi:10.4271/2011-01-2096.

[31] Jaroonjitsathian S, Tipdecho C, Sukajit P, Namthirach N. Et al., Bio-Hydrogenated Diesel (BHD): Renewable Fuel for Advanced Diesel Technology, SAE Technical Paper 2013-01-0070, 2013, doi:10.4271/2013-01-0070.

[32] Erkkilä K, Nylund N, Hulkkonen T, Tilli A. et al., Emission performance of paraffinic HVO diesel fuel in heavy duty vehicles, SAE Technical Paper 2011-01-1966, 2011, doi:10.4271/2011-01-1966.

[33] Hulkkonen T, Hillamo H, Sarjovaara T, and Larmi M. Experimental Study of Spray Characteristics between Hydrotreated Vegetable Oil (HVO) and Crude Oil Based EN 590 Diesel Fuel, SAE Technical Paper 2011-24-0042, 2011, doi:10.4271/2011-24-0042.

[34] Jaroonjitsathian S, Saisirirat P, Sivara K, Tongroon M. et al., Effects of GTL and HVO Blended Fuels on Combustion and Exhaust Emissions of a Common-Rail DI Diesel Technology, SAE Technical Paper 2014-01-2763, 2014, doi:10.4271/2014-01-2763.

[35] Matti H, Tero L, Maria E. M, Teemu S, Martti L, Reine W, Annele V, Jorma K., The comparison of particle oxidation and surface structure of diesel soot particles between fossil fuel and novel renewable diesel fuel. Fuel 89 (2010), p.4008-4013, doi: 10.1016/j.fuel.2010.06.006

[36] Matti H, Juha H, Timo M, Kalle L, Teemu S, Martti L, Jorma K, Annele V., Reductions in particulate and NOx emissions by diesel engine parameter adjustments with HVO fuel, Environmental Science & Technology, 2012, 46 (11), pp 6198–6204, doi: 10.1021/es300447t.

[37] Mizushima N, Kawano D, Ishii H, Takada Y. et al., Evaluation of Real- World Emissions from Heavy-Duty Diesel Vehicle Fueled with FAME, HVO and BTL using PEMS, SAE Technical Paper 2014-01-2823, 2014, doi:10.4271/2014-01-2823.

[38] Singh D, Subramanian K. A, and Singal S. K., Emissions and fuel consumption characteristics of a heavy duty diesel engine fueled with Hydroprocessed Renewable Diesel and Biodiesel, Applied Energy 155 (2015) 440–446, doi: 10.1016/j.apenergy.2015.06.020

[39] Westphal A. G, Krahl J, Munack A, Rosenkranz N, Schröder O, Schaak J, Pabst C, Brüning T, and Bünger J., Combustion of hydrotreated vegetable oil and jatropha methyl ester in a heavy duty engine: emissions and bacterial mutagenicity, Environ. Sci. Technol., 2013, 47 (11), pp 6038–6046, doi: 10.1021/es400518d.

[40] Richard van Basshuysen and Fred Schäfer. Internal combustion engine handbook, 2nd edition, SAE International, 2016, eISBN: 978-0-7680-8287-6.

[41] Payri R, Gimeno J, Novella R, Bracho G. On the rate of injection modeling applied to direct injection compression ignition engines, International journal of engine research, 2016, doi: 10.1177/1468087416636281

[42] Yu G, Li L, Deng J, Zhang Z, Yu L. Research on the Effect of the Parameters of Common-Rail System on the Injection Rate, SAE-China, FISITA (eds) Proceedings of the FISITA 2012 World Automotive Congress, doi: 10.1007/978-3-642-33841-0_30

[43] Mulemane A, Han J, Lu P, Yoon S, Lai M. Modeling Dynamic Behavior of Diesel Fuel Injection Systems, SAE Technical Paper 2004-01-0536, 2004, doi:10.4271/2004-01-0536.

[44] Henein N, Lai M, Singh I, Zhong L, Han J. Characteristics of a Common Rail Diesel Injection System under Pilot and Post Injection Modes, SAE Technical Paper 2002-01-0218, 2002, doi:10.4271/2002-01-0218.

[45] Lucio P, Giacomo B, Francesco C. P, Claudio C. Zeuch method-based injection rate analysis of a common-rail system operated with advanced injection strategies, Fuel 128, 2014, 188-198, doi: 10.116/j.fuel.2014.03.006

[46] Ishikawa S, Ohmori Y, Fukushima S, Suzuki T, Takamura A, Kamimoto T. Measurement of Rate of Multiple-Injection in CDI Diesel Engines, SAE Technical Paper 2000-01-1257, 2000, doi:10.4271/2000-01-1257.

[47] Arcoumanis, C., Baniasad, M. Analysis of consecutive fuel injection rate signal obtained by the Zuech and Bosch method. SAE-Journal of Engines 102, 3, 93021, 1993.

[48] Hwang J, Kal H, Kim M, Park J. et al., Effect of Fuel Injection Rate on Pollutant Emissions in DI Diesel Engine, SAE Technical Paper 1999-01-0195, 1999, doi:10.4271/1999-01-0195.

[49] Nishimura T, Satoh K, Takahashi S, and Yokota K. Effects of Fuel Injection Rate on Combustion and Emission in a DI Diesel Engine, SAE Technical Paper 981929, 1998, doi:10.4271/981929.

[50] Tanabe K, Kohketsu S, and Nakayama S. Effect of Fuel Injection Rate Control on Reduction of Emissions and Fuel Consumption in a Heavy Duty DI Diesel Engine, SAE Technical Paper 2005-01-0907, 2005, doi:10.4271/2005-01-0907.

[51] Benajes J, Molina S, Rudder D. K. Influence of injection rate shaping on combustion and emissions for a medium duty diesel engine, KSME Int, J, Vol. 20, No. 9, pp 1436-1448, 2006, doi: 10.1007/BF02915967.

[52] Tinprabath P, Hespel C, Chanchaona S, and Foucher F. Influence of Biodiesel and Diesel Fuel Blends on the Injection Rate and Spray Injection in Non-Vaporizing Conditions, SAE Technical Paper 2013-24-0032, 2013, doi:10.4271/2013-24-0032.

[53] Dernotte J, Hespel C, Foucher F, Mounaim-Rousselle C. Influence of physical fuel properties on the injection rate in a diesel injector. Fuel 96, 153–160, 2012, doi: 10.1016/j.fuel.2011.11.073

[54] Bang S. H, Lee C S. Fuel injection characteristics and spray behavior of DME blended with methyl ester derived from soybean oil, Fuel, 2010,89:797-800.

[55] Seykens X L J, Somers L M T, and Baert R S G. Modeling of common rail fuel injection system and influence of fluid properties on injection process, In: Proceedings of VAFSEP, Dublin, Ireland; July 6-9, 2004.

[56] Som S, Longman D E, Ramirez A I, Aggarwal S K. A comparison of injector flow and spray characteristics of biodiesel with petro-diesel, Fuel, 2010, 89:4014-4024.

[57] Desantes J.M, Payri R, Garcia A, and Manin J. Experimental study of biodiesel blends' effects on diesel injection processes, Energy & Fuels, 2009, 23:3227-3235.

[58] Dong Han, Yaozong D, Chunhai W, He L, Zhen Huang. Experimental study on injection characteristics of fatty acid esters on a diesel engine common rail. Fuel 123, 19-25, 2014.

[59] Tinprabath P, Hespel C, Chanchaona S, and Foucher F. Influence of biodiesel and diesel fuel blends on the injection rate under cold conditions, Fuel, 144, 80-89, 2015, doi: 10.1016/j.fuel.2014.12.010

[60] Desantes J, Payri R, Salvador F, and Gimeno J. Measurements of Spray Momentum for the Study of Cavitation in Diesel Injection Nozzles, SAE Technical Paper 2003-01-0703, 2003, doi:10.4271/2003-01-0703.

[61] Payri F, Bermudez V, Payri R, Salvador j. F. The influence of cavitation on the internal flow and the spray characteristics in diesel injection nozzles, Fuel 83, 4-5, 419-431, 2004, doi: 10.1016/j.fuel.2003.09.010

[62] Benajes J, Pastor V. J, Payri R, Plazas H. A. Analysis of the Influence of Diesel Nozzle Geometry in the Injection Rate Characteristic, journal of fluid engineering, 126, 1, 2004, doi: 10.1115/1.1637636.

[63] Payri R, Salvador J. F, Gimeno J, Venegas O. Study of cavitation phenomenon using different fuels in a transparent nozzle by hydraulic characterization and visualization, Experimental thermal and fluid science, 44, 235-244, 2013, doi: 10.1016/j.expthermflusci.2012.06.013

[64] Badock C, Wirth R, Fath A, Leipertz A. Investigation of cavitation in real size diesel injection nozzles, Int. J. Heat and Fluid Flow, 20, 5, 538, 544, 1999, doi: 10.1016/S0142-727X(99)00043-0

[65] Munsin R, Laoonual Y, Jugjai S, Matsuki M, Kosaka H. Effect of glycerol ethoxylate as an ignition improver on injection and combustion characteristics of hydrous ethanol under CI engine condition. Energy Conversion and Management 98, 282-289, 2015.

[66] Borhanipour M, Karin P, Tongroon M, Chollacoop N. et al., Comparison Study on Fuel Properties of Biodiesel from Jatropha, Palm and Petroleum Based Diesel Fuel, SAE Technical Paper 2014-01-2017, 2014, doi:10.4271/2014-01-2017.

[67] Pandey K. R, Rehman A, Sarviya M. R. Impact of alternative fuel properties on fuel spray behavior and atomization. Renewable and sustainable energy reviews, 16 (3) (2012) 1762-1778, doi: 10.1016/j.rser.2011.11.010

[68] André L, David M, James S. The Impact of the bulk modulus of diesel fuels on fuel injection timing, Energy Fuel, 18 (6) (2004) 1877-1882.

[69] Boudy F, and Seers P. Impact of physical properties of biodiesel on the injection process in a common-rail direct injection system, Energy conversion and Management, 50 (12) (2009) 2905-2912.

[70] Hiroyasu H. and Arai M., Structures of Fuel Sprays in Diesel Engines, SAE Technical Paper 900475, 1990, doi:10.4271/900475.

[71] Dernotte J, Hespel C, Houille S, Foucher S, Mounaim-Rousselle C. Influence of fuel properties on the diesel injection process in nonvaporizing conditions, Atomization and Sprays, 2012, doi: 10.1615/AtomizSpr.2012004401

[72] Hillamo H, Sarjovaara T, Vuorinen V, Larmi M. et al., Diesel Spray Penetration and Velocity Measurements, SAE Technical Paper 2008-01-2478, 2008, doi:10.4271/2008-01-2478.

[73] Wang X, Gao J, Jiang D, Huang Z, Chen W. Spray characteristics of high-pressure swirl injector fueled with methanol and ethanol, Energy & Fuel, 2005, 2394-2401, doi: 10.1021/ef050135w.

[74] Delacourt E, Desmet B, Besson B. Characterisation of very pressure diesel spray using digital imaging techniques, Fuel 84, 2005, 859-867, doi: 10.1016/j.fuel.2004.12.003.

[75] Suh k. H, Park W. S, Lee S. C. Effect of piezo-driven injection system on the macroscopic and microscopic atomization characteristics of diesel fuel spray. Fuel 86, 2007, 2833–2845, doi: 10.1016/j.fuel.2007.03.015

[76] Payri R, Salvador J. F, Soare V. Determination of diesel sprays characteristics in real engine In-cylinder air density and pressure conditions, KSME Int. J, Vol. 19, No. 11, pp.2040-2052, 2005.

[77] Chen C. P, Wang C. W, Roberts L. W, and Fang T. Spray and atomization of diesel fuel and its alternatives from a single-hole injector using a common rail fuel injection system, Fuel 103, 2013, 850-861, doi: 10.1016/j.fuel.2012.08.013

[78] Kihm KD, Terracina DP. Synchronized droplet size measurements for coal-water slurry sprays generated from a high-pressure diesel injection system. Department of Mechanical Engineering, Texas A&M University; June 1993.

[79] Suh K. H, Roh G. H, Lee S. C. Spray and combustion characteristics of biodiesel/diesel blended fuel in a direct injection common-rail diesel engine. J. Eng. Gas Turbines Power, 130(3):032807, 2008, doi: 10.1115/1.2835354.

[80] Labs J, Parker T. Two-dimensional droplet size and volume fraction distributions from the near-injector region of high-pressure diesel sprays. Atomization Spray, 2006;16-7; page 843–855, doi: 10.1615/AtomizSpr.v16.i7.90

[81] Gao Y, Deng J, Li C, Dang F, Liao Z, Wu Z, Li L. Experimental study of the spray characteristics of biodiesel on inedible oil. Biotechnology Advance 27, 2009;p. 616–624, doi: 10.1016/j.biotechadv.2009.04.022.

[82] Ghurri A, Kim D. J, Kim G. H, Jung Y. J, Song K. K. The effect of injection pressure and fuel viscosity on the spray characteristics of biodiesel blends injected into an atmospheric chamber, J. Mechanical Science and Technology 26, 9, 2012, 2941-2947, doi: 10.1007/s12206-012-0703-1

[83] Lee S, Jeong S, Lim O. An investigation on the spray characteristics of DME with variation of ambient pressure using the common rail fuel injection system, J. Mechanical Science and Technology 26, 10, 2012, 3323-3330, doi: 10.1007/s12206-012-0806-8.

[84] Settles S. G. Schlieren and shadowgraph techniques: Visualizing phenomena in transparent media, Springer 200a, ISBN: 978-3-642-63034-7.

[85] Grimaldi C, and Postrioti L. Experimental Comparison Between Conventional and Bio-derived Fuels Sprays from a Common Rail Injection System, SAE Technical Paper 2000-01-1252, 2000, doi:10.4271/2000-01-1252.

[86] Song k. K, Sim C. S, Jung K. B, Kim G. H, Kim H. J. Effect of the injection parameters on diesel spray characteristics, KSME Int. J., Vol. 19, No. 6, pp. 1321-1328, 2005.

[87] Wang X, Huang Z, Kuti A. Experimental and analytical study on biodiesel and diesel spray characteristics under ultra-high injection pressure, Int. J. Heat fluid flow, 31, p.659-66, 2010.

[88] Dung N. N, Ishida H, Shioji M., Gas-to-Liquid Spray at Different Injection and Ambient Conditions, Journal of engineering for gas turbines and power, 133/032804-1, 2009.

[89] Dodge L, Simescu S, Neely G, Maymar M. et al., Effect of Small Holes and High Injection Pressures on Diesel Engine Combustion, SAE Technical Paper 2002-01-0494, 2002, doi:10.4271/2002-01-0494.

[90] Wang X, Huang Z, Kuti O, Zhang W, Nishida K., An experimental investigation on spray, ignition and combustion characteristics of biodiesels, Proceedings of the combustion institute, 33, 2071- 2077, 2011, doi: 10.1016/j.proci.2010.07.037.

[91] Masjuki H, Abul K., An Overview of Biofuel as a Renewable Energy Source: Development and Challenges, Procedia Engineering 56 (2013), p.39-p.53, doi: 10.1016/j.proeng.2013.03.087.

[92] Ali Y, Hanna A. M., Alternative diesel fuels from vegetable oils, Bioresource technology 20, 2, p.153-163, 1994, doi: 10.1016/0960-8524(94)90068-X.

[93] Liu X, He H, Wang Y, Zhu S, Piao X., Transesterification of soybean oil to biodiesel using CaO as a solid base catalyst, Fuel 87, 2, p.216-221, 2008, doi: 10.1016/j.fuel.2007.04.013

[94] Nwafor O.M.I, Rice G, Ogbonna A.I., Effect of advanced injection timing on the performance of rapeseed oil in diesel engines, Renewable Energy 21, 3-4, p. 433-444, 2000, doi: 10.1016/S0960-1481(00)00037-9.

[95] Zainal M, Yusof M, Aziz A. A, Mukti A. A. M., Performance of Palm Oil Methyl Esters as Alternative Fuel for Diesel Engines, SAE Paper No. 871151, 1998.

[96] Hashimoto N, Ozawa Y, Mori N, Yuri I, Hisamatsu T., Fundamental combustion characteristics of palm methyl ester (PME) as alternative fuel for gas turbines, Fuel, 87, 15-16, p.3373-3378, 2008, doi: 10.1016/j.fuel.2008.06.005

[97] Reksowardojo I, Lubis I, Manggala W, Brodjonegoro T. et al., Performance and Exhaust Gas Emissions of Using Biodiesel Fuel from Physic Nut (Jatropha Curcas

L.) Oil on a Direct Injection Diesel Engine (DI), SAE Technical Paper 2007-01-2025, 2007, doi:10.4271/2007-01-2025.

[98] Tapanes N. C. O, Gomes Aranda D. A, de Mesquita Carneiro J. W, Ceva Antunes O. A, Transesterification of Jatropha curcas oil glycerides: Theoretical and experimental studies of biodiesel reaction, Fuel 87, 10-11, p.2286-2295, 2008, doi: 10.1016/j.fuel.2007.12.006

[99] Meng X, Chen G, Wang Y., Biodiesel production from waste cooking oil via alkali catalyst and its engine test, Fuel Processing Technology, 89, 9, p.851-857, 2008, doi: 10.1016/j.fuproc.2008.02.006

[100] Bhatti H. N, Hanif M. A, Qasim M, Ata-ur-Rehman, Biodiesel production from waste tallow, Fuel, 87, 13-14, p.2961-2966, 2008, doi: 10.1016/j.fuel.2008.04.016.

[101] Schablitzky H W, Lichtscheidl J, Hutter K, Hafner Ch, Rauch R, Hofbauer H., Hydroprocessing of Fischer-Tropsch biowaxes to second-generation biofuels, Biomass conversion and biorefinery, 1, pp. 29-37, 2011, doi: 10.1007/s13399-010-0003-x.

[102] Schablitzky H W, Lichtscheidl J, Rauch R, Hofbauer H., Investigations on hydrotreating of Fischer Tropsch-biowaxes for generation of bio-Products from lignocellulosic biomass, Modern applied science, vol.6, no.4, 2012, doi: 10.5539/mas.v6n4p28.

[103] Unruh D, Pabst K, Schaub G., Fischer-Tropsch synfuels from biomass: Maximizing carbon efficiency and hydrocarbon yield, Energy fuels, 24, p. 2634-2641, 2010, doi: 10.1021/ef9009185.

[104] Gill S. S, Tsolakis A, Dearn K. D, Rodríguez-Fernández J., Combustion characteristics and emissions of Fischer-Tropsch diesel fuels in IC engines, Progress in energy and combustion science, 37, p. 503-523, 2011, doi: 10.1016/j.pecs.2010.09.001.

[105] Zhang W., Automotive fuels from biomass via gasification, Fuel processing technology, 91, 8, p. 866-876, 2010, doi: 10.1016/j.fuproc.2009.07.010

[106] Leckel D., Diesel production from Fischer-Tropsch: The past, the present, and new concepts, Energy & Fuels, 23, p.2342-2358, 2009, doi: 10.1021/ef900064c

[107] Oguma M, Goto S, Oyama K, Sugiyama K. et al., The Possibility of Gas to Liquid (GTL) as a Fuel of Direct Injection Diesel Engine, SAE Technical Paper 2002-01-1706, 2002, doi:10.4271/2002-01-1706.

[108] Moon G, Lee Y, Choi K, Jeong D., Emission characteristics of diesel, gas to liquid, and biodiesel-blended fuels in a diesel engine for passenger cars, Fuel, 89, 12, p. 3840-3846, 2010, doi: 10.1016/j.fuel.2010.07.009.

[109] Lehto K, Elonheimo A, Hakkinen K, Sarjovaara T. et al., Emission Reduction Using Hydrotreated Vegetable Oil (HVO) With Miller Timing and EGR in Diesel Combustion, SAE Int. J. Fuels Lubr. 5(1):218-224, 2012, doi:10.4271/2011-01-1955.

[110] Ladommatos N, Abdelhalim S, Zhao H., The effects of exhaust gas recirculation on diesel combustion and emissions. Int. J. engineresearch, vol. 1, no. 1, 2000.

[111] Shi Q, Li T, Zhang X, Wang B., Measurement of temperature and soot (KL) distributions in spray flames of diesel butanol blends by two color method using high speed RGB video camera. SAE international, no. 2016-01-2190, doi: 10.4271/2016-01-2190.

[112] Zhang J, Jing W, Roberts W L., Fang T., Effects of ambient oxygen concentration on biodiesel and diesel spray combustion under simulated engine conditions. Energy, 57, p.722-732, 2013, doi: 10.1016/j.energy.2013.05.063.

[113] Pickett M. L, Siebers L. D., Soot in diesel fuel jets: Effects of ambient temperature, ambient density, and injection pressure, Combustion and Flame 138, p.114-p.135, 2004, doi: 10.1016/j.combustflame.2004.04.006

[114] Wang X, Kuti A. O, Zhang W, Nishida K, Huang Z., Effect of injection pressure on flame and soot characteristics of the biodiesel fuel spray, Combust. Sci. and Tech., 182:1369-1390, 2010, doi:10.1080/00102201003789139.

[115] Kitamura Y, Mohammadi A, Ishiyama T, and Shioji M., Fundamental Investigation of NOx Formation in Diesel Combustion Under Supercharged and EGR Conditions, SAE Technical Paper 2005-01-0364, 2005, doi:10.4271/2005-01-0364.

[116] Soltic P, Edenhauser D, Thurnheer T, Schreiber D, Sankowski A., Experimental investigation of mineral diesel fuel, GTL fuel, RME and neat soybean and rapeseed oil combustion in a heavy duty on-road engine with exhaust gas aftertreatment, Fuel, 88, 1, p.1-8, 2009, doi: 10.1016/j.fuel.2008.07.028

[117] Shi L, Cui Y, Deng K, Peng H, Chen Y., Study of low emission homogeneous charge compression ignition (HCCI) engine using combined internal and external exhaust gas recirculation (EGR), Energy, 31, 14, p. 2665-2676, 2006., doi: 10.1016/j.energy.2005.12.005.

[118] Ganesh D, Nagarajan G, Mohamed Ibrahim M., Study of performance, combustion and emission characteristics of diesel homogeneous charge compression ignition (HCCI) combustion with external mixture formation, Fuel. 87, 17-18, p. 3497-3503, 2008, doi: 10.1016/j.fuel.2008.06.010

[119] Raeie N, Emami S, Sadaghiyani O. K., Effects of injection timing, before and after top dead center on the propulsion and power in a diesel engine, Propulsion and power research, 3, 2, p. 59-67, 2014, doi: 10.1016/j.jppr.2014.06.001

[120] Deqing M, Junnan Q, Ping S, Yan M, Shuang Z, and Yongjun C., Study on the combustion process and emissions of a turbocharged diesel engine with EGR, journal of combustion, 2012, doi: 10.1155/2012/932724.

[121] Buyukkaya E, Cerit M., Experimental study of NOx emissions and injection timing of a low heat rejection diesel engine, Int. J. of thermal sciences, 48, p. 1096-1106, 2008, doi: 10.1016/j.ijthermalsci.2007.07.009.

[122] Ito T, Kitamura T, Ueda M, Matsumoto T. Et al., Effects of Flame Lift-Off and Flame Temperature on Soot Formation in Oxygenated Fuel Sprays, SAE Technical Paper 2003-01-0073, 2003, doi:10.4271/2003-01-0073.

[123] Zhang J, Jing W, Roberts L. W, Fang T., Soot temperature and KL factor for biodiesel and diesel spray combustion in a constant volume combustion chamber, Applied energy 107, 52-65, 2013, doi: 10.1016/j.apenergy.2013.02.023

[124] Kamimoto T, Uchida N, Aizawa T, Kondo K and Kuboyama T., Diesel flame imaging and quantitative analysis of in-cylinder soot oxidation, Int. J. of engine research, IMechE 2016, doi: 10.1177/1468087416629282.

[125] Hottel H. C, and Broughton F. P., Determination of true temperature and total radiation from luminous gas flame. Ind. Eng. Chem. Anal. Ed., 1932, 4 (2), pp 166–175, doi: 10.1021/ac50078a004.

[126] Dale R. T, Kenth I. S., Soot process in compression ignition engine, Progress in energy and combustion science 33, 3, p.272-p.309, 2007, doi: 10.1016/j.pecs.2006.03.002.

[127] Nishiumi R, Yasuda A, Tsukasaki Y, and Tanaka T., Effects of Cetane Number and Distillation Characteristics of Paraffinic Diesel Fuels on PM Emission from a DI Diesel Engine, SAE Technical Paper 2004-01-2960, 2004, doi:10.4271/2004-01-2960.

[128] Xiaojie B, Haifeng L, Ming H, Cai S, Xinqi Q, Chia-fon F. L., Experimental and numerical study on soot formation and oxidation by using diesel fuel in constant volume chamber with various ambient oxygen concentrations, Energy conversion and management 84, p.152-p.163, 2014, doi: 10.1016/j.enconman.2014.04.023.

[129] Haifeng L, Chia-fon L, Ming H, Mingfa Y., Combustion characteristics and soot distributions of neat butanol and neat soybean biodiesel, Energy & Fuel, 25, p.3192-3203, 2011, doi: 10.1021/ef1017412.

[130] Fujimoto H, Higashi K, Yamashita T, and Senda J., Effects of Ambient Temperature and Oxygen Concentration on Soot Behavior in Diesel Flame, SAE Technical Paper 2005-24-007, 2005, doi:10.4271/2005-24-007.

[131] Haifeng L, Ming H, Yu L, Xin W, Hu W, Mingfa Y, and Chia-fon F. L., Time-resolved spray, flame, soot quantitative measurement fueling n-butanol and soybean biodiesel in a constant volume chamber under various ambient temperatures, Fuel 133, 317-325, 2014, doi: 10.1016/j.fuel.2014.05.038.

[132] Idicheria C. and Pickett L., Soot Formation in Diesel Combustion under High-EGR Conditions, SAE Technical Paper 2005-01-3834, 2005, doi:10.4271/2005-01-3834.

[133] Gomes P. and Yates D., Analysis of the Influence of Injection Timing on Diesel Combustion by the Two-Colour Method, SAE Technical Paper 982890, 1998, doi:10.4271/982890.

[134] Haifeng L, Xiaojie B, Ming H, Chia-fon F. L, Mingfa Y., Soot emissions of various oxygenated biofuels in conventional diesel combustion and low-temperature combustion condition, Energy & fuel, 26, 1900-1911, 2012, doi: 10.1021/ef201720d.

[135] Haifeng L, Xin W, Zunquing Z, Jingbo G, Hu W, Mingfa Y., Experimental and simulation investigation of the combustion characteristics and emissions using n-butanol/biodiesel dual-fuel injection on a diesel engine, Energy 74, 741-752, 2014, doi: 10.1016/j.energy.2014.07.041.

AUTHOR BIOGRAPHY

Author	: Mr. Vo Tan Chau
Date of birth	: May 27th, 1987
Address	: Ho Chi Minh City, Vietnam
Education	: 2005-2010 Bachelor degree in Transportation Engineering
	: Ho Chi Minh City University of Technology, Vietnam
	: 2011-2013 Master degree in Mechanical Engineering
	: Institute of Technology Bandung (ITB), Indonesia
	: 2013-2017 Doctoral degree in Mechanical Engineering
	: King Mongkut's Institute of Technology Ladkrabang (KMITL), Thailand
	: Tokyo Institute of Technology (TIT), Japan
Email	: votanchau_brvt@yahoo.com